U.PORTO

FEUP FACULDADE DE ENGENHARIA
UNIVERSIDADE DO PORTO

DESIGN OF A PRE-STRESSED BRIDGE DECK WITH ULTRA-HIGH PERFORMANCE CONCRETE

RUI MACÁRIO GOMES VALENTE

Dissertação submetida para satisfação parcial dos requisitos do grau de

MESTRE EM ENGENHARIA CIVIL — ESPECIALIZAÇÃO EM ESTRUTURAS

Orientador: Professor Doutor Pedro Álvares Ribeiro do Carmo Pacheco

Coorientador: Engenheiro Gilberto Castro Alves

Junho de 2017

MESTRADO INTEGRADO EM ENGENHARIA CIVIL 2016/2017

DEPARTAMENTO DE ENGENHARIA CIVIL

Tel. +351-22-508 1901

Fax +351-22-508 1446

✉ miec@fe.up.pt

Editado por

FACULDADE DE ENGENHARIA DA UNIVERSIDADE DO PORTO

Rua Dr. Roberto Frias

4200-465 PORTO

Portugal

Tel. +351-22-508 1400

Fax +351-22-508 1440

✉ feup@fe.up.pt

🌍 http://www.fe.up.pt

Aos meus Pais

ACKNOWLEDGMENTS

I would like to thank not only who directly helped me to develop this work but also the ones who had an important role in my academic course. I would particularly like to acknowledge:

- Professor Pedro Pacheco for his motivational words, timely and experienced advices, and the readiness to answer my questions. I would also like to thank by making possible my attendance on High Tech Concrete Symposium in Maastricht which I will never forget.
- Engineer Gilberto Alves for his availability to help me whenever I needed. All our discussions about issues that arose along work process have enriched me. Finally, I should thank him for his predisposal to let me know about deeper subjects that aroused my interest, and for make understand how important is to face the difficulties by going through them as soon as possible.
- Professor Mário Pimentel for receive me to discuss about the particularities of Ultra-High Performance Concrete and also for providing me useful scientific documentation and bibliographic references.
- Professor Miguel Castro for introduce me computational programming in the point of view of structural optimization. It is a subject that interests me and which soon or later I will go back to it again.
- CSI Portugal technical support for elucidate me about software considerations on creep effects.
- My cousin, Daniela Valente, for her readiness to assist me in text revision as well as my friends Luis Tiago Costa and Andreia Cardoso.
- Above all, to my parents for all the effort to attend all my needs, since ever.

RESUMO

Este trabalho inclui duas soluções diferentes resultantes do dimensionamento de um tabuleiro de uma ponte com Betão de Desempenho Ultra-Elevado (UHPC). No primeiro caso (Caso 1) o tabuleiro foi inteiramente dimensionado com UHPC, enquanto no segundo caso (Caso 2) é uma solução mista onde o UHPC é colocado onde surgem maiores esforços e no restante tabuleiro é colocado betão normal. O objetivo prende-se com a avaliação da viabilidade económica e comparar estas duas soluções com o projeto da ponte existente, que é um tabuleiro em viga caixão feito de betão normal pré-esforçado. Adicionalmente, análise modal seguida de análise sísmica são realizadas com o intuito de avaliar possíveis mudanças nos esforços máximos que se instalam na substrutura.

Devido às elevadas propriedades mecânicas do UHPC, espera-se que a massa da superestrutura possa ser reduzida. Contudo, com um material de características soberbas vem um custo elevado que pode comprometer a viabilidade económica das soluções em estudo. Por essa razão, o estudo deve ser realizado para que seja avaliado se o dimensionamento com UHPC em lugar do betão normal conduz a soluções viáveis ou não.

A análise estrutural é executada após a elaboração do modelo de cálculo da ponte no software *CSiBridge* ter sido feita. Além da análise estrutural no modelo da ponte completa, a análise da construção faseada não linear é também considerada para controlar tensões durante a execução da obra. Esta última análise requere a definição da evolução das propriedades dos materiais ao longo do tempo e do planeamento construtivo. O método de dimensionamento passa por realizar verificações das tensões durante o processo construtivo e verificações do estado limite de serviço e do estado limite último durante o período de serviço da estrutura. O dimensionamento dos elementos de UHPC é apoiado por uma norma adequada, NF P18-710, e por uma ferramenta numérica propositadamente desenvolvida para realizar análise da secção transversal durante o dimensionamento ou verificação a flexão e ao corte em estado limite último. Finalmente, para que a solução final da secção transversal seja validada, são realizadas análises de estabilidade quer durante a construção, quer durante a fase em que a estrutura se encontra em serviço para que seja avaliado se o estado limite último é condicionado pela instabilidade ou pela capacidade resistente do material.

É alcançada uma redução da massa da superestrutura na ordem dos 36% para a o Caso 1 e 26 % para o Caso 2, e a quantidade de cordões de pré-esforço é também reduzida para 36% e 32%, respetivamente. Ao contrário do que era esperado, a ação sísmica na direção do alinhamento do tabuleiro não muda nos dois casos, mas na direção transversal o corte basal reduziu cerca de 14.6% para o Caso 1 e 8% para o Caso 2. Existe grande variedade de preço para o UHPC mas não foi encontrada nenhuma solução economicamente viável em ambas as soluções alcançadas. Contudo, é necessário continuar o estudo no sentido da otimização estrutural e quantificação das armaduras.

PALAVRAS-CHAVE: Dimensionamento estrutural, Betão de Desempenho Ultra-Elevado, Ponte, Cimbre Auto lançável, Viga Caixão.

ABSTRACT

A bridge deck is designed with two different solutions where is used Ultra-High Performance Concrete (UHPC) as structural element. The first Case 1, involves a deck thoroughly using UHPC. And the second, Case 2, is a mixed solution with UHPC being placed where the internal forces are higher and the remaining deck is casted with regular concrete. The purpose of this study is to assess the economic feasibility and compare those solutions with the existing bridge which is a multi-span box girder deck made of regular pre-stressed concrete. Additionally, modal analysis preceded by seismic analysis are performed to evaluate eventual changes that may occur on substructure internal forces.

Due to high mechanical properties of this material, it is expected a superstructure with less material. However, with a superb material comes a high cost which may comprise economic feasibility. For that reason, the study must be go forward in order to assess whether the application of UHPC in turn of regular concrete leads to a feasible solution or not.

The structural analysis is executed after the development of bridge numerical model on the software CSiBridge have been done. Besides the analysis on bridge integral model, nonlinear staged construction analysis is also considered to control stresses during execution. This last analysis requires the definition of time dependent properties of the materials and of constructive schedule. The method of design goes through stress verifications during constructive stage, serviceability limit state and ultimate limit state verifications during service stage. The design of UHPC elements is aided by proper design code, NF P18-710, and by a numerical tool purposely developed to perform sectional calculations on both flexural and shear design or verifications in ultimate limit state. Finally, to validate the final solution for the cross-section, buckling analysis is performed in both service and constructive stages to assess if the ultimate limit state is governed by instability issues or by material strength.

It is achieved a reduction on superstructure mass of 36% for Case 1 and 26% for Case 2 and the amount of pre-stress tendons is also reduced to 36% and 32%, respectively. On the contrary to expected, seismic action along superstructure alignment does not change in both cases, but in transverse direction the global base reaction decreased about 14.6% for Case 1 and 8% for Case 2. There is high scatter about the UHPC cost but no economic feasibility was found on both solutions achieved. However, a deeper study on it is required regarding structural optimization and also the quantification of steel reinforcement.

KEYWORDS: Ultra-High Performance Concrete, Movable Scaffolding System, Box Girder, Structural design.

TABLE OF CONTENTS

INDEX OF FIGURES

INDEX OF TABLES

SYMBOLS, ACRONYMS AND ABBREVIATIONS

A_c - Area of concrete cross-section

A_{fv} - Area of fiber effect

A_k - Area enclosed by the center-lines of the connecting walls, including inner hollow areas

A_p - Area of pre-stressing steel

A_s - Area of steel reinforcement

$b_{(i)}$ - Width of layer i

b_w - Web thickness

$b_{w,nom}$ - Web thickness deducted by ducts

d - Effective depth

E_{cm} - Mean Elasticity Modulus

E_s - Elasticity modulus of steel reinforcement

$F_{(i)}$ - Resultant force on layer i

f_{cd} - Design value of concrete compressive strength

f_{ck} - Characteristic compressive strength

f_{cm} - Mean compressive strength

$f_{ctf1\%,k}$ - Characteristic post-cracking stress corresponding to a crack width of 0.01H

$f_{ctf1\%,u}$ - Ultimate post-cracking stress corresponding to a crack width of 0.01H

f_{ctfk} - Characteristic maximal post-cracking stress

$f_{ctfk,u}$ - Ultimate maximal post-cracking stress

f_{ctfm} - Mean maximal post- cracking stress

$f_{ctk,el}$ - Characteristic limit of elasticity under tension

$f_{ctm,el}$ - Mean limit of elasticity under tension

$f_{p0.1k}$ - Characteristic 0,1% proof-stress of pre-stressing steel

f_{pk} - Characteristic tensile strength of pre-stressing steel

F_s - Total force installed on steel reinforcement

$F_{s,corrected}$ - Corrected force of steel reinforcement

$F_{s,correction}$ - Force deducted from UHPC because of steel reinforcement presence

f_{ywd} - Yield stress of steel reinforcement

H - Depth of the tested prism with dimensions complying with the structures dimensions

h_0 - Notional size of the cross-section

i - Layer i

K - Fiber orientation factor

L_c - Characteristic length used to calculate equivalent strain from the crack width

L_f - Fibers length

n_{ducts} - Number of ducts on the same horizontal plan

N_{ed} - Design axial force

P_{max} - Maximum force applied to the tendon

r - Degree of reaction

RH - Relative Humidity

t - Equivalent time

t_0 - Age of the concrete which is subjected to permanent load

T_{ed} - Design value of longitudinal torsion force

t_s - Age of the concrete at the beginning of drying shrinkage

V_{ed} - Design value of longitudinal shear force

$V_{ed,i,t}$ - Design value of shear force in one wall due to longitudinal torsion force

$V_{ed,i,tot}$ - Total design value of shear force in one wall

$V_{ed,i,v}$ - Design value of shear force in one wall due to shear longitudinal force

$V_{rd,c}$ - Contribution to shear resistance brought by the concrete matrix

$V_{rd,f}$ - Contribution to shear resistance brought by the fibers

$V_{rd,max}$ - Resistance of the concrete compressive struts

$V_{rd,s}$ - Contribution to shear resistance brought by the vertical shear reinforcement

w - Crack width

$w_{1\%}$ - Crack width of 0.01H

w_{pic} - Crack width corresponding to local peak in post-cracking phase or to a crack width equal to 0.3 mm if there is no peak

x - neutral axis depth or height of the compression zone

x_i - Position of Layer i

z - Lever arm of internal forces

z_i - Lever arm of internal forces in one wall

α - Shear reinforcement inclination angle

α_{cc} - Coefficient that takes into account the long-term effects on the compressive strength

$\varepsilon_{(i)}$ - Strain of the layer i

ε_{c0d} - Design value of maximum compressive elastic strain

ε_{ca} - Autogenous shrinkage strain

ε_{cd} - Drying shrinkage strain

ε_{cs} - Total shrinkage strain

ε_{cud} - Design value of ultimate compressive strain

ε_{s} - Steel reinforcement strain

ε_{syd} - Yield strain of steel reinforcement

ε_{u} - Ultimate tensile strain in the extreme fiber

$\varepsilon_{u,el}$ - Elastic tensile strain at ULS

"$\varepsilon_{u,el}$" - Truncated elastic tensile strain at ULS

$\varepsilon_{u,lim}$ - Ultimate strain beyond which fibers participation is no longer taken into account at ULS

$\varepsilon_{u,pic}$ - Ultimate equivalent strain corresponding to the local peak in post-cracking phase or to a crack width equal to 0.3 mm if there is no peak

$\varepsilon_{u,1\%}$ - Ultimate equivalent strain corresponding to a crack width of 0.01H

θ - Strut inclination angle

v - Poisson's ratio

ρ - Reinforcement ratio

$\sigma_{(i)}$ - Stress installed on layer i

σ_{c} - Stress installed on concrete

σ_{cp} - Average cross-section stress

$\sigma_{f(w)}$ - Stress law as a function of crack width

$\sigma_{p,max}$ - Maximum stress applied to the tendon

σ_{pm0} - stress in the tendon immediately after tensioning or transfer

$\sigma_{Rd,f}$ - Residual strength of the fiber-reinforced cross-section

σ_{s} - Steel reinforcement stress

$\sigma_{t,averege}$ - Average stress along the crack

Υ_{c} - Partial factor on compression

Υ_{cf} - Partial safety factor on fibers

φ - Curvature

φ_{b} - Basic creep coefficient

φ_{d} - Drying creep coefficient

Φ_{ducts} - Ducts diameter

AFGC - Association Française de Génie Civil

CC - Conventional Concrete

DSPs - Densified with small particles

EC2 - Eurocode 2

FHWA - Federal Highway Administration

JSCE - Japan Society of Civil Engineers

LMSS - Large Movable Scaffolding System

MDF - Micro-Defected-Free

MSS - Movable Scaffolding System

OPS - Organic Pre-Stressing System

PS - Pre-stressing

RCP - Reactive Powder Concrete

SLS - Serviceability limit state

TS - Tandem System

UDL - Uniformed Distributed Load

ULS - Ultimate limit state

US - United States

W/B - Water-Binder ratio

W/C - Water-Cement ratio

Eq. - Equation

Fig. - Figure

1
INTRODUCTION

1.1. PREFACE

History have been showed us that structural form is closely interrelated with the material of which it is made of. For this reason, when some new material emerges new structural geometries may also appear so that the material properties can be fully exploited. Arches were early built with stone and then steel brought other structural geometries as trusses, suspension and tied bridges. Consequently, and as already have been proven, UHPC will also provide structural designers with superb mechanical properties to develop new structural concepts.

With the increasing mobility and accessibility needs comes a growing demand on infrastructures like bridges either in quantity or load bearing capacity. Consequently, the search for economical solutions is indispensable. The emergence of a new material such as UHPC, which is characterized by its compressive strength higher than 150MPa and tensile strength provided by steel fibers around 10MPa, certainly leads to lighter structures once that there is required less material to resist the same loading. However, a major hindrance emerges and which is related with material high cost. Therefore, to evaluate whether UHPC application is economical or not, studies on that should be performed.

This study bases in a real project of an existing multi-span continuous bridge whose cross-section is re-designed with UHPC material. A pair of different solutions are proposed, designed and then compared with the initial and existing solution. In the first case, the bridge deck is thoroughly designed with UHPC and, in the second case, it is designed with a mixed solution of conventional concrete (CC) and UHPC.

Even before reaching design phase, there was a need of studying and understanding several matters without which it would be impossible to go forward. It starts by a deeper understanding on material properties and composition. Then, a review over existing codes and guidelines referred to UHPC structural design allowed making a reasonable choice on what would be the proper document to follow during design. The differences between internal and external tendons are described so that can support design and modeling procedures as well as the constructive method and its implications on structural analysis and design.

1.2. OBJECTIVES

The focus of this study is on the design of a bridge deck with UHPC. In order to accomplish that, it is necessary to go through the following works:

- Material characterization (composition and properties);

- Identify existing design standards;
- Study of the constructive process;
- Load characterization;
- Develop numerical structural models in the software *CSiBridge*;
- Comparative analysis.

2
STATE OF THE ART

2.1. HISTORICAL OVERVIEW

Several experiments and studies were carried out aiming to increase concrete strength. Most developments occurred during two decades between 1970's and mid-1990's. In Table 1.1. is shown a brief chronological explanation of most significate advances during that period.

Table 2.1. - Summary of concrete compressive strength developments

Source	f_{cm} [MPa]	Name	Conditions/Technics
Roy, Gouda and Bobrowsky (USA, 1972) [20]	510	-	▪ Only cement paste with high heat treatment (250ºC) and high-pressure treatment (50MPa).
Yudenfreund, Odler and Brunauer (USA, 1972) [21]	240	-	▪ Only cement paste with very thin clinkers (Blaine surface areas ranging from 6000 to 9000cm^2/g); ▪ Low water-cement ratio (0.2-0.3); ▪ Use of additives to increase workability; ▪ Vacuum mixing to reduce air entrainment.
Birchall, Howard and Kendall (UK, 1981) [22]	200	Micro-Defected-Free (MDF) Paste	▪ Only cement paste; ▪ Removal of large voids on cement undetected by conventional methods.
Bache (Denmark, 1981) [23]	Up to 270	High-Strength Densified with small particles (DSPs) Concrete	▪ Mortar made of sand (up to 4mm); ▪ Densely packed cement with ultra-fine particles arranged in the space between the cement; ▪ Heat treatment during cure (80ºC); ▪ Extremely low water content (0.13-0.18 by weight of cement and ultra-fine particles); ▪ Large quantity of superplasticizer.
Richard and Cheyrezy (France, 1995) [24]	Up to 810	Reactive Powder Concrete (RPC)	▪ Excluding coarse aggregate; ▪ Heating (250-400ºC) and pressure (50MPa) treatments; ▪ Steel fibers and steel aggregate.

Two major lines of research have been followed aimed to achieve high mechanical performance with cementitious matrix materials. The first concerns high-strength DSPs concrete, with high superplasticizer and silica fume content, also incorporating ultra-hard aggregate [23]. Another approach was oriented towards improving the strength of the paste, based on the concept of the so called MDF [22].

But high-strength DSPs concrete was developed further by Scientific Division of Bouygues [24]. This research considered not only different aggregates and steel fiber lengths but also different curing treatments. In one of their tests neither pressuring treatment nor heat-treatment was applied (20ºC) which can be compared to field cast conditions. Steel straight fibers were added to the cementitious material matrix (2-2.5% per volume) and compressive strength reached 170MPa. Moreover, it was concluded that steel fibers enhanced ductile behavior on rupture. With the Lafarge cooperation, a new mix formulation was developed and called of "Reactive Powder Concrete" (RCP) which continues to exist in the commercial form of "Ductal" [25].

RCP is a branch of UHPC family whose maximum grain sizes is approximately 0.8 mm whereas it generally may reach approximately 5.0mm [26]. In section Proportions where different mix formulations are presented, that particularity can be verified.

Since then, this material was the starting point for researchers and engineers who have begun extensive investigation studies. The objective was to improve and characterize even better its behavior. Only this way would be possible to industrialize it and provide engineers with technical normalization to apply it in design and construction.

After UHPC have become commercially available in the United States in 2000, the Federal Highway Administration (FHWA) started to investigate its use in highway infrastructure in 2001. FHWA along with State Transportation Department have worked to deploy the technology since 2002. Simultaneously, several universities were doing research work on UHPC. All of this led engineers to apply this material in bridges in many ways. The most common usage was in bridge joints but in 2006 the first highway bridge was constructed in the US [27].

In 2002, France came with the first design recommendation on UHPC. This document results from multiple checks and tests carried out during the development of nuclear-power-plant cooling towers and Bourg-lès-Valence bridges [28]. It addresses mechanical characteristics, structural design methods and durability of UHPC [29]. Consequently, several bridges have been built in France since then. As design standards were missing elsewhere, this recommendation had been also used out of France [25]. Later in 2013 this recommendation was updated mainly motivated by compatibility with entering in force of Eurocodes [30] and, in 2016, a French national annex to EC2 arose.

Since 2004, International Symposium on Ultra-High Performance Concrete have taken place in Kassel (Germany) every 4 years. But later in 2012, the international symposium extended its focus towards nanotechnology in construction materials. A 12-million-euros Research Program on UHPC was launched by German Research Foundation. It begun in 2005 with the contribute of more than 20 institutes to investigate about 40 projects. In the end (2012), the research results were supposed to provide a strong basis to develop reliable technical standards. The goal was to enable industries to produce reliable UHPC using regionally available raw materials and provide engineers with guidelines to design proper structures [27].

Other Asian countries have shown interest in this material too. Japan's first guideline appeared in 2004 which represents a modified version of the French recommendations [16]. Korea Institute of Construction Technology launched a 6 years' research program (Super Bridge 200) started in 2007 to

investigate the use of UHPC in cable-stayed bridges. The total budget was about 10 million euros [31]. Bridge construction cases on these countries are as well referred in Bridges made of UHPC chapter. In Malaysia, UHPC has been used as a sustainable way of construct bridges and, in 2014, it had already been built 24 bridges with this material [32].

According to State-of-The-Art Report of FHWA [27] there are several countries spread all over the globe which adopted UHPC as main structural material for bridge construction. It shows, therefore, that UHPC potentials are being recognized and receiving worldwide attention.

2.2. BRIDGES MADE OF UHPC

2.2.1. FOREWORD

The report made by U.S. Department of Transportation, that approaches the UHPC state of the art [27], lists several bridges where this material had been applied before 2013. This list covers North America, Europe, Asia, and Australia. Some cases, UHPC is used on local repairs, or wet joints or even connecting adjacent precast beams. Other cases it is applied as the main structural element and is about this last case the following examples are referred to.

2.2.1. FOOTBRIDGES

Footbridges are interesting structures in the point of view of UHPC potential. That is justified by architectural requirements, for instance visual lightness. The material higher strength allows the design of slender structures. Herein are mentioned some remarkable UHPC footbridges and their main features.

The first UHPC bridge is located at Sherbrooke in Canada in 1997. It is a pre-stressed pedestrian/bikeway bridge (Fig.2.1.) made of six precast segments each 10m long and spanning a total of 60m long. The precast segments are open-web space trusses without conventional steel reinforcement. Upper and lower chord members are made from UHPC with 200MPa compressive strength. The top chord is materialized with a ribbed slab with 30mm thickness, and transverse pre-stressing was applied with sheathed monostrands. The bottom chord is made of two pre-stressed beams. In the web diagonal members, UHPC is confined in stainless steel tubes. Finally, the precast segments are assembled with external pre-stressing tendons [19].

Fig.2.1 - The Sherbrooke Footbridge in Sherbrooke, Quebec, spans 60 m across the Magog River with a precast truss made of reactive powder concrete [1, 19].

The Seon Yu Footbridge (2001) was erected in Seoul, South Korea, with 430m of total length (Fig.2.2.). To allow pedestrians crossing the Han River, the structure is composed by an arch which accomplishes 120m span. It consists of six precast elements with double-T (or π-shape) cross-section

supporting a UHPC ribbed slab [18]. Due to UHPC mechanical properties, it was possible to design a very slender arch with thin sections, resulting in a lighter perception.

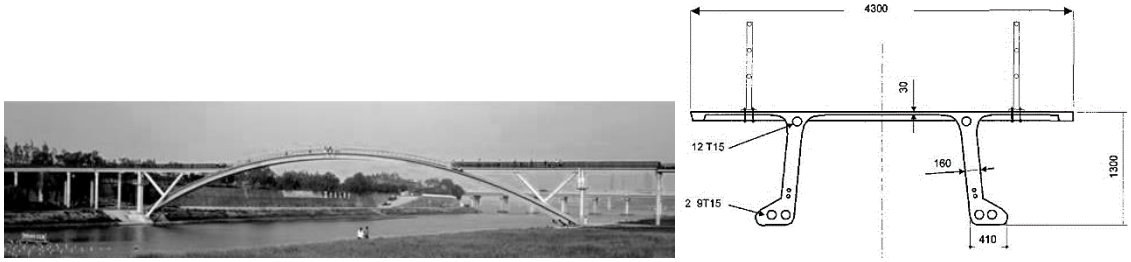

Fig.2.2. - Seon Yu Footbridge: a) Arch [1]; b) Cross-section [18].

Other structures, with the same function but with different forms, have been built since then in many countries. For instance, the Sakata-Mirai footbridge (Fig.2.3.) was built in 2002 and it was the beginning of bridge design using UHPC in Japan. It is a post-tensioned box girder structure with perforated webs. The self-weight of the deck resulted in about 25% of that of ordinary pre-stressed concrete bridge. The deck is also constituted with 6 precast segments that when combined with external pre-stressing it achieves 50m span length [33].

Fig.2.3. - General view of Sakata-Mirai Footbridge [1]

2.2.3. ROAD BRIDGES

The Bourg-Les-Valence Bridges (Fig.2.4.) are known to be the two first UHPC road bridge applications. They have two 20-m-long-spans each constructed by mean of π-shaped pre-stressed beams without any passive reinforcement (Fig.2.5.). These spans are statically determinate and the joint connecting longitudinal beams was made *in situ* using internal reinforcement and UHPC too [7].

Fig.2.4. - General view of one of the Bourg-Les-Valence Bridges, France, 2001 [1].

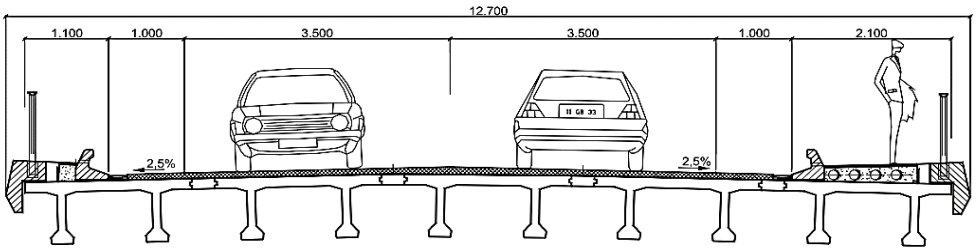

Fig.2.5. - Standard cross-section of Bourg-Les-Valence Bridges, France, 2001 [7].

Still in France, a single span bridge with 47.40m of length was constructed during 2004. Its name is Pont de la Chabotte (Fig.2.6.) and it comprises 22 glued segments with some of them having different geometry to anchorage external pre-stressing tendons. The depth of the cross-section is 1.6m and the upper slab width is 4.4m. So, this bridge slenderness is characterized by span-to-depth ratio of 30. The webs and the lower slab have a constant thickness of 0.12m whereas the upper slab has 0.14m. When compared with an eventual conventional C35/45 concrete solution, this bridge only needs 40% of that concrete volume and 1/3 of that assembling duration. Furthermore, this box girder bridge is free of longitudinal passive reinforcement [11].

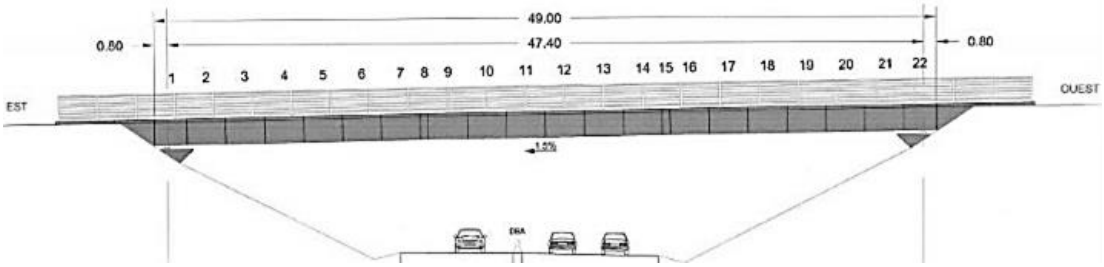

Fig.2.1. - Elevation of the Pont de la Chabotte. [11].

The construction of first highway bridge in the US making use of UHPC dates to 2006 (Iowa, USA) and it is called The Wapello County Mars Hill Bridge (Fig.2.6.). It comprises three 33.5m long precast UHPC beams with bulb-tee cross-section form. Each beam is pre-stressed and there is no need of shear reinforcement. All together support a cast-in-place bridge deck [14].

Fig.2.2. - The Wapello County Mars Hill Bridge [14].

Malaysia have been adopted UHPC has a mainstream material for bridge construction. It is there that the world's longest single span road bridge was constructed. Batu 6 Bridge (Fig.2.7.) is constructed with precast segments of 4 m high, 2.5m long and 5m wide. The typical mid-span section has very slender elements (Fig.2.8.) but the webs are locally thickened to accommodate the shear keys and the bottom slab at the ends is also thickened to accommodate anchorages. There is no passive

reinforcement to stand ultimate bending moment forces. However, it is uniquely used as anti-bursting reinforcement in the anchorages and to transfer longitudinal shear between webs and upper slab [34].

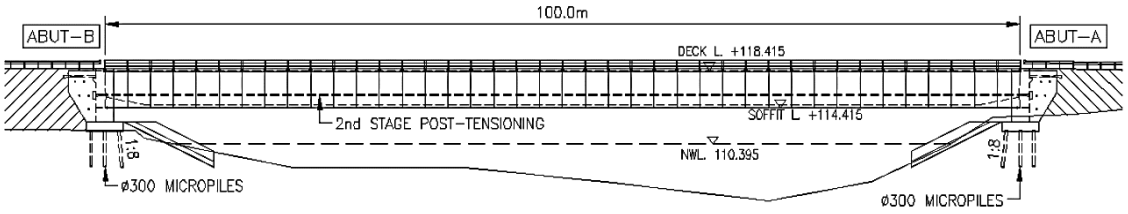

Fig.2.3. - Elevation view of Batu 6 Bridge [34].

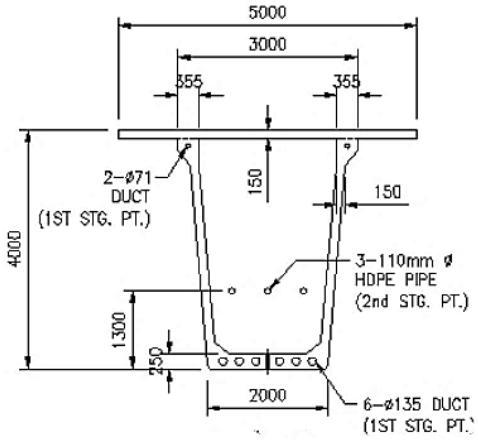

Fig.2.4. - Detail of UHPC box girder of Batu 6 Bridge [mm] [34].

One last existing example is given. Sungai Nerok Bridge is another bridge in Malaysia with integral beam-deck system (Fig.2.9.). This multi-span, continuous road bridge has a total width of 15m and three spans of 30 m each, creating a total bridge length of 90m. The structural component cost was USD906/m^2 which is lower than the homologous value of CC bridges in Malaysia, USD1.100 to USD1.400/m^2. The immediate cost saving s amounts 17% even knowing that durability may increase that value at long-term.

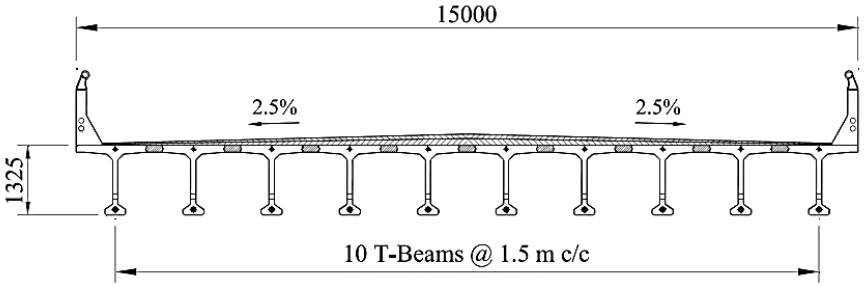

Fig.2.5. - Typical section view of Sungai Nerok Bridge [mm] [32].

2.3. SUMMARY

In the last 5 decades have been published works that show the interest in enhancing concrete overall performance mainly its maximum compressive strength. The material formulation has been changed until mid-90's. Since then the formulation have remained practically unchanged and studies started to

focus in the characterization of mechanical properties. There are 3 work fronts which have an interdependent relationship between each other. They are researching, standard development, and real structures applications. Most of the continents have been doing that resulting in UHPC bridges all over the world.

All the bridges introduced are examples of how bridges have been designed with UHPC. Most of the times bridge elements are pre-cast and then assembled at their final position which is justified by the high controlled conditions during material production. With UHPC is possible to design slender and lighter solutions and, in some particular cases, it may compete against CC structures regarding immediate costs.

3
UHPC AS A STRUCTURAL MATERIAL

3.1. COMPOSITION

3.1.1. CEMENT

UHPC mixtures usually are designed of ordinary Portland cement (generally combined with silica fume). As result of dense packing, a very low water-cement ratio is achieved. Consequently, binder components do not hydrate completely and they will also work as filler [35]. Furthermore, cement selection cannot be dissociated from that of superplasticizer [24].

3.1.2. AGGREGATE

Fine quartz sand aggregate combined is frequently used as this material is readily available, has low cost, is very strong and promotes excellent paste/aggregate interfaces. The most common maximum particle size of sand used in UHPC is limited to over 5 or 6 mm [26, 36]. Both angular or natural sand can be used but is preferred the second one because of lower water requirements [24].

In some cases, quartz powder may be used. It has particle size distribution ranging from 0.1 to 100μm and usually acts like a filler. However, this ultra-fine material is an essential ingredient for heat-treated UHPC whose maximum reactivity is obtained for particle size of between 5 and 25 μm [24].

3.1.3. SILICA FUME

Silica fume is an industrial byproduct and has a typical diameter of 0.2μm. This admixture is usually combined with cement. The implementation of this admixture has three main functions:

- Filling the empty space between the cement particles
- Improvement of rheological behavior through the lubrication effect resulting from the perfect sphericity of the basis particles
- Secondary hydrates resulting from pozzolanic reaction with the calcium hydroxide

In order to control impurities, that the Blaine finesses must be limited to $22m^2/g$. It was also proposed that silica fume content should be about 25% of Portland cement weight. [24].

If heat treatment is applied (80-90°C) there will be formation of additional strength-forming hydrate phases. Contrary, without that treatment the filler effect remains [37].

3.1.4. SUPERPLASTICIZER

It was concluded that a combination of selectively adsorbing polycarboxylate superplasticizers is more effective than individual polymers [38] for dispersion of the cement/silica blend. This chemical admixture is a dispersing agent that allow to reduce water content. But superplasticizers also exhibit a retarding characteristic on cement hydration which can present a problem for practical applications [24].

The main characteristics of the polycarboxylate based superplasticizers are the following:

- High water reduction (up to 40%)
- High flowability
- Polymer-design allows to control the main characteristics (setting time and workability)
- Blending of different polymers is possible: formulation of customized solutions

As mentioned previously, cement and superplasticizer cannot be chosen individually. With these main characteristics, it is possible to adapt the superplasticizer to the cement conditions and to achieve a perfect optimization of the cement paste. The binder content of UHPC can be 4 times higher when compared to a CC, which leads to an increased admixture content of up to 15 times. This shows the importance of the choice of the right superplasticizer type. Studies show that big differences occur mainly in setting time and early strength development, whereas the influence on final strength is not significantly influenced [39].

3.1.5. STEEL FIBERS

There are several types of fibers that can be integrated in UHPC mixture. In the current work only steel fibers are used. Depending on fiber content, UHPC attains the following characteristics [26]:

- Increase of fracture energy, subsequent improvement of ductility;
- Increase of strength (manly tensile strength);
- Reduction of tendency for cracking.

In order to enhance ductility in their compressive tests, Richard and Cheyrezy [24] used straight steel fibers with 12mm long and a diameter of 0.15mm.

In Malaysia, several bridges have been constructed using UHPC whose steel fibers are from two different type. One of them is straight with 20mm length and 0.2mm of diameter. And the other type is end-hooked and had dimensions of 25mm length by 0.3mm diameter [32]. Moreover, Japanese Recommendation [40] suggests the use of fibers 10 to 20 mm in length and 0.1 to 0.25 mm in diameter, with a tensile strength of 2000MPa or more and 2% volume fraction.

3.1.6. PROPORTIONS

In CC, water-binder ratio (W/B) is between 0.4 and 0.6. But in UHPC that ratio is reduced to below 0.25 thanks to two major aspects. First, the addition of superplasticizer has a deflocculating effect on binder. And second, thin granulometry is used and which requires higher content of cement. In summary, binder content increases whereas water content remains practically the same. Silica fume amounts about 20% of the cement weight [41].

The very compact UHPC induces not only very high compressive strength but also more pronounced fragile behavior with complete loss of any plastic domain. Steel fibers are added to ensure non-brittle

behavior. It is currently used a fiber content of 2% by volume [24, 32, 41]. Moreover, regulations on UHPC structures indirectly control fibers quantity through a minimum ductility condition [6].

The proportions of UHPC composition may vary among the suppliers and it also depends on raw materials locally available. Some of the few patents in the world market are presented in Table 3.1..

Table 3.1. - Dosages and properties of the most common commercial UHPC. [36]

Element	Ductal®		BSI®		CEMTEC$_{multiscale}$®		BCV®	
	Type	Kg/m^3	Type	Kg/m^3	Type	Kg/m^3	Type	Kg/m^3
Cement	Portl.	746	-	1114	CEM I 52.5	1050		
Silica fume	-	242	-	169	-	275		2115
Quartz flour	-	224	-	-	-	-		(premix)
Sand (mm)	0.1-0.6	1066	0-6	1072	<0.5	730	2-3	
Water	W/C	0.19	W/C	0.19	W/C	0.181	W/C	0.25
Admixture	Chryso	9	SIKA	40	Chryso	35	-	21.5
Fiber (mm)	13/0.2	161	20/0.3	234	10/0.2	470	$20_{2/3}13_{1/3}$	156
Slump (mm)		700		640		-		750
$F_{ct,28}$ (MPa)		8		8.8		-		8
$F_{cm,7}$ (MPa)	20º	101	20º	165	20º	-	20º	98
$F_{cm,28}$ (MPa)	20º/90º	124/198	20º	199	20º	168	20º/90º	130-150

3.2. FRESH STATE

3.2.1. MIXING

Any CC mixer is capable of mix UHPC but it requires more mixing energy when compared to CC, which means that mixing time should be longer. This fact combined with fine grain size and low water-binder ratio may lead to undesirable overheat during mixing. It can be avoided by using a high-energy mixer, or lowering the temperatures of the constituents, or even replacing the mix water with ice [42].

The UHPC production requires long mixing times that depends on the ambient temperature. It easily lasts 12 minutes of mixing time. Thus, it restrains plant production and increases costs significantly. The mixing time of UHPC can be reduced by optimizing the particle size distribution by means of replacement of cement and quartz flour by silica fume, matching the type of superplasticizer and cement in the mix and increasing the speed of mixing [43].

3.2.2. PLACING

Placing operations have a fundamental role on UHPC fibers orientation. Therefore, UHPC ultimate tensile strength and ductile behavior are highly influenced by placement method [41]:

- Fiber reinforcement tends to show a preference for aligning in the direction of flow during casting;
- The fibers close to the walls tend to be oriented parallel to the formwork. The thinner the element, the greater will be the impact on the tensile strength;
- A preferred orientation of fibers in the direction of gravity can sometimes occur due to the natural behavior of fibers in the viscous liquid phase of the UHPC before setting.

These phenomena must be considered during development of casting sequence. In an advanced phase of this work it will be explained how fiber scatter and element fineness is considered on design.

Internal vibration is not recommended so that fibers orientation don't be interfered. However, limited external form vibration can be applied in order that entrapped air could be released. Despite that, packing rarely is a problem due to UHPC self-compacting ability. Placement shall be performed using tremie pipes or buckets. Additionally, continuous poring until the completion in one area shall be planned. Overlay placing and merging areas shall be avoided (Fig.3.1.) during casting process because they become weak points [16, 42]. UHPC must be dropped up to 0.50 m and if this indication cannot be satisfied, a test should be done beforehand to ensure that there is no segregation of fibers nor fiber clustering [30].

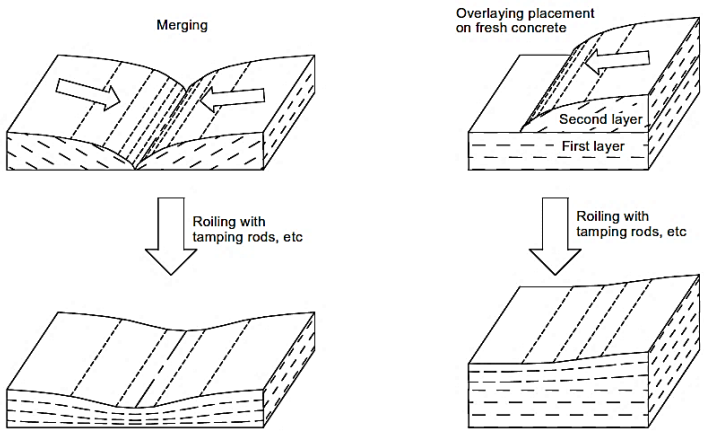

Fig.3.1. - Examples of treatment for overlaying placement and merging [3]

The French recommendation [30] gives some instructions that should be considered in adverse weather conditions. Concreting is not recommended when the outdoor temperature falls below +5°C. However, special arrangements can be made to overcome this issue allowing proper concreting process:

- Heating of aggregate and/or mix water;
- Use of thick timber or insulated forms;
- Use of setting and hardening accelerators.

High outdoor temperature (>35°C) induces undesirable high temperatures inside thick components during hydration process. The precautions pointed are similar to those which can be adopted for CC for example cooling of mixing water.

3.2.3. CURING AND HARDENING

The reduced water-binder ratio in a UHPC mix necessitates careful attention to prevent water to escape prior to hydration. That is why, right after casting, UHPC surface must be covered with an impermeable layer. When UHPC surface is properly covered, avoiding any space between seal and UHPC, the possibility of surface dehydration is eliminated. That avoids cracking and significant degradation of final material properties [42]. Additionally, the surface of constructive joints should be systematically cured so that surface drying and also micro-cracking during setting may be prevented [30].

Heat (90ºC) and steam (RH=95%) treatment may be applied to UHPC to accelerate hydration and enhance final mechanical properties including durability. These treatments are only feasible in precast plant [42]. When comparing compressive strength of UHPC cured at 90ºC (until 7 days) and 20ºC, it was concluded that without heat treatment the compressive strength decreases (≈20%) whereas compressive ductility increases. The UHPC cured at 20ºC, like *in situ* curing conditions, could lead to a more economical and sustainable option. Despite of compressive strength reduction, cast-in-place must be considered so that expenses of both high-temperature curing and pre-casting procedures can be avoided [44].

A study on mechanical properties development [45] at 20ºC, demonstrate that hydration reaction starts after 26h after water addition. This period is denominated of "dormant period" which is longer than in CC and that is governed by high amount of superplasticizer in the mix. Mechanical properties started to develop at approximately 32h after water addition. 7 days after, the UHPC compressive strength reached 140MPa (81% of final strength). This high rate of mechanical properties development on early ages may be advantageous to accelerate the construction process. And finally, 90 days after, the development of mechanical properties practically stopped.

3.3. HARDENED STATE

3.3.1. MECHANICAL PROPERTIES

3.3.1.1. Behavior in compression

The typical compressive strength of UHPC is in the range of 150 to 250MPa. UHPC shows a linear elastic behavior until about 70 to 80 % of the ultimate compressive strength. The scatter of compressive strengths tests results is usually low due to homogeneity of the material [41]. The strain at peak stress for UHPC is approximately 4.4 ‰. Thanks to the fibers, a pronounced descending branch can be developed (Fig.3.2.). Its configuration is influenced by the following aspects [8]:

- Fiber content;
- Fiber orientation;
- Fiber geometry;
- Fiber stiffness (in case of using different fiber types);
- Relation between fiber length and maximum aggregate dimension.

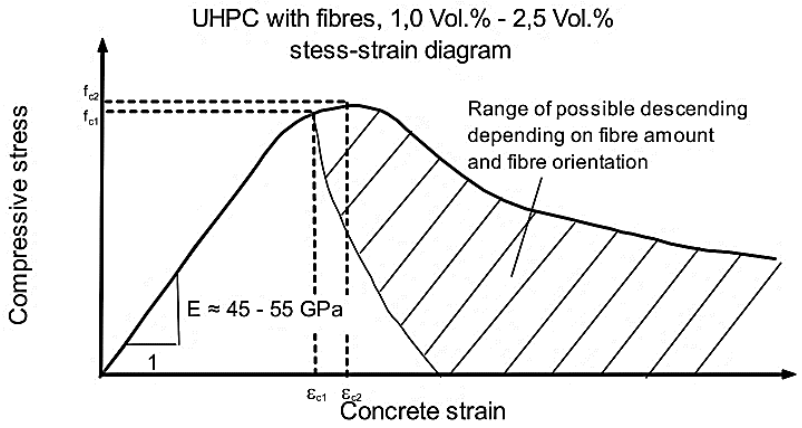

Fig.3.2. - Typical stress-strain-diagrams of UHPC [8].

3.3.1.2. Behavior in tension

Graybeal and Baby [9] characterized uniaxial tensile response of UHPC specimen after a set of direct tension tests (Fig.3.3.). The response can be divided into four phases:

- Phase I - Linear elastic domain;
- Phase II - Multiple tightly spaced cracks occur in the cementitious matrix whereas fibers are bridging those cracks. The cracks occur sequentially whenever the stress overpass the matrix cracking strength;
- Phase III - It occurs crack saturation where additional cracking is unlikely so individual cracks extend;
- Phase IV - Individual crack has reached its extension limit and the fibers bridging that crack begin to pull out of the matrix.

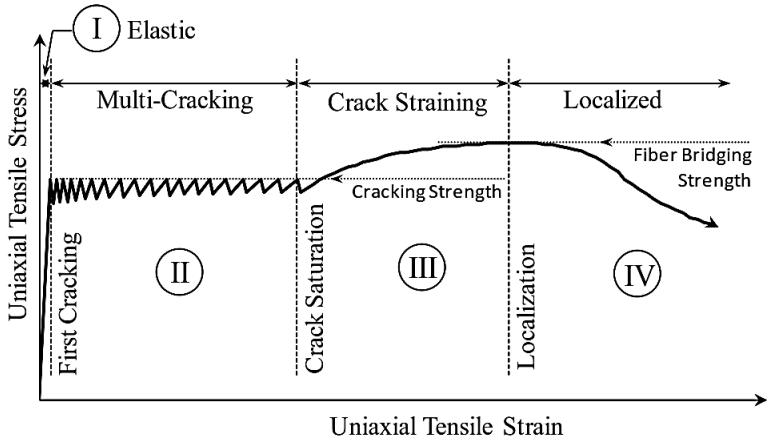

Fig.3.3. - Idealized response of UHPC element subjected to uniaxial tensile force [9].

It is important to mention that only was considered strain hardening behavior which is associated with a limited minimum fiber content and appropriate fiber orientation. Otherwise, neither multi-cracking phase would be possible nor the consequent phases. Therefore, a softening post peak behavior would occur subsequently to phase I.

In their experiments, Graybeal and Baby tested UHPC produced in different curing conditions and with different compositions [9]. The mechanical response results of direct tensile test had the fallowing values:

- First cracking strength from 6 to 9MPa;
- Multi-cracking stress from 7.8 to 11.5MPa;
- Maximum tensile stress from 8.5 to 11.5MPa;
- Strain at crack saturation from 3 to 5.4‰;
- Strain at localization from 3.4 to 6.5‰.

French recommendations [29, 30] identify three different tensile behaviors after cracking for design purpose:

- High strain-hardening which the post-cracking peak is higher than elastic resistance because of high fiber content.
- Low strain-hardening which corresponds to most of the UHPCs currently on the market.
- Strain-softening is characterized by crack localization once the matrix strength is reached, when a tensile force is applied. This type of constitutive law can be found in UHPCs with a low fiber content or containing fibers that are not very efficient.

Additionally, a new French standard [46] gives expressions to classify post-cracking behavior of a given UHPC material from specific tests results.

3.3.1.3. Shrinkage

The shrinkage of UHPC barely depend on humidity and elements dimensions, because it is primarily influenced by endogenous processes [47]. In the case of a heat treatment during the first few hours, shrinkage partly occurs during heat treatment and 550 μm/m total shrinkage is expected for outdoor environment. In the case of heat treatment after the UHPC has hardened, it is considered that there will be no further shrinkage once the treatment is finished. And finally, if there is no heat treatment, to the 550 μm/m for endogenous shrinkage is added the 150 μm/m for drying shrinkage in an outdoor environment [30].

3.3.1.4. Creep

Like CC, creep is mainly influenced by the age of loading, permanent load magnitude and its duration. Heat treatment at early age before or after UHPC has hardened may significantly stabilize creep effects [47]. Indicative values of the long-term creep for UHPC with heat treatment before or after UHPC has hardened, and UHPC without heat treatment normally round 0.4, 0.2, and 0.8, respectively [30].

3.3.1.5. Other mechanical properties

In the Table 3.2. are summarized indicative or recommended values by different countries for predesign calculations. Those values are referred to elasticity modulus (E), poisson´s ratio (ν), thermal expansion coefficient (α), and density (ρ).

Table 3.2. – Usual values elasticity modulus, poisson´s ratio, thermal expansion coefficient, and density.

Country	E	v	α	ρ
	[GPa]	-	[10^{-6} m/m/ºC]	[kg/m^3]
France	45 - 65	0.2	11	2200 - 2800
Japan	50	0.2	13.5	-
Switzerland	45 - 65	0.2	10	-
Australia	50	0.2	-	2400 - 2650

3.3.2. DURABILITY

It has been mentioned that UHPC is very homogeneous concrete thanks to its high packing density and its ultrafine particles. Its dense matrix prevents from being penetrated by aggressive agents. Consequently, durability properties are significantly better than those of CC [9, 30].

Considering the main objective of this study, durability has not an important role and that is why it is not deeper detailed, even knowing that it may assure low maintenance and then life-cycle cost savings. However, these enhanced durability properties have positive influence on UHPC cover thickness by reducing it.

3.4. AFFORDABILITY

It can be seen in the Table 2 that UHPC has not a unique formulation and, therefore, high range of material cost can be expected. UHPC is characterized by its high performance but it comes along with a price which makes it difficult to fight against reinforced CC solutions.

During 2013, there was only one commercial supplier for transportation infrastructure in the United States. That blend was sold for about USD2600/m^3 (≈2000€/m^3 at that time) and it includes not only the raw materials cost and fiber reinforcement but also costs related with production and delivery. It means that UHPC may cost 20 times higher than CC. This discrepancy is justified by proprietary nature, high material cost and high production quality control.

A non-proprietary UHPC was developed with local raw materials which accomplishes compressive strength not lower than 155MPa. This material costs 1110$/m^3 (≈850€/m^3) whose steel fibers (1.5%/volume) cost amounts half of the total material total cost [48]. Moreover, there is a company [49] that claims its UHPC technology is 3 to 4 times cheaper than other regular UHPC commercially available and, the author was informed that the UHPC produced by Dura Technology® costs USD475-500/m^3 in Malaysia.

4
UHPC STANDARDS

4.1. AUSTRALIA

DESIGN GUIDELINES FOR DUCTAL PRESTRESSED CONCRETE BEAMS [15]

Australian guidelines on UHPC are based on a study of the existing literature at that time, research undertaken at University of New South Wales (UNSW) and information gained from the performance of existing UHPC structures constructed overseas. This document emerged in 2000 and it was the first specification concerning UHPC in structural design.

However, this document is only applicable on design of pre-stressed concrete beams manufactured from the Reactive Powder Concrete (RPC) known as Ductal. As result, it addresses a limited material and structural field of application. Where possible, these guidelines are consistent with the limit states design philosophy of Australian Standard for Concrete Structures (AS3600-1994).

Stress-strain curves in compression and tension are provided as well as values for modulus of elasticity, density, Poisson's ratio, creep, and shrinkage. Design guidelines are provided for strength in flexure, shear, and torsion followed by specifications for flexural crack control and deflection at service loads. It is slightly referred issues like resistance to fire and fatigue. It ends with indications for pre-stressing losses and anchorage zones calculations.

The idealized stress-strain curve shown in Fig.4.1. may generally be used for the evaluation of ultimate limit state (ULS). For the evaluation of serviceability limit state (SLS) stress-strain diagram may be regarded as linear.

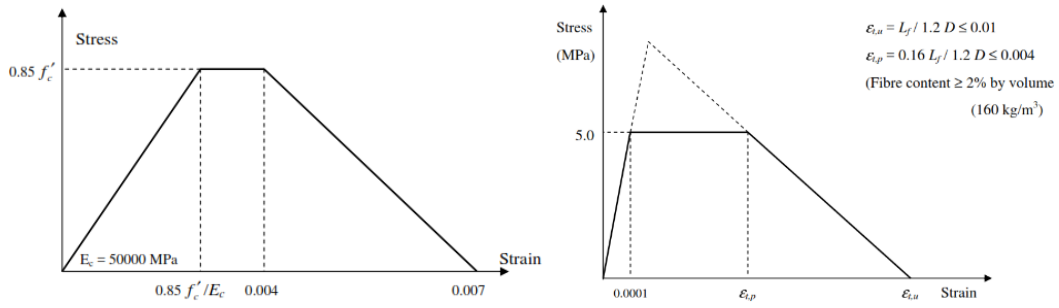

Fig.4.1. - Design stress-strain relationship recommended in Design Guidelines for Ductal Pre-Stressed Concrete Beams: in compression (left) and in tension (right) [15].

Design flexural strength is based on equilibrium of forces and strain compatibility using constitutive laws in compression and tension for UHPC. Ductility is provided by limiting the ratio of neutral axis depth to effective depth (x/d) to a maximum value of 0.4.

Shear strength of the UHPC in beams is based on limiting the principal tensile stress either at the centroidal axis or at the junction of the web and the flange of the cross-section, whichever is the smaller, to a maximum value based on a section uncracked in flexure. Shear reinforcement and pre-stress can contribute to shear strength but steel fibers contribution is not considered.

In this document appendix could be found numerical examples illustrating the behavior of pre-tensioned concrete beams and unreinforced elements are included together with detailed design calculations.

4.2. JAPAN

Recommendations for Design and Construction of Ultra High Strength Fiber Reinforced Concrete Structures (Draft)

Concrete Committee of Japan Society of Civil Engineers (JSCE) established a subcommittee for the research on UHPC in 2003 to publish recommendations for design and construction. The research was based on the results of a technical examination of Sakata-Mirai footbridge and the guidelines from French Association of Civil Engineers. JCSE published UHPC recommendations in 2004 and English version in 2006 [40], which provide basic principles for design and construction [16].

Most of the design values for UHPC are determined through pre-existing Japanese standards for CC or fiber reinforced concrete. JSCE recommendation provides those values that can be used under standard material mix and standard curing conditions (Fig.4.2.).

Components	Mixing ratios (wt.%)
Low-heat Portland cement	33 ~ 45
Silica fume	7 ~ 22
Intermediate materials	10 ~ 24
Aggregate	28 ~ 42

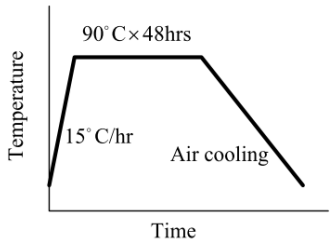

Fig.4.2. - JSCE composition of standard mixed ingredients (left) and conditions of standard heat curing (right) [16].

Constitutive law of UHPC is shown in the Fig.4.3. and is used for ultimate limit state (ULS). For tensile behavior, and based on Association Française de Génie Civil (AFGC) recommendations, it is defined the orientation factor with which it is considered the difference in fiber orientation between test specimens and in the actual structure. Under service loads, stress-strain diagram may be regarded as linear.

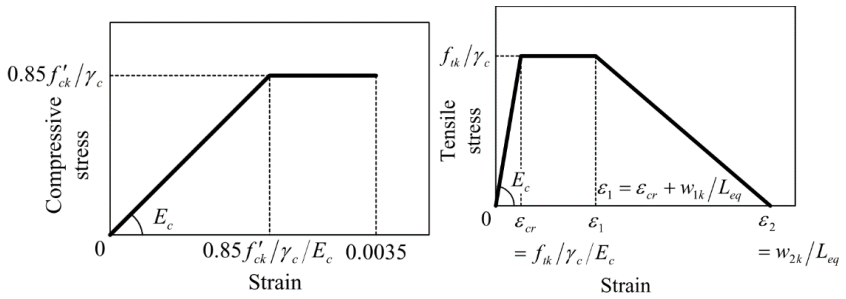

Fig.4.3. - JSCE Compressive stress-strain curve (left) and tensile stress-strain curve (right) [16].

No strain hardening behavior is considered not even steel rebar reinforcement are permitted according to this recommendation. This constitutes a limitation for designers when using this document.

Usual section analysis using the stress-strain curves are performed during flexural design. Identical to French recommendations, shear capacity provided by steel fibers bridging the diagonal crack surface is considered. For verification of serviceability (SLS), tensile stress in UHPC should not exceed the first cracking strength. Determination of tensile stresses induced by flexure, shear force, torsional moment and axial force shall be performed in accordance with the elastic assumption. The following chapters address fatigue resistance, structural details, pre-stressed concrete, durability, construction, and concreting conditions.

4.3. SWITZERLAND

SNR 592052:2016 - *Béton Fibré Ultra-Performant (BFUP) - Matériaux, Dimensionnement et Execution*

This technical specification is based on Swiss Society of Engineers and Architects structure norms and was submitted for consultation in 2014 [47]. In the following year, it was validated by Swiss Society of Engineers and Architects and in 2016 it became effective.

This specification aims to regulate the use of UHPC in the design, construction, and execution of load-bearing structures. It is essentially based on two basic concepts:

- The construction of structures of UHPC elements, generally pre-casted elements, reinforced and/or pre-stressed.
- Rehabilitation and reinforcement of existing structures made of CC. This concept is equally applicable to the construction of new load-bearing structures.

Like many other documents on this subject, this technical specification forwards the designer to proper tests so that UHPC mechanical properties can be assessed. However, ranges of common values for those properties are provided.

The section that addresses structural analysis in ultimate and serviceability limit states is split in two parts. One for UHPC elements with or without reinforcement steel bars, and the other part for UHPC-CC composite elements where UHPC is completely compressed or tensioned.

Constructive detailing for reinforcement, UHPC precast elements and UHPC-CC composite elements are referred. Additionally, execution rules are mentioned regarding fabrication, placement and cure.

This technical report does not deal with the behavior of UHPC load-bearing structures subjected to seismic action, or with punching in the case of slabs.

4.4. FRANCE

4.4.1. RECOMMENDATIONS

Ultra High Performance Fibre-Reinforced Concretes - Interim Recommendations

This recommendation [29] was requested by the *Association Française de Génie Civil* (AFGC) to *Service d'études Techniques des Routes et Autoroutes* and at the beginning of 2002 it was ready to be used. It was elaborated from experience with the first industrial applications, and experimental structures, as well as 10 years of laboratory research. These recommendations are composed of three major chapters:

- Characterization of UHPC;
- Design and analysis of UHPC structures;
- Durability of UHPC.

Ultra High Performance Fibre-Reinforced Concretes – Recommendations

With the Eurocodes entrance came a request from AFGC to elaborate a new version of the previous recommendations due mainly to compatibility reasons. In 2013, the update was made [30] and it comprised the following changes:

- Improves of UHPC characterization and testing methods;
- Structural design methods were totally rewritten respecting design principles of EC2;
- Updated fire resistance and durability performance chapters as well as addition of abrasion resistance topic;
- Implementation of a new chapter about this material in terms of sustainable development.

4.4.2. STANDARDS

Two French standards related to UHPC have been published in 2016. These documents are technically based on the AFGC recommendations that were previously referred. One major aim was to conform with the arrangement of Eurocode 2. This resulted in the consistent elaboration of two documents [6, 46]:

- NF P18-470 essentially concerns about the construction product and it describes test protocol as well as standardized methods to assess material characteristics.
- NF P18-710 is a standard for the design of UHPC structures.
- PR NF P P18-451 is a draft document about UHPC that was not been published yet. Its publication is planned for the 4th quarter of 2017 [50]. It addresses issues related with execution of UHPC structures

NF P 18-470 - Concrete - Ultra-high performance fibre-reinforced concrete - Specifications, performance, production and conformity

In this standard, classes are defined aiming to become UHPC specification easier. Those classes are referred to compressive strength, tensile behavior, workability, thermal treatment, durability characteristics, and resistance to abrasion.

NF P 18-470 gives basic requirements that UHPC has to meet and that concerns mix-proportions, properties of UHPC at the fresh state and properties of hardened UHPC. There are also defined phases of evaluation and validation of UHPC supply along with who is responsible for doing so:

- Evaluation of the conformity of constituents according to this standard;

- Validation of the design study which evaluates conformity to the project requirements;
- Validation of the suitability test based on trial production regarding expected production conditions;
- Validation of the production control of UHPC at both fresh and hardened state.

NF P 18-710 - National addition to Eurocode 2 - Design of concrete structures: specific rules for Ultra-High Performance Fibre-Reinforced Concrete

This standard constitutes a French national annex to EC2 (Part 1 and 2) and it follows the same architecture and content as the EC2. It is given design rules for this material while is indicated the applicability or nonrelevance of clauses of EC2. This way it easy to correlate this new standard with the pre-existing one.

One of the most remarkable changes in the design has to do with the consideration of the tensile contribution of the UHPC due to fibers, not only in serviceability but also in ultimate limit state design and verifications. With that comes a different approach about the minimum required reinforcement ratio which in some cases reinforcement is not even needed.

Considering the high compacity of UHPC, this standard adjusts anchor lengths of reinforcement bars and cover thickness that generally become lower when compared with CC elements.

Contrary to what happens in EC2, this standard does not allow to estimate UHPC mechanical properties as function of compressive characteristic strength. Each mechanical parameter should be estimated through tests described in NF P 18-470. For preliminary design, this norm provides a set of ranges and values for each one of mechanical properties. Moreover, the designer may also use "identity cards" of UHPC from suppliers whose material is well defined due to repetition of production and tests. In order to validate design solution, the mechanical parameters must be determined from trial production as mentioned in NF P 18-470.

4.5. SUMMARY

At this point it is possible to review and discuss what should be the right standard to follow looking forward to structural analysis and design.

Australian and Japanese documents are applicable in very restricted cases. The first is only applicable in pre-stressed beams made from RPC, the second only gives material properties values for a strict cure condition and material mix.

Swiss norm is predisposed for pre-cast elements or reinforcement of existing structures. Besides that, the Swiss norm is a very brief document that despite of addressing several issues, it does not go deep into it.

Finally, France counts with expertise evidences in UHPC matters including regulation. In 2002, France came up with a complete recommendation for that time and which allowed engineers to design bridges like The Bourg-Les-Valence Bridges, Footbridge Seon Yu, and Sakata Mirai Footbridge, already introduced in section 2.2.. Later in 2013, it was updated mainly due conformity reasons with Eurocode 2. In 2016, France provided engineers with a national annex where every issue addressed in Eurocode 2 are also mentioned and review for UHPC applications.

Concluding, NF P 18-710 shows to be the most reliable and embracing UHPC design code. Moreover, this code comes in line with previous French recommendations which had shown practical evidences of their application. That is why NF P 18-710 is the main reference during the case study.

5
PRE-STRESS

5.1. TECHNIQUES

Pre-stressing is an induced and deliberated permanent action in a structure to improve its behavior. It is known that concrete is strong in compression and for design purposes its tensile resistance is neglected. Then, compressive stresses induced by pre-stressing will counteract tensile stresses promoted by external loadings [51]. Several techniques of pre-stressing are available but they may be divided into two major groups: pre-tensioning and posttensioning.

In the first group, the pre-stressing tendons are strained to a predetermined tension and anchored to fixed molds. The concrete is poured around the tendons, cured, and after hardening process the tendons are released. The bonding between the materials allows the concrete to oppose the shortening of the tendons while it becomes compressed.

In the second group, the tendons are strained and anchored after the hardened concrete member has attained sufficient strength. The tendons must therefore be enclosed in ducts which may be either embedded in concrete (internal pre-stressing) or outside of the concrete section (external pre-stressing). In the case of internal pre-stressing, the tendons can be either bonded or unbonded to concrete. The first is achieved by filling the void in the duct with mortar grout whereas the last is achieved by filling it with grease instead of mortar grout. In the case of external pre-stressing, the grout that fills the duct is only a mean of protecting the tendons [51, 52].

Additionally, pre-tensioning technique is frequently used to produce precast concrete elements because it offers a great potential industrialization and the costs of anchors and grouting can be eliminated. Although posttensioning can also be used in pre-cast elements, it may be most useful in cast-in-place construction where bridge girders are too large to be transported [51, 52]. Once the current work is focused in cast-in-place bridges, post-tensioning is the technique which is considered. Internal bonded pre-stressing and external unbonded pre-stressing are detailed in this chapter leaving aside internal unbonded pre-stressing. These two techniques are further ahead involved in the Case Study: *Río Cabriel* Bridge.

5.2. INTERNAL VS. EXTERNAL

5.2.1. TENDON LAYOUT

In internal pre-stressing method, tendons are placed before concrete poring and they remain their position during and after that. Once tendons are thoroughly in contact with concrete element, the pre-stressing equivalent loads are continuously transmitted to it. Then, parabolic layout is usually adopted

for the tendons because that is the most effective way of counterbalance dead loads (Fig.5.1.) and because it does not cause increased constructive effort.

External pre-stressing tendons are not embedded in concrete member but, in case of box girder decks, tendons may be positioned inside the void of the box girder which is assumed for this work. In order to transmit equivalent pre-stressing force to concrete element, tendons are connected to it on its ends and by mean of deviation blocks (Fig.5.1.). In this case, the layout has a polygonal shape due to constructive constrains mainly related to deviators placement.

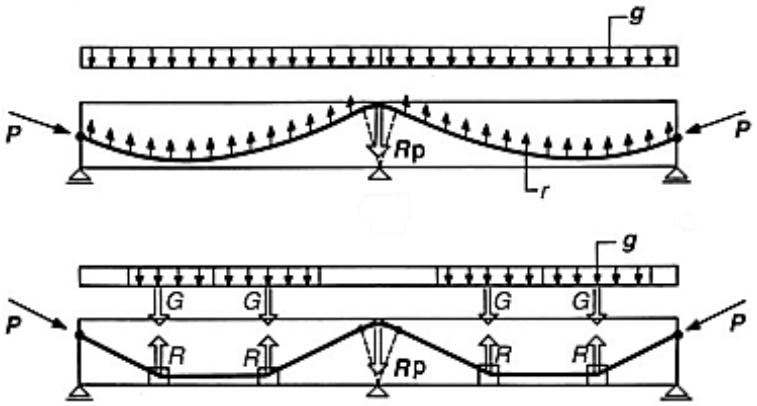

Fig.5.1. - Balancing of the dead load in a two-span beam by internal tendons (above) and external tendons (below) [17]. g = uniform dead load; G = resultant of the dead load; P = pre-stressing force; r = uniform radial forces from pre-stressing; R= radial force from pre-stressing at support; Rp = radial force from pre-stressing.

5.2.2. EQUIVALENT LOADS

Given an infinitesimal segment of pre-stressing tendon, the concrete element actions on this last where:

- dβ – Infinitesimal deviation angle;
- R - Radius of curvature;
- ds - infinitesimal length;
- q* - Concrete load on tendon;
- dP – infinitesimal variation of pre-stressing force.

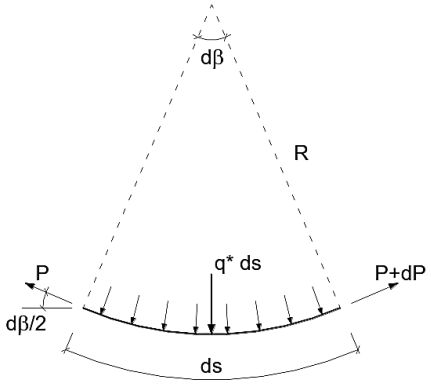

Fig.5.2. - Equilibrium of an infinitesimal segment of pre-stressing tendon [10]

$$ds = R\ d\beta \Leftrightarrow \frac{d\beta}{ds} = \frac{1}{R} = \varphi = curvature$$

Considering a very small deviation angle,

$$\sin\frac{d\beta}{2} \cong \tan\frac{d\beta}{2} \cong \frac{d\beta}{2}$$
$$\cos\frac{d\beta}{2} \cong 1$$

From the vertical equilibrium of forces,

$$\sum F_v = 0 \Leftrightarrow P\ \frac{d\beta}{2} + (P + dP)\frac{d\beta}{2} = q^* ds \overset{dP\approx 0}{\Longleftrightarrow} P\ d\beta = q^*\ ds$$
$$q^* = P\ \frac{d\beta}{ds} \Leftrightarrow q^* = P\ \varphi$$

It is possible to understand that the action of the concrete element on the tendon is proportional to both tendon axial force and how its slope varies (φ). Then, the action of pre-stressing tendons on concrete element is symmetric, opposite direction with the same intensity. So, when a pre-stressing tendon has a parabolic layout, its rotation changes linearly and the curvature is constant. If we assume pre-stressing axial force (P) constant, the equivalent load (q*) would be constant too.

However, in a polygonal layout of a pre-stressing tendon the rotation is constant with discontinuities at deviation blocks. It means that there is no vertical equivalent load in between discontinuities and at the deviation blocks occur a vertical point load (Fig.5.3.).

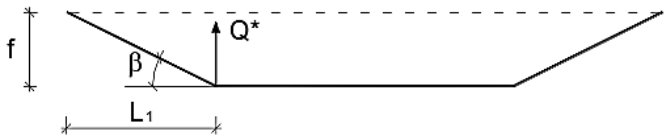

Fig.5.3. - Equivalent load due to a polygonal tendon [10]

$$\tan\beta = \frac{f}{L_1}$$
$$Q^* = P\tan\beta = P\frac{f}{L_1}$$

5.2.3. COMPATIBILITY

In the internal (bonded) pre-stressing technique, before even grouting, the tendon can move almost freely within the duct. After the ducts have been grouted, there is strain combability between the tendon and the surrounding concrete. This means that the tendon strain depends on concrete element curvature at each cross-section.

In case of external pre-stressing, the deformation of the tendons and the concrete element are independent and, consequently, there is movement of tendons through the deviation blocks. The tendon strains are averaged over the length of the tendon and depends on global deformation of the concrete element.

When exists compatibility between materials the stiffness to bending and the resisting bending moment of the element counts with tendons contribution. Otherwise, pre-stressing tendons practically act as only an imposed load.

5.2.4. LOSSES

Both techniques involve short-term losses due to friction, anchorage slip and elastic-shortening. But, friction losses only occur at deviation blocks for external pre-stressing tendons resulting in reduced short-term losses. Long-term losses due to creep, shrinkage and relaxation are inherent to both techniques.

5.2.5. PARTICULARITIES OF EXTERNAL PRE-STRESSING

Most of the times, web thickness design is restricted by constructive constrains related to internal pre-stressing tendons. Therefore, external pre-stressing has been used to reducing the structures weight, essentially by reducing the thickness of the webs [53].

Besides of the differences between internal and external pre-stressing solutions already mentioned which are relevant for a proper analysis and design in the current work, there are other few particular characteristics on external pre-stressing that should be considered during an advanced design stage [54]:

- Better accessibility of tendons;
- Tendons can be replaced without major effort;
- Fatigue advantages due to lower stress fluctuation under live load;
- Issues related with tendons vibration and fretting at the deviation blocks;
- Reduced ductility;
- Concentrated forces at the anchorages and deviation blocks.

6
CONSTRUCTIVE METHODS

6.1. FOREWORD

In this chapter are only addressed constructive methods that, at first, are feasible for cast-in-place bridges, deck at more than 45 m high, and spans with about 70 m long. The cast-in-place solution comprises methods based on ground scaffolding system, movable scaffolding system, balanced cantilever method, and incremental launching. From these four methods, ground scaffolding system starts to be an unfeasible solution for decks at more than 40 m high [13]. The other three methods are conceivable solutions for 70 m long spans. Movable scaffolding system is the one more detailed herein because of its importance on Case Study: *Río Cabriel* Bridge. Balanced cantilever method and incremental launching are detailed enough to understand their constructive particularities, equipments, and impact on internal forces during constructive process. Where relevant, some considerations about internal forces redistribution during time are also taken.

6.2. BALANCED CANTILEVER METHOD

6.2.1. DESCRIPTION AND EQUIPMENT

The construction of bridges with large spans and with decks at high altitude is closely related with this constructive method. The economical range of span lengths for this method goes from 70m to beyond 250m.

The deck is divided into segments whose common length ranges between 3 and 5 m (6 and 7m is also possible) which are sequentially casted outward from pier to form a cantilever structure. Two cantilevers are simultaneously and symmetrically constructed from each pier and the metallic scaffolding is supported by the last segment already casted. A complete sequence of operations to build a segment usually lasts one week and it comprises the following steps:

1. Launching of the balanced cantilever carriage;
2. Leveling of the equipment;
3. Reinforcement and pre-stressing tendons placement;
4. concreting and curing;
5. Tensioning of the pre-stressing tendons and formwork removal.

An important step during construction occurs in the beginning of the cantilever when the advance starts in both pier sides. To overcome that, it is necessary to stablish a provisional scaffolding system supported at each pier side so that the first segments may be casted (Fig.6.1). Without this step, it would not be possible to place the constructive equipment at the top of the pier.

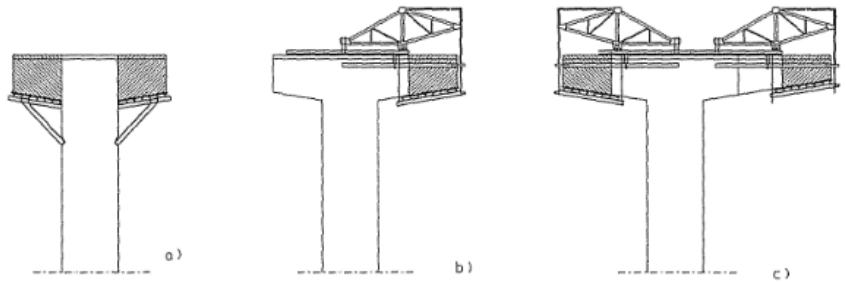

Fig.6.1. - Balanced cantilever method with provisional scaffolding system [13].

However, some advanced systems allow the construction of those initial segments without provisional scaffolding system. A special structural element is used to unify both equipments until the two first segments have been casted. Then, the unifying element is released and the typical constructive sequence starts (Fig.6.2.).

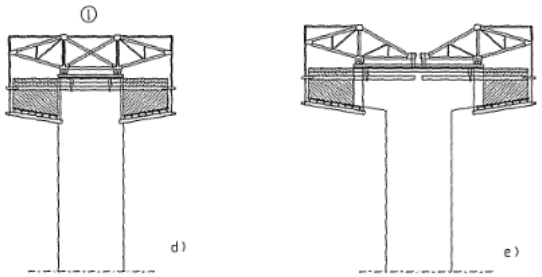

Fig.6.2. - Balanced cantilever method without provisional scaffolding system [13]

6.2.2. IMPACT ON INTERNAL FORCES

In Fig.6.3. is qualitatively illustrated how bending moments change during balanced cantilever method construction. At the end of constructive process all the segments are under negative bending moments by only considering the dead load acting on structure.

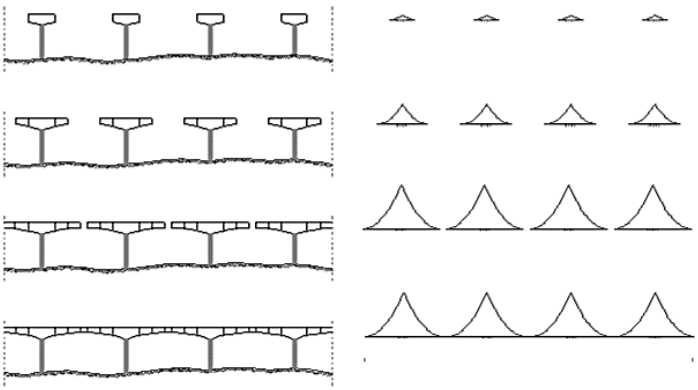

Fig.6.3. - Dead load internal forces resulting from balanced cantilever method [12].

As soon as viscoelastic phenomenon starts to act, internal forces start to redistribute and the bending moments at the end of constructive process (M_0) evolve toward that would exist if dead load was

hypothetically applied after the structure had been ended (M_e). When this phenomenon stabilizes, bending moments diagram (M_∞) lays at an intermediate position between those aforementioned (Fig.6.4.).

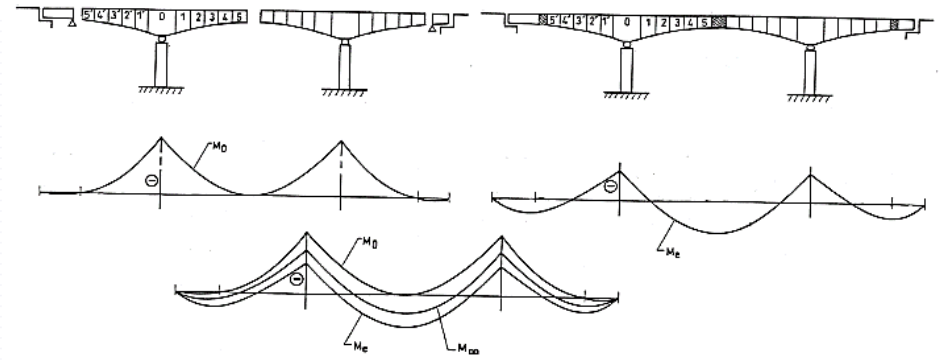

Fig.6.4. - Balanced cantilever method - Dead load internal forces redistribution caused by creep [5]

6.3. INCREMENTAL LAUNCHING METHOD

6.3.1. DESCRIPTION AND EQUIPMENT

This constructive method is recommended for bridges with spans ranging between 30 and 70 m. This method is also restricted to bridges with horizontal lay-out either circular or straight along all its extent. Otherwise it is not possible to coincide bridge deck with piers top. The economic advantage of this method resides on a casting plant stationed at a bridge end where deck segments (15 to 20 m long) are casted and pushed forward by successive displacements by means of hydraulic jacks. Thus, bridge deck travels over all piers top until it reaches the other abutment with no scaffolding system needed.

There is a steel nose at the front of the traveling deck (Fig.6.5.) which has two main purposes. One of them is to reduce internal forces due to the cantilever dead load. The other one is to facilitate the deck to pass over the piers.

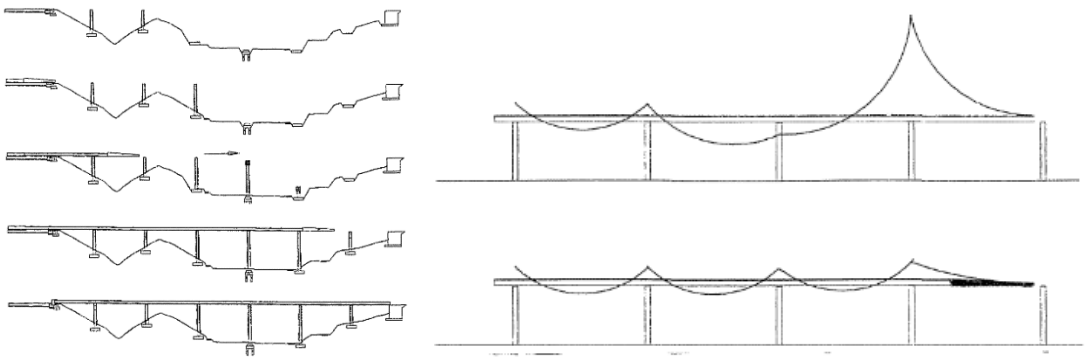

Fig.6.5. - Effect of the steel nose on internal forces during incremental launching [13]

6.3.2. IMPACT ON INTERNAL FORCES

Once that the segments occupy different positions during construction, each cross-section is submitted to changes of internal forces during constructive process (Fig.6.6.). For instance, when it is positioned

at mid-span it is subjected to positive bending moments and when it is positioned at pier it is subjected to negative bending moments.

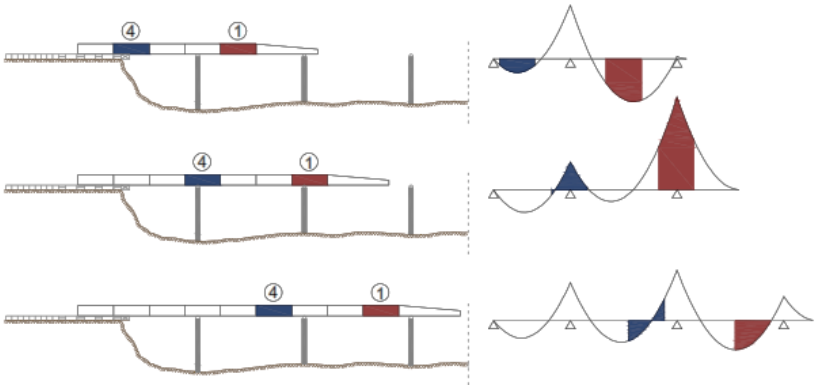

Fig.6.6. - Dead load internal forces resulting from incremental launching method [12].

In Fig.6.7. is represented the bending moments diagram envelope resulting of dead load action during constructive process. This envelope shows how this constructive method can be conditioning for deck design. Besides that, it requires the existence of provisional external pre-stressing to avoid tensile stresses during construction.

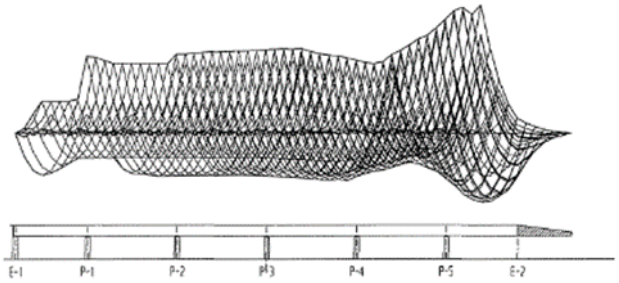

Fig.6.7. - Dead load internal forces envelope resulting from incremental launching method [13].

6.4. MOVABLE SCAFFOLDING SYSTEM

6.4.1. DESCRIPTION AND EQUIPMENT

This is a sophisticated procedure to construct bridge decks *in situ* where scaffolding operations are fully automated. This span-by-span construction system also overcomes limitations inherent to ground scaffolding system related with soil influence and deck height. However, considering its high performance as well as the high investment on it, movable scaffolding system becomes profitable in applications of long bridge constructions. Usually, this procedure has been used to construct bridges with common spans within 30 and 40 m long [13].

Every span construction follows these steps summarized below (Fig.6.8.):

1. Once a span is casted and pre-stressed, each set of beams is released from its support (A) by being lowered slightly with help of vertical jacks;
2. Beams move transversely on the brackets (3) supported by the piers (4). These two steps refer to the transition from a) to b);

3. The scaffolding system slides over the brackets attached to the piers until it reaches the following span;
4. When it has reached its final position, the system is leveled, the formwork (2) is closed, longitudinal beams are supported by the cantilever of the last casted span;
5. Placement of ordinary reinforcement, concreting, curing and pre-stressing procedures.

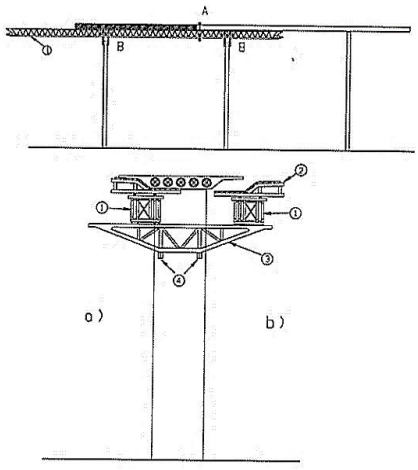

Fig.6.8. - Movable scaffolding system equipment [13].

Movable Scaffolding System (MSS) allows the construction of curved deck bridges but some adjustments must be performed. The space between beams must be such that the curve of the bridge stays inscribed between them. Additionally, the formwork needs to be segmented to fit the curve shape. Precautions should be taken to the deflections of scaffolding system due to their self-weight, that of the formwork and that of the fresh concrete. These deflections must be opposed with a pre-camber.

Recently, the state of the art of this construction method has changed with the Organic Pre-Stressing System (OPS) which is a concept inspired in muscle behavior (Fig.6.9.). It consists in an active control system whose main target is decrease deflections and stresses of scaffolding system during casting process. It is achieved by tensioning external pre-stressing tendons while the load over MSS increases [55].

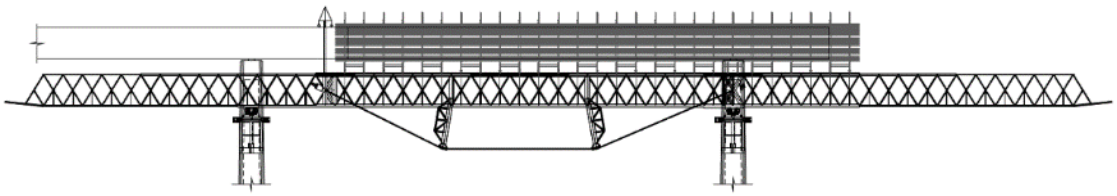

Fig.6.9. - Movable scaffolding system equipped with organic pre-stressing system (OPS).

With OPS implementation is possible to use MSS to cast deck segments with 60m long where the scaffolding system can perform in two ways, under or above the deck. Even more recently, this system has met a new development and now it is possible to cast 90m spans with large movable scaffolding system (LMSS) [56]. These developments on MSS technology have made possible its use on long spans applications while avoiding undesirable loads in the structure during constructive process which would become its use infeasible.

LMSS was firstly used to build the superstructure of *Río Cabriel* Bridge with 70m spans. This equipment (M70-S) is characterized by its "Bowstring" arch behavior where the lower chord is actively controlled by OPS during the concrete pouring stage which prevents the opening of the arch (Fig.6.10.). Consequently, this active control promotes a reduction deformations during the concrete pouring stage, with a maximum mid-span deflection lower than L/2000. However, the cantilever concrete pouring extension has no OPS influence. Yet, its deformations are limited thanks to stiffness provided by the inclusion of two superior passive ties.

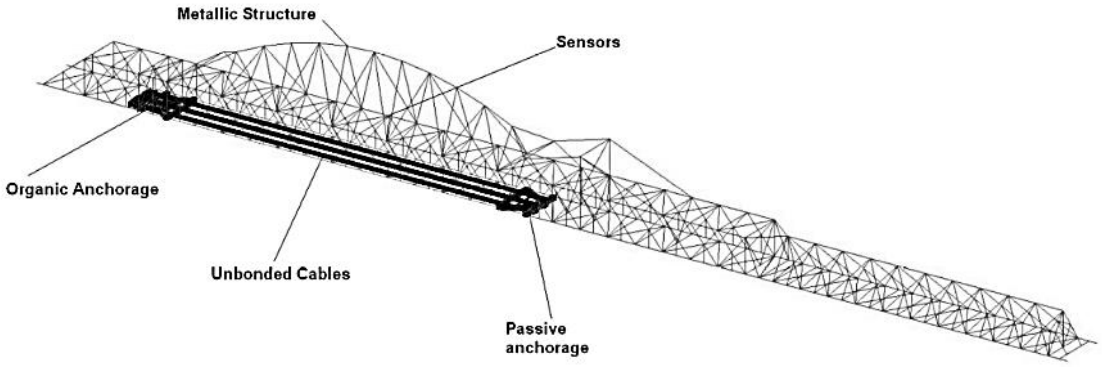

Fig.6.10. - Schematic representation of large movable scaffolding system (LMSS).

Like the regular MSS without OPS, M70-S is supported by the following pier and by the end of previews casted deck during the casting of the following deck segment (Fig.6.11.). Right after the pushing of pre-stressing tendons, formworks move transversely (Fig.6.12.) thanks to a hydraulic system so that all the M70-S can cross the intermediate pier to achieve the next span.

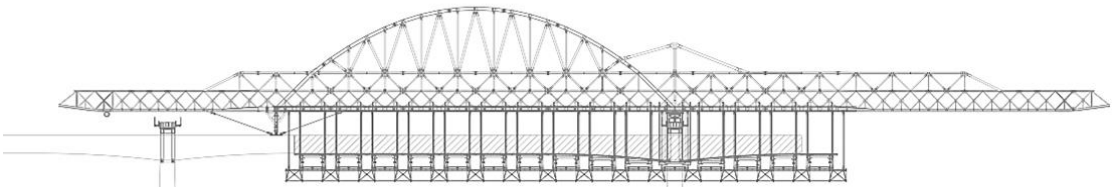

Fig.6.11. - Positioning of the M70-S during casting works.

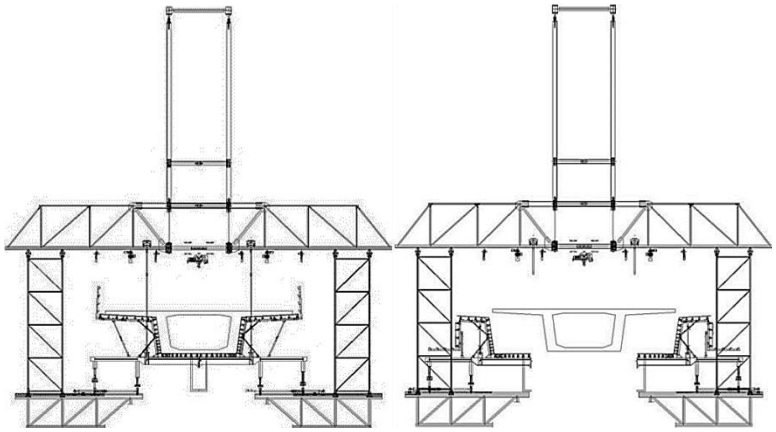

Fig.6.12. - Preparing M70-S for launching by opening formwork system.

In order to launch M70-S to the following span, the rear support is replaced by another one near mid-span, designated by “launching frame” from now on (Fig.6.13.). The main purpose of bringing supports closer is to increase the room for maneuver M70-S. Therefore, the equipment is easily adjustable during launching in curved decks. Then, M70-S starts to move forward until it reaches the front pier where is placed a provisional support (Fig.6.14.). At this point, the rear support is again replaced by a support at the cantilever end, the support at the back pier is also removed. Then, M70-S moves until its final position to start the cycle again (Fig.6.11.).

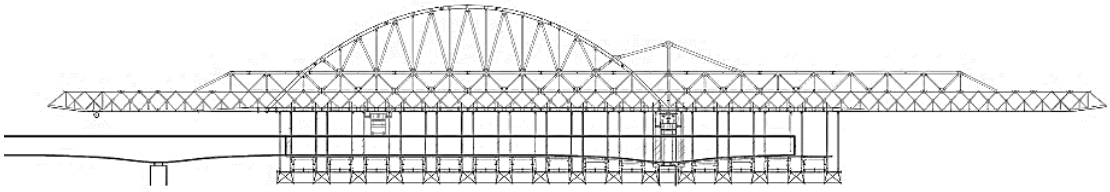

Fig.6.13. - Preparing M70-S for launching by bringing supports closer.

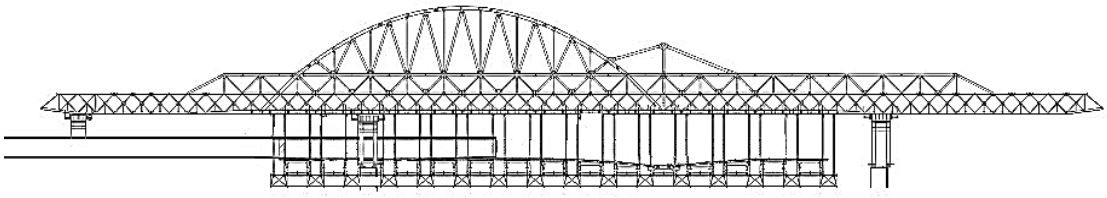

Fig.6.14. - M70-S reaching the support above the pier of the following span.

6.4.2. IMPACT ON INTERNAL FORCES

In order to understand the influence of this constructive method on structural analysis, it is illustrated a simplified scheme where is only considered deck self-weight loading the structure. As can be seen in Fig.6.15., every time that is added a new deck segment its self-weight is also “activated”. This self-weight is applied when occurs formwork removal. The same is applied to pre-stressing loads. Equipment loads during staged construction are relevant and must be considered for limit states verifications.

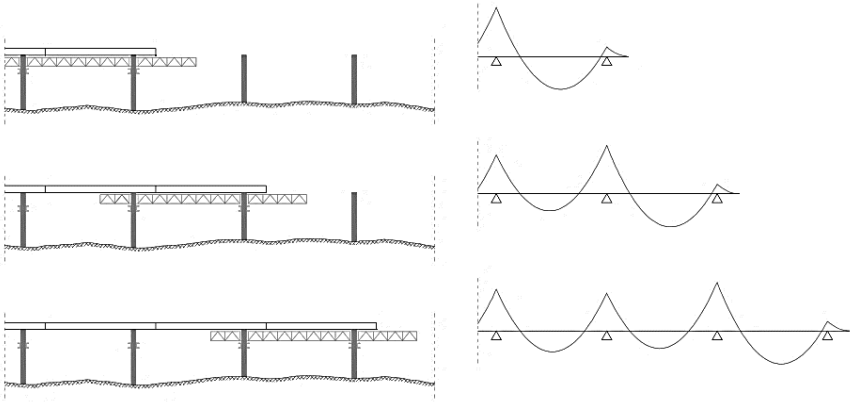

Fig.6.15. - Dead load internal forces resulting from construction with movable scaffolding system (MSS) [12].

After staged construction is ended occurs internal forces redistribution during time. In the Fig.6.16. is illustrated how bending moments diagram changes from built-up distribution (M_0) towards that for monolithic construction (M_e).

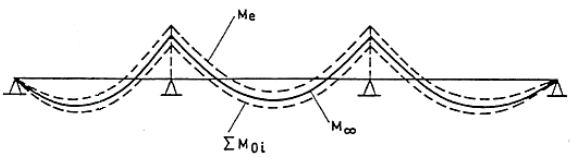

Fig.6.16. - Construction with movable scaffolding system – Dead load internal forces redistribution caused by creep [5].

7

DESIGN PRINCIPLES AND ASSUMPTIONS

7.1. FOREWORD

As already said, the design methods described in NF P 18-710 are based on EC2. Some articles have remained unchanged, some are not applied anymore, and others which have been changed or have been added are thoroughly described. In this chapter, the topics about properties modeling which are relevant for UHPC structural design in the current study are summarized. Some assumptions related to material properties are also detailed because of lack of material characterization data.

Some particularities about structural analysis are also addressed with regard to time dependent effects and box girder beams design.

7.2. MATERIALS

7.2.1. MECHANICAL PROPERTIES

According with what is said in the NF P 18-470 about thermal treatment class, compressive strength class, and tensile behavior class, and due to the lack of that information some assumptions should be done.

The case study is developed considering a field cast procedure, therefore, no thermal treatment neither steam treatment is presumed to be applied. Consequently, the thermal treatment class is "STT". This assumption has direct influence on shrinkage and creep magnitudes, as previously explained in chapter 3.

French norm provides indicative values of UHPC characteristics at 28 days of age. These values are tabulated in the Appendix A.1. in form of ranges. It can be said beforehand that the UHPC material assumed for the case study comprises the minimum values for the strengths (Table 7.1.).

Table 7.1. – Mechanical properties assumed for UHPC during the current study.

Property	Symbol	Value
Elasticity Modulus	E_{cm}	45GPa
Characteristic compressive strength	f_{ck}	150MPa
Mean compressive strength	f_{cm}	160MPa
Characteristic limit of elasticity under tension	$f_{ctk,el}$	7.0MPa
Mean limit of elasticity under tension	$f_{ctm,el}$	8.0MPa

Property	Symbol	Value
Characteristic maximal post-cracking stress	f_{ctfk}	6.0MPa
Mean maximal post-cracking stress	f_{ctfm}	7.0MPa
Fibers length	L_f	16mm
Global fiber orientation factor	K_{global}	1.25
Local Fiber orientation factor	K_{local}	1.75
Thermal expansion coefficient	α_t	11 µm/m/ºC
Crack opening corresponding to local peak	w_{pic}	0.3
Mean post-cracking stress corresponding to a crack with of 0.01H	$f_{ctf1\%}$	4.8MPa

From now on, any time that is intended to refer to this material it will be designated by **UHPC150**, because of its characteristic compressive strength.

7.2.2. CONSTITUTIVE LAW FOR DESIGN

In this section is intended to introduce to the reader the stress-strain relationship in ultimate limit state safety verifications when elements are subjected to bending moments and/or axial forces. Similar stress-strain relationships with average or characteristic values are also provided in French norm to use on serviceability limit state verifications, for instance cracking control, which is not going to be needed in the current work.

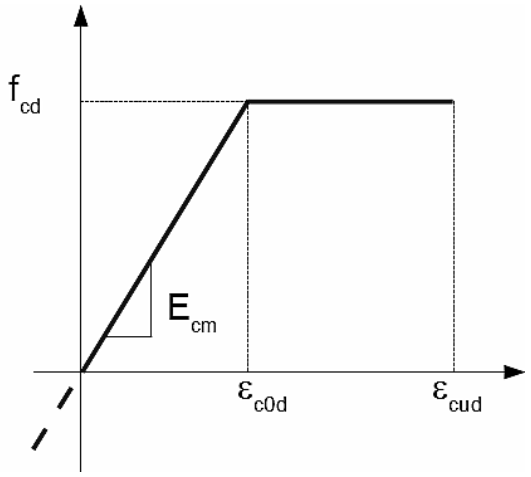

Fig.7.1. - NF P 18-710 Design stress-strain relationship in compression [6].

$$f_{cd}=\alpha_{cc} f_{ck}/\gamma_c \quad (7.1.)$$

$$\varepsilon_{c0d} = f_{cd}/E_{cm} \quad (7.2.)$$

$$\varepsilon_{cud} = \left[1 + 14\ \frac{f_{ctm}}{K_{global}\ f_{cm}}\right]\varepsilon_{c0d} \quad (7.3.)$$

Material constitutive law in tension depends on two aspects:

- Whether it is a thick element or a thin element. There are expressions which classify elements regarding their thickness.
- Tensile behavior class according to NF P 18-470

In the current work the elements are in the domain of the thick elements and with tensile behavior class "T1" (softening behavior). So, the constitutive law in tension comes with the shape illustrated in the image.

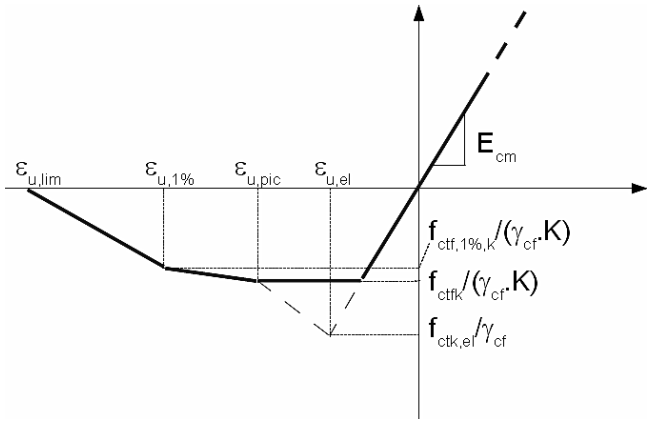

Fig.7.2. - NF P 18-710 Design stress-strain relationship in tension [6].

A safety factor (γ_{cf}=1.3) is introduced regarding manufacturing defects and it is applied to tensile strength of UHPC. The key points of tensile constitutive law are defined in the following equations.

$$\varepsilon_{u,pic} = \frac{w_{peak}}{L_c} + \frac{f_{ctk,el}}{\gamma_{cf}\, E_{cm}} \tag{7.4.}$$

$$\varepsilon_{u,1\%} = \frac{w_{1\%}}{L_c} + \frac{f_{ctk,el}}{\gamma_{cf}\, E_{cm}} \tag{7.5.}$$

$$\varepsilon_{u,lim} = \frac{L_f}{4\, L_c} \tag{7.6.}$$

$$L_c = \frac{2}{3} h \tag{7.7.}$$

With "h" as being cross-section depth. This means that post cracking constitutive law depends not only on the material but also cross-section geometry. Its presence on those formulas is supposed to express the scale effect on tensile constitutive law after crack opening.

How fibers are distributed influence the nonlinear part of the tensile constitutive law. Their distribution depends on the placing method and element geometry. In order to take this into account, a K factor is implemented to correct the tensile resistance in nonlinear behavior. Moreover, K factor may take different values depending on the analysis direction at the same structural point.

In a real design situation, and before implementing the validation process, the designer is allowed to use recommended values for K factor (Appendix A.1.). Then, suitability tests should be carried out to validate those values.

7.2.3. TIME DEPENDENT PROPERTIES

How material strength and stiffness evolve during time has major importance during staged construction analysis. The results achieved by Habel et al. [45] in determining the models of mechanical properties development are used in this study. That paper is based in a proprietary UHPC (CEMTECmultiscale®). The development of the mechanical properties is function of degree of reaction, which in turn is function of time. All specimens were demolded after three days and then water-cured at 20°C until testing. The model of development of the degree of reaction with time comes is in equation (7.8.), thus, any mechanical property "p" studied by Habel et al. can be modeled by the general equation (7.9.).

$$r = \frac{0.038\ (t - 26)}{1 + 0.038\ (t - 26)} \tag{7.8.}$$

$$p(r) = \left(\frac{r - r_0}{1 - r_0}\right)^a \times p(r = 1) \tag{7.9.}$$

Where

- p - Considered mechanical property;
- r_0 - Degree of reaction at the beginning of the strength development, and takes the value of 0.16;
- a - Parameter which depends on mechanical property to be evaluated (Table 7.2.).

Table 7.2. - Values of a-parameter determined by Habel et al. [45].

Mechanical Property	Symbol	a
Elasticity Modulus	E_{cm}	0.8
Mean compressive strength	f_{cm}	1.1
Mean limit of elasticity under tension	$f_{ctm,el}$	2.5

French norm also provides indicative models for creep and shrinkage which are described in the appendix (A.1.). For the parameters whose values come in range form, it is assumed their intermediate values (Table 7.3.).

Table 7.3. – Assumed values to characterize creep and shrinkage based on the suggestions of NF P18-710 [6]

β_{ca}	450 µm/m
β_{cd}	0.005 days/mm^2
β_{bc1}	2
φ_{d0}	35

In the appendix (A.2.) can also be found the diagrams which illustrate UHPC150 time dependent properties during time.

For pre-stressed members, the redistribution of moments and stresses is particularly important for the serviceability limit state design, as it can lead to unacceptable cracking and serviceability stresses, if creep effect is not considered properly. To attend this issue during case study, it was modeled the creep coefficient development during time for each age that concrete is loaded by permanent actions along constructive process. The curve of shrinkage strain along time is also defined. Finally, all time dependent data is inputted on structural analysis software and then it will perform step by step calculation which is the general method mentioned in EN1992-2 for assessment of structural effects of time dependent behavior [57].

7.3. ULTIMATE LIMIT STATE CAPACITY

7.3.1. BENDING

The resistant bending moment and/or axial force are calculated regarding a linear variation of strains. The limits of a strain linear diagram for a given cross-section is different whether it includes reinforcement and/or pre-stress or not. The following images show those limits whether it is plain UHPC element (Fig.7.3.) or not (Fig.7.4.).

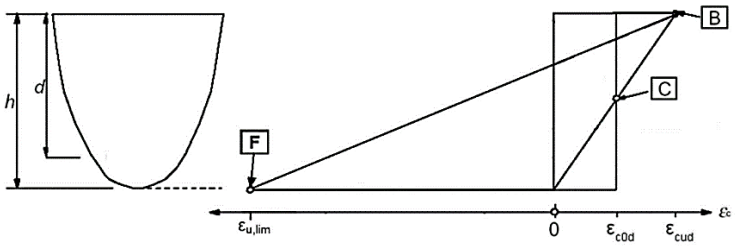

Fig.7.3. - Limit strains diagram in ULS for plain UHPC [6].

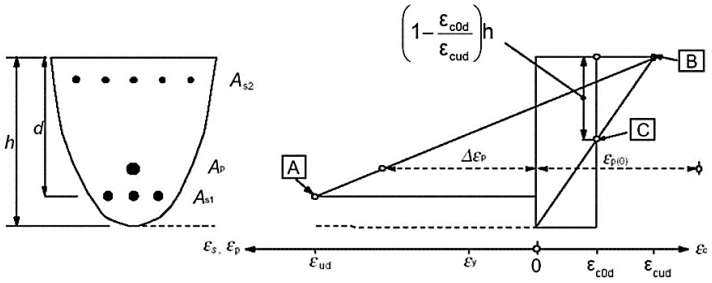

Fig.7.4. - Limit strains diagram in ULS for reinforced and/or pre-stressed UHPC [6].

- A - Reinforcing steel tension strain limit;
- B - UHPC compression strain limit;
- C - UHPC strain limit under pure compression;
- F - UHPC tension strain limit.

An important particularity for this study is that in parts of cross-sections which are subjected to approximately concentric loading (e/h < 0.1), such as compression flanges of box girders, the mean

compressive strain in that part of the section should be limited to ε_{c0d}. This information is relevant because during case study it is dealt with box girder beams where this rule must be applied either for negative or positive bending moments.

Contrary to what is stated in EC2, no minimum flexural reinforcement area neither shear reinforcement is required in UHPC elements. This is justified by the fact that NF P18-710 is only applicable for UHPC materials that fulfill the ductility requirement expressed in equation (7.10.).

$$\frac{1}{w_{0.3}} \int_0^{w_{0.3}} \frac{\sigma_f(w)}{1.25}\, dw \geq max\left(0.4\, f_{ctm,el}\,; 3\, MPa\right) \tag{7.10.}$$

7.3.2. SHEAR

Unlike EC2, NF P 18-710 allows the superposition of shear strength of the UHPC matrix and shear reinforcement. Besides that, a shear strength component due to fibers bridging cracks is considered when determining the total shear strength of a given cross-section as expressed in equations (7.11.), (7.12.), and (7.13).

$$V_{Rd} = min\{V_{Rd,max}\,;\, V_{Rd,c} + V_{Rd,s} + V_{Rd,f}\} \tag{7.11.}$$

$$V_{Rd,f} = A_{fv}\, \sigma_{Rd,f} \cot\theta \tag{7.12.}$$

$$A_{fv} = b_w\, z \tag{7.13.}$$

The equation (7.14.) represents the mean value of the post-cracking stress resistance along the shear crack. The parameter w_u is the ultimate opening of the cracks on the extreme fiber, under the moment and axial force acting in the same cross-section, and is characterized by equation (7.15.).

$$\sigma_{Rd,f} = \frac{1}{K\, \gamma_{cf}} \frac{1}{w^*} \int_0^{w^*} \sigma_f(w)\, dw \tag{7.14.}$$

$$w^* = max\{w_u\,;\, 0.3mm\} \tag{7.15.}$$

Characterization testes should be previously performed in order to know $\sigma_f(w)$. However, it is possible to know $\sigma_f(\varepsilon)$ from recommended values provided by the code. Then, it was assumed that equation (7.14.) would be equivalent to the equation (7.16.), which also gives the mean value of the post-cracking stress resistance along the shear crack. Consequently, with that transformation comes equation (7.17.) and (7.18.). This transformation can be better explained with Fig.7.5., which shows the analogy between domain of integration of crack opening and strains diagram. Furthermore, is also shown the correspondent stresses diagram inherent to those domains. The parameter ε_u is the ultimate strain of the cracks on the extreme fiber. Notice that this simplification is only an assumption of the author, it is not mentioned on French norm.

$$\sigma_{Rd,f} = \frac{1}{K\,\gamma_{cf}} \frac{1}{\varepsilon^* - "\varepsilon_{u,el}"} \int_{"\varepsilon_{u,el}"}^{\varepsilon^*} \sigma_f(\varepsilon)\, d\varepsilon \tag{7.16.}$$

$$"\varepsilon_{u,el}" = \frac{f_{ctfk} / (\gamma_{cf}\, K)}{E_{cm}} \tag{7.16.}$$

$$\varepsilon^* = max\{\varepsilon_u\,;\, \varepsilon_{u,pic}\} \tag{7.17.}$$

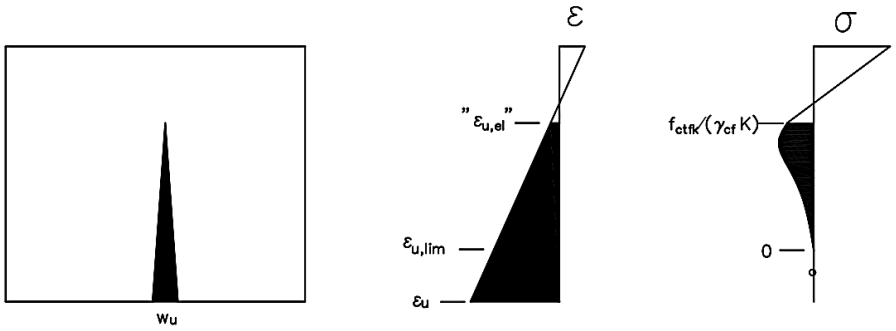

Fig.7.5. – Analogy between crack width-stress diagram and strain-stress diagram.

The UHPC matrix contribution to shear strength is similar to that is described on EC2 and the shear reinforcement contribution is exactly the same as EC2. The shear strength provided by UHPC matrix ($V_{Rd,c}$), depending whether it is a steel reinforced cross-section (7.18.), pre-stressed cross-section (7.19.) or none of them (7.20.).

$$V_{Rd,c} = \frac{0.21}{\gamma_{cf}\,\gamma_E} k\, {f_{ck}}^{1/2} b_w\, d \tag{7.18.}$$

$$V_{Rd,c} = \frac{0.24}{\gamma_{cf}\,\gamma_E} k\, {f_{ck}}^{1/2} b_w\, z \tag{7.19.}$$

$$V_{Rd,c} = \frac{0.18}{\gamma_{cf}\,\gamma_E} k\, {f_{ck}}^{1/2} b_w\, h \tag{7.20.}$$

Where k (7.21.) is a parameter that takes into account the positive effect of compressions usually induced be pre-stressing.

$$k = 1 + 3\frac{\sigma_{cp}}{f_{ck}} \tag{7.21.}$$

When determining the compressed strut strength (7.22.), no positive direct influence provided by pre-stressing is considered, contrary to what described in EC2.

$$V_{Rd,max} = 2.3\ \frac{\alpha_{cc}}{\gamma_c} b_w\ z\ {f_{ck}}^{2/3} \left[\frac{V_{Rd,s}(\cot\theta + \cot\alpha)}{1 + \cot^{\,2}(\theta)} + V_{Rd,f} \tan\theta\right] \cdot \left[\frac{1}{V_{Rd,s} + V_{Rd,f}}\right] \qquad (7.22.)$$

7.3.3. CALCULATION TOOL

A worksheet in Excel was developed aiming to assist ULS sectional analysis. It was useful to avoid repetitive and complex hand calculations considering the complex shape of tensile constitutive law of UHPC. The concept is similar to that used by Yoo and Yoon to predict the flexural behavior of UHPC beams with steel reinforcement [58].

Firstly, the cross-section under analysis is discretized into horizontal layers along its height. For a given neutral axis position (x) and a given cross-section curvature (φ), the strains and stresses at each layer are calculated based on the usual assumption of linear strain distribution (Fig.7.6.). Then, the Solve module on Excel may be defined to iteratively search for the best result for a given objective function, for instance:

- Maximum resisting bending moment for a given axial force;
- Minimum steel reinforcement required for a given solicitation.

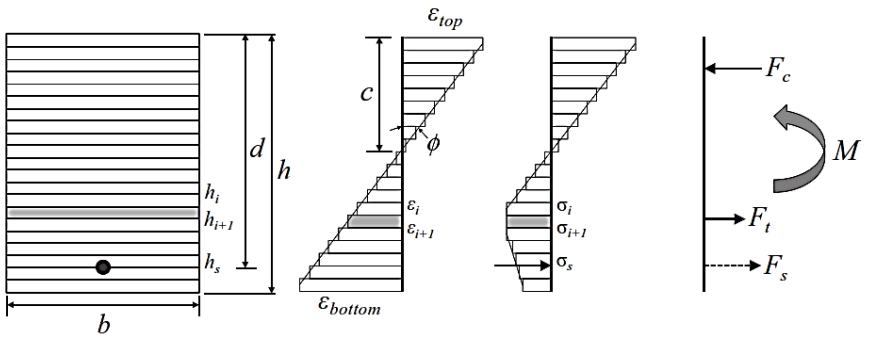

Fig.7.6. - Schematic explanation of stress and strain distributions in cross-section [58].

This operation is always performed with verification of equilibrium condition of external forces and moments with the resulting forces of stress field on materials. At the same time, shear equations use the results from bending analysis to calculate shear strength.

An example (in appendix A.4.) is given for a cross-section geometry with 1 m width and 0.25 m depth and material class of UHPC150 which is supposed to resist 260 kN.m bending moment. It is also possible draw Moment-curvature (M-φ) diagrams just by assuming several curvature values, and ask for the corresponding bending moment that satisfies equilibrium conditions. It may be useful to assess the cross-section flexural ductility.

7.3.4. SHEAR AND TRANSVERSE BENDING

According with what is said in the EN1992-2, the interaction between transverse bending and longitudinal shear in the webs of box girder sections should be considered in the design. That norm guides the designer to annex M where is explained an appropriate method for concrete structures based on “sandwich model”.

In the current work, no interaction will be performed and the webs are supposed only to resist the longitudinal shear force. Moreover, French norm states that that annex is no longer applicable for UHPC and does not come with other alternative methods or expressions.

8

CASE STUDY: *RÍO CABRIEL* BRIDGE

8.1. DESCRIPTION AND GEOMETRY

The case study bridge was constructed in 2009-2010, it is located in Spain (Cofrentes, Valencia), and integrates the national road N-330. It passes over the river *Cabriel* and counts with 8 spans which amounts 520m length. The common span has 70m of length and 11m of width. The highest pier has approximately 45m. The superstructure was built with an overhead movable scaffolding system (MS70-S) as mentioned in chapter 6. It is assumed a structural class S4 and with an exposure class of XC2 or XC3 (inferred from cover thickness).

The horizontal alignment (Fig.8.1.) configures a compound curve with a circular part and two clothoid spiral parts before and after the first mentioned. The minimum radius of curvature is 1170 m and the A parameter of the two spirals are 196.8 and 163.5 m, respectively. For simplicity reasons, and attending to the high value of the curvature radius, a straight line is assumed for the horizontal alignment during numerical calculations. The vertical alignment (Fig.8.2.) is slightly sloped but, again, for simplicity reasons and without induce significant errors, a horizontal straight line is assumed during numerical calculations.

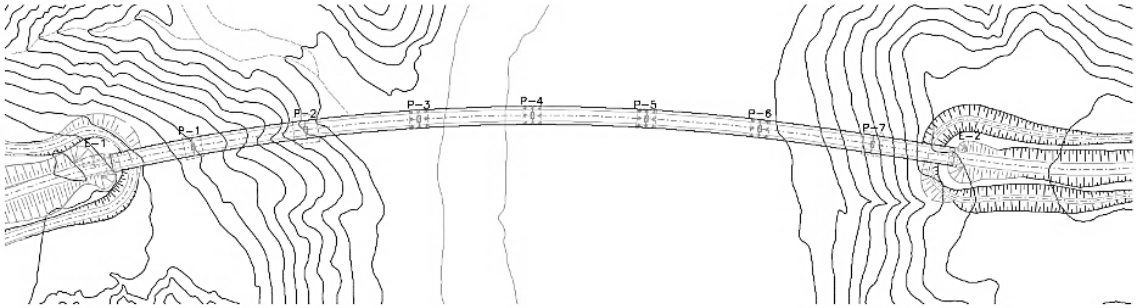

Fig.8.1. - *Río Cabriel* Bridge - Plan view.

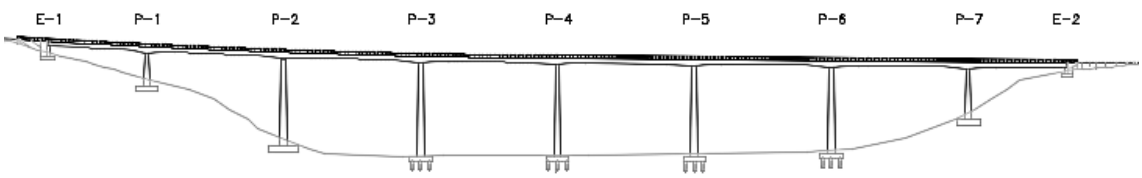

Fig.8.2. - *Río Cabriel* Bridge - Elevation view.

The superstructure is concrete box girder with variable inertia and 11 m width. The girder depth at mid span is 2.5 m (Fig.8.3.) whereas over the piers it reaches 3.47 m (Fig.8.4.). Other geometrical parameters like bottom slab thickness are variable and they are all modeled according to a parabolic variation law. No web thickening to accommodate pre-stress anchorages neither deck superelevation are considered. The diaphragms at the abutments and above the piers are only included in shell numerical models.

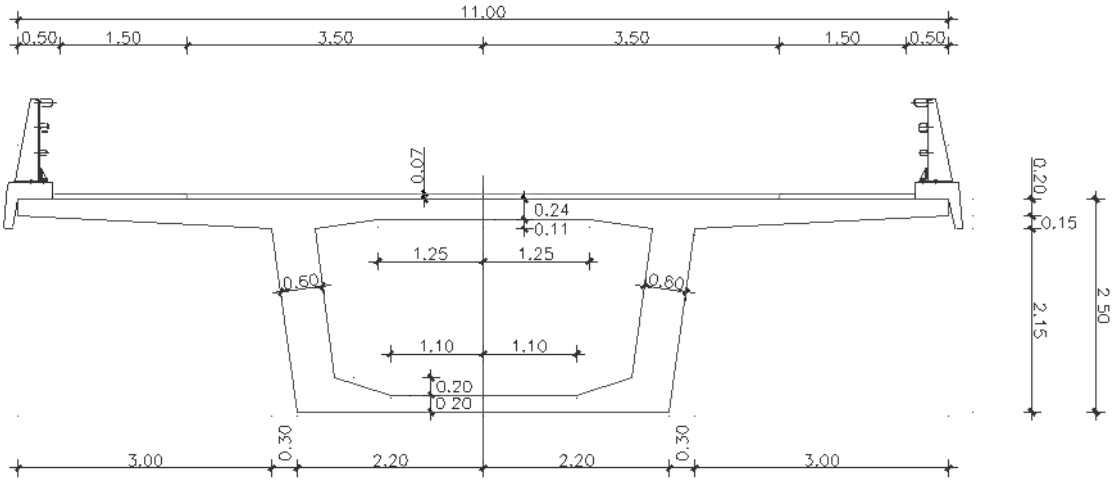

Fig.8.3. - *Río Cabriel* Bridge - Cross-section at mid span

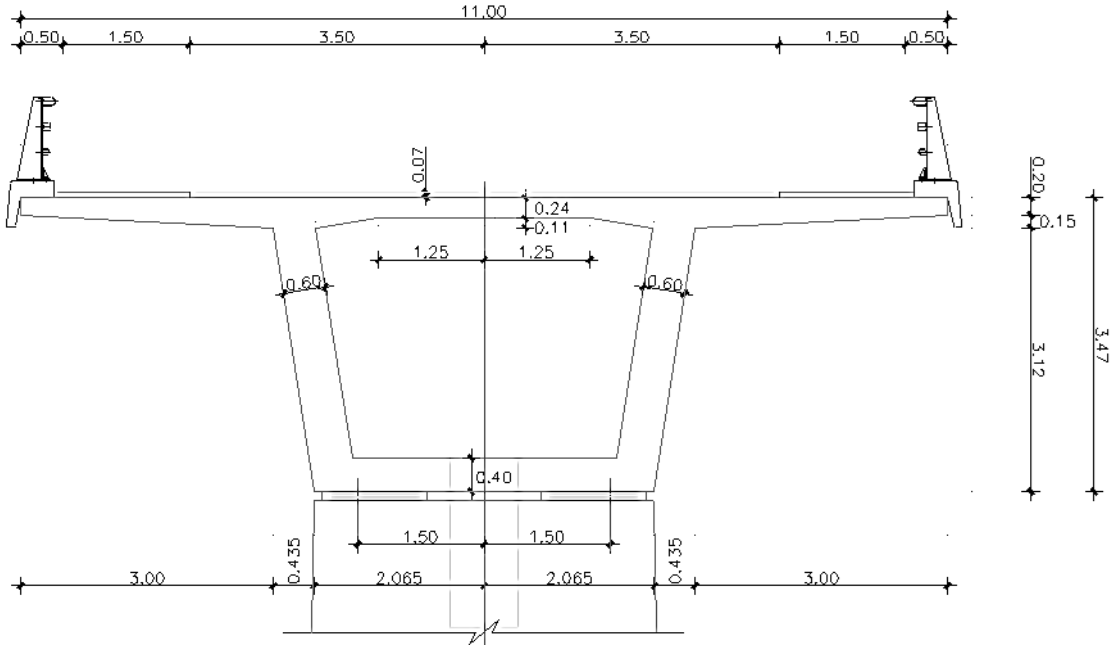

Fig.8.4. - *Río Cabriel* Bridge - Cross-section at above the piers

The abutments (E-1 and E-2) are fixed to the ground and they provide support to the girder by means of elastomeric bearings in the bottom of the girder. The superstructure is also supported by 7 single piers (Table 8.1.) which are non-prismatic elements whose cross-section geometry changes linearly

between its ends (Fig.8.5.). Some piers are supported by pile foundation and others by shallow foundation but all of them are idealized as fixed supports throughout analysis.

Table 8.1. - Characterization of piers' geometry and foundation.

Pier	H [m]	Section		Foundation
		Bottom	Top	
P-1	16.690	a)	b)	Shallow
P-2	44.285	a)	b)	Shallow
P-3	47.247	a)	c)	Piles
P-4	46.137	a)	c)	Piles
P-5	45.982	a)	c)	Piles
P-6	43.331	a)	c)	Piles
P-7	25.686	a)	b)	Shallow

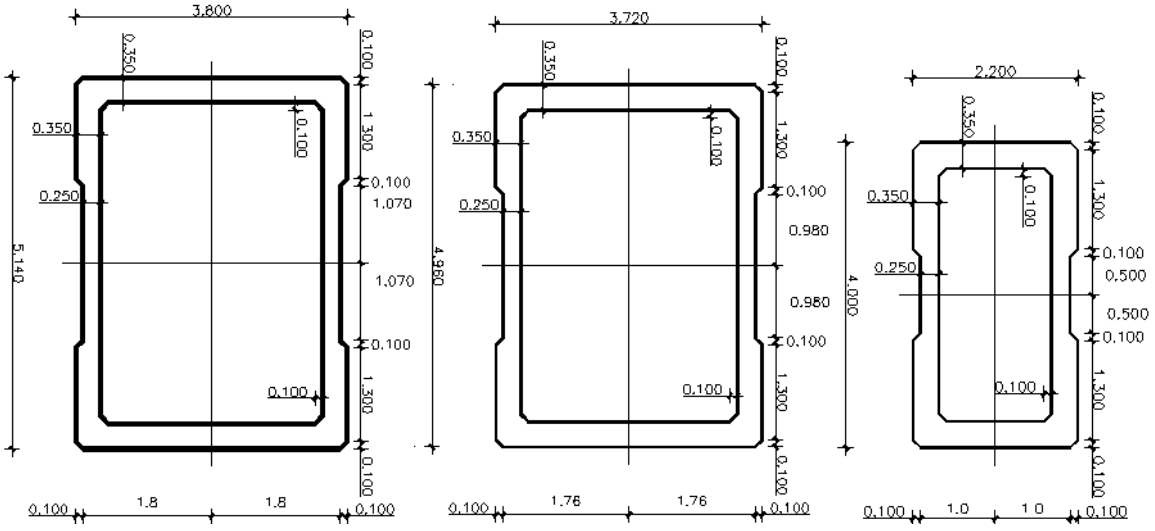

Fig.8.5. - Piers cross-section geometry.

The real pot bearings lay-out is represented in Fig.8.6. However, equivalent single bearings per piers and abutments were modeled as illustrated in Fig.8.7. The rotation about normal to bridge alignment is free for all bearings and the rotation about vertical is free for abutments, P-2, and P-7.

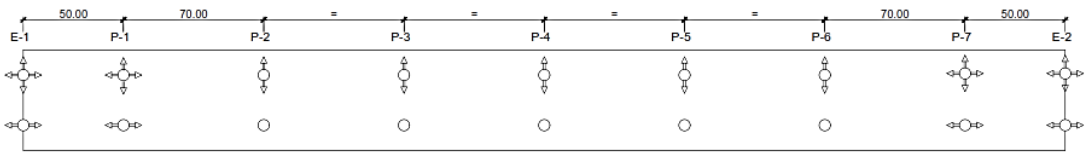

Fig.8.6. - Real pot bearings lay-out.

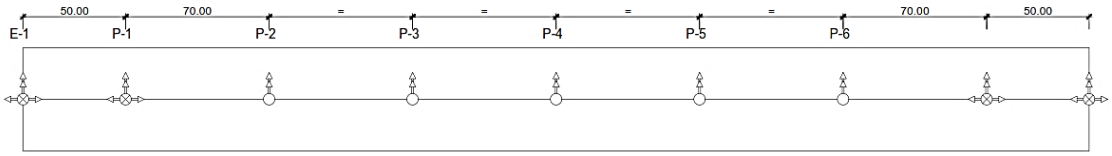

Fig.8.7. - Equivalent pot bearings lay-out.

8.2. LOAD CASES

8.2.1. STAGED CONSTRUCTION

This bridge was built span-by-span with Movable Scaffolding System (MSS), more precisely with the equipment M70-S as previously described. During equipment launching to the following span, its support conditions changes as well transmitted forces to the structure. The load that M70-S transmits to the structure during constructive process is simply modeled as equivalent point loads when and where they are most unfavorable. Furthermore, only loads acting on the deck are considered because loads on the piers have no interest in the current study. Those loads were provided by the company responsible for developing the M70-S, "BERD - Bridge Engineering Research & Design". Each stage of constructive process (Fig.8.8.) comprises the following tasks:

1. Add a new deck segment with its self-weight and add the corresponding pre-stressing tendons with their tensioning force;
2. Remove Concreting Frame (CF = 2545kN ↑);
3. Add Launching Frame (LF = 2600kN ↓);
4. Remove Launching Frame (LF = 2600kN ↑);
5. Add Concreting Frame (CF = 2545kN ↓);
6. Add Concrete Load (CL = 3706kN ↓);
7. Remove Concrete Load (CL = 3706kN ↑) which occurs simultaneously with task 1 of the following stage.

In the appendix A.5. can be found a table where this procedure is sequenced for all the stages until the construction is completed. The tasks are identified with numbers that correspond to the numbering of Fig. 8.8. and they are accompanied by the strength development of UHPC and CC.

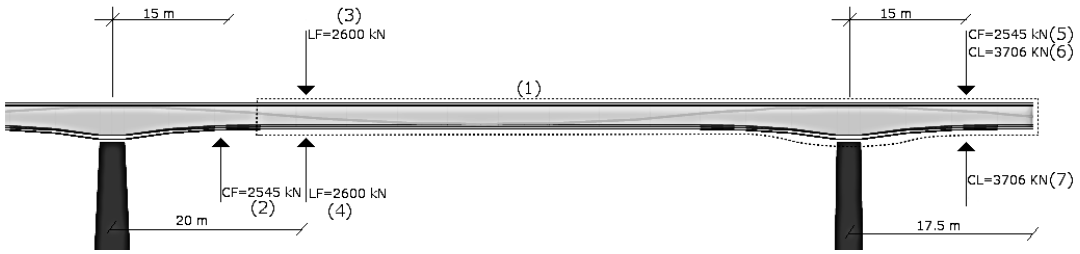

Fig.8.8. - Schematic sequence of tasks which represents M70-S loads on structure during a constructive cycle.

8.2.2. PERMANENT LOADS (G_K)

The specific-weight, either for CC or for UHPC, is assumed to be 25kN/m^3. In Fig.8.9. is illustrated the roadway and where can be seen non-structural elements whose self-weight must be modeled along bridge length. Those elements are:

- 2 parapets
- 2 cornices
- Asphalt layer

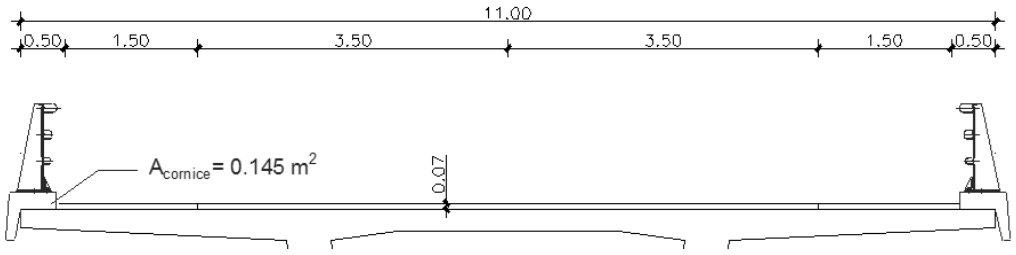

Fig.8.9. - Non-structural elements.

It is considered that asphalt layer has a constant thickness of 7 cm and is bounded by cornice inner edges. Asphalt is inputted as a surface load:

$$q_{asphalt} = 24 \times 0.07 = 1.68 \ kN/m^2$$

Parapet is considered to weight 1kN by linear length and both parapet and cornice are conservatively modeled as a linear load at the overhang ends.

$$p_{parapet} = 1 \ kN/m$$

$$p_{cornice} = 25 \times 0.145 = 3.63 \ kN/m$$

In Fig.8.10 is summarized the RPL locations and values.

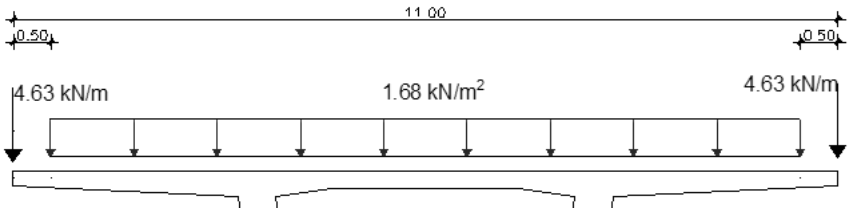

Fig.8.10. - Transverse positioning of the remaining permanent loads (RPL)

8.2.3. TRAFFIC LOADS (TS AND UDL)

Load models defined in EN1991-2 [2], which approaches traffic loads on bridges, should be used for bridges with loaded lengths lesser than 200 m. However, for bridges longer than 200 m is also said these load models result safe-sided. The carriageway width is 10 m and from that results 3 notional lanes of 3 m width each and a remaining area with a total width of 1 m.

The load model for global analysis is the Load Model 1 (LM1) and the class assigned to the bridge is, as suggested by EN1991-2, international heavy vehicle traffic. With these considerations comes a load distribution for global analysis that is similar to the one represented in Fig.8.11.

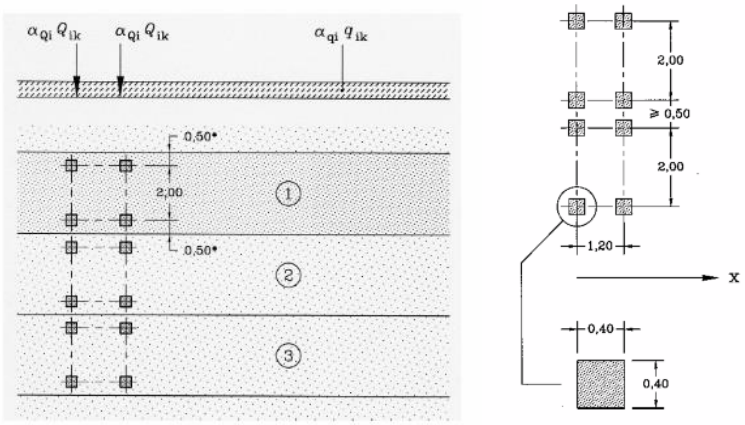

Fig.8.11. - Application of load Model 1 for global (left) and local (right) verifications.

The Tandem System (TS) vehicles are placed side by side to run all deck length such that an internal forces envelope for every TS position may be determined. The uniformed distributed loads (UDL) are properly placed to increase internal forces over the 4th pier and in the mid-span of the odd spans where will appear the most conditioning internal forces. In Fig.8.12. can be found axle loads and UDL used for each lane.

Location	**Tandem system *TS***	***UDL* system**
	Axle loads Q_{ik} (kN)	q_{ik} **(or** q_{ik}**)** (kN/m^2)
Lane Number 1	300	9
Lane Number 2	200	2,5
Lane Number 3	100	2,5
Other lanes	0	2,5
Remaining area (q_{rk})	0	2,5

Fig.8.12. - Load model 1: characteristic values [2].

In order to intensify torsion forces, notional lanes are positioned near the edge of the carriageway with Lane n.1 being the one placed closest to it (Fig.8.13.). Only one axle loads per vehicle are represented.

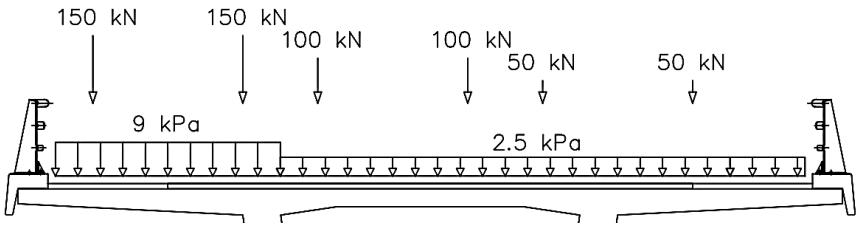

Fig.8.13. - UDL and TS positioning in order to intensify global internal forces.

Tandem system 1 is also used to perform local verifications in a shell model. In this kind of verifications, axle loads must be characterized more realistically with surface loads which represents the contact pressure of the wheels. Besides that, dispersal of the load up to slab middle plan must be considered (Fig.8.14.). It is simply assumed that the slab has constant thickness of 0.20 m. The surface loaded is a square 0.74 x 0.74 m where the point load is now uniformly distributed.

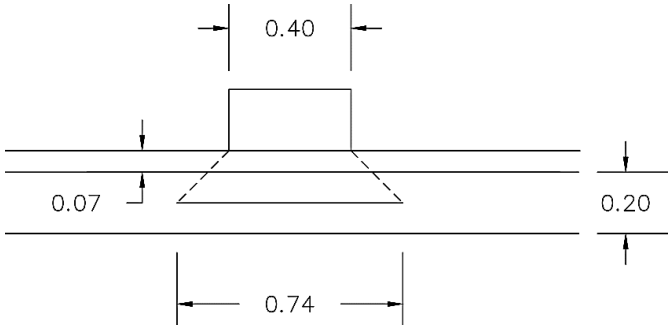

Fig.8.14 - Dispersal of TS loads.

Load arrangement of Fig.8.15. is supposed to, first, maximize shear forces and negative bending moments in the cantilever-slab connection and, second, promote positive bending moments in the inner slab. Fig.8.16. and Fig.8.17. shows to different load arrangement considered to maximize internal forces in the inner slab.

Fig.8.15 – Traffic load arrangement for local verifications 1.

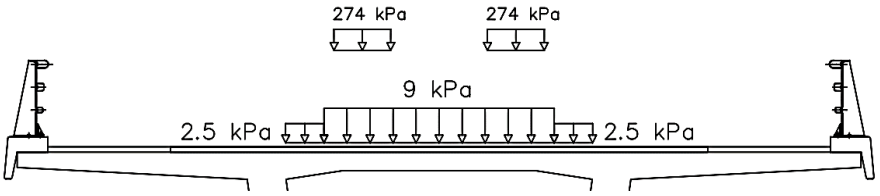

Fig.8.16 - Traffic load arrangement for local verifications 2.

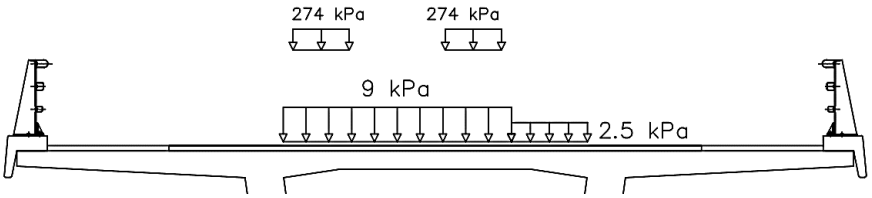

Fig.8.17 - Traffic load arrangement for local verifications 3.

8.2.4. THERMAL ACTIONS (T_K)

The thermal actions can be divided into 4 components (Figure 49):

- Uniform temperature component (a);
- Horizontal temperature difference component (b);

- Vertical temperature difference component (c);
- Non-linear temperature component (d).

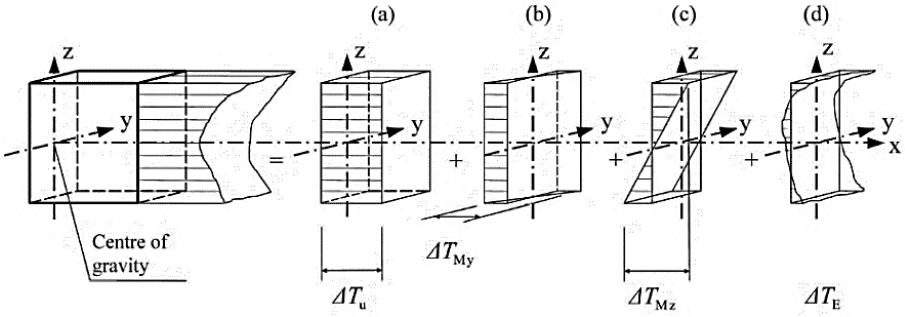

Fig.8.18. - Diagrammatical representation of constituent components of a temperature profile [4]

The component (a) induces a variation in length of the bridge deck which is restrained by the piers. Then, internal forces will appear in the deck and in the piers. It is assumed that thermal actions on the existing bridge can be characterized by NP EN1991-1-5 for Zone A in both winter and summer conditions. Thus, maximum (T_{max}) and minimum temperature (T_{min}) which the bridge will achieve are:

$$T_{max} = 45ºC$$

$$T_{min} = -5ºC$$

And if initial bridge temperature at the time the structure is restrained is:

$$T_0 = 15ºC$$

Then, the characteristic values of the maximum expansion ($\Delta T_{N,exp}$) and maximum contraction ($\Delta T_{N,con}$) range of uniform bridge temperature component are:

$$\Delta T_{N,exp} = 30ºC$$

$$\Delta T_{N,con} = 20ºC$$

For superstructure design purposes, vertical temperature difference component (c) governs the problem by imposing relevant bending moments. NP EN1991-1-5 defines two extreme values for this component, one corresponding to heating and the other corresponding to cooling of the deck [4]. In bridges Type 3 (concrete box girder) with 7 cm of asphalt thickness, vertical temperature difference component (ΔT_{Mz}) comes:

$$\Delta T_{Mz,heat} = 13.2ºC$$

$$\Delta T_{Mz,cool} = 5ºC$$

To model the difference temperature component, the gravity center is assumed 63% of girder depth away from box girder bottom along all bridge length. It is true for mid-span cross-section and almost true near de piers which actually is 57%.

The non-linear component (d) is not included in the approach specified in the national annex of the same norm. Finally, according to NP EN1991-1-5, the combination of actions corresponding to uniform and difference components are the following:

$$\Delta T_{Mz,heat} + 0.8\,\Delta T_{N,exp}$$

$$0.8\,\Delta T_{Mz,heat} + \Delta T_{N,exp}$$

$$\Delta T_{Mz,cool} + 0.8\,\Delta T_{N,con}$$

$$0.8\,\Delta T_{Mz,cool} + \Delta T_{N,con}$$

The characteristic internal forces envelope resulting from these four combinations is referred as being T_k, from now on.

8.3. LOAD COMBINATIONS AND VERIFICATIONS

8.3.1. EXECUTION STAGE

For execution stage, no ultimate limit state (ULS) verifications are performed even though EN1992-2 requires that both ultimate and serviceability limit states (SLS) must be verified during structure execution. However, information about stresses limits to be respected in SLS is not clear. Therefore, the SLS verifications assumed during execution stage are performed by restricting concrete compressive (Eq.8.1.) and tensile stresses (Eq.8.2.). Furthermore, the displacement in the end of the cantilever at the moment of casting of the following segment (see task 6 in section 8.2.1.) is determined. The prediction of this value is important to provide the cantilever with a pre-deflection such that cantilever end may have approximately null deflection right before the following span is casted.

$$\sigma_c \leq 0.6\, f_{ck}(t) \tag{8.1.}$$

$$\sigma_c \leq f_{ctm}(t) \tag{8.2.}$$

Moreover, tensile stresses on pre-stressing tendons are also controlled with Eq.8.3. and Eq.8.4.

$$\sigma_{p,max} \leq \min\left(0.8\, f_{pk}; 0.9\, f_{p0.1k}\right) \tag{8.3.}$$

$$\sigma_{pm0} \leq \min(0.75\, f_{pk}; 0.85\, f_{p0.1k}) \tag{8.4.}$$

The stresses under those restrictions result from nonlinear staged analysis whose loads involved are applied with their characteristic values. Only structure self-weight, equipment loads, and pre-stressing loads are considered. No thermal actions during execution are considered in the analysis.

8.3.2. SERVICE STAGE

The load combinations used for this study came from the most common combinations of actions for road bridges in persistent design situations suggested by Designers' Guide to Eurocode 1: Action on Bridges [59]

These pair of fundamental combination of actions (Eq.8.5.) are used to perform ULS safety verifications on shear and bending strength capacity of cross-sections.

$$E_d = 1.35\ G_k + P_k + \begin{cases} 1.35\ (TS + UDL) + 1.5{\times}0.6\ T_k \\ 1.5T_k + 1.35\ (0.75\ TS + 0.4\ UDL) \end{cases} \tag{8.5.}$$

The characteristic (Eq.8.6.), frequent (Eq.8.7.) and quasi-permanent (Eq.8.8.) combination of actions are used to verify serviceability limited state. All limit states during service stage are performed assuming that has passed enough time to occur all pre-stress losses, thus, pre-stressing effects on the structure (P_k) take into account those losses.

$$E_d = G_k + P_k + \begin{cases} (TS + UDL) + {\times}0.6\ T_k \\ T_k + (0.75\ TS + 0.4\ UDL) \end{cases} \tag{8.6.}$$

$$E_d = G_k + P_k + \begin{cases} (0.75\ TS + 0.4\ UDL) + {\times}0.5\ T_k \\ 0.6\ T_k \end{cases} \tag{8.7.}$$

$$E_d = G_k + P_k + 0.5\ T_k \tag{8.8.}$$

Under characteristic load combination, three conditions related with concrete (Eq.8.9.), pre-stress tendons (Eq.8.10.), and steel reinforcement (Eq.8.11.) must be respected. However, the verification of steel reinforcement stresses may be neglected because it will be studied pre-stressed elements and, consequently, lower tensions on reinforcement will occur. Furthermore, the E.8.11. is useless in unbonded tendons solutions because they barely contribute to element stiffness and as result they do not develop internal forces due to vertical loads. The frequent load combination would be useful during cracking control verifications in case of bonded pre-stressing tendons. However, it is not used because it is adopted external and unbonded pre-stressing solution. Finally, it is required to verify the Eq.8.12. under quasi-permanent load combination.

$$\sigma_c \leq 0.6\ f_{ck} \tag{8.9.}$$

$$\sigma_p \leq 0.7\ f_{pk} \tag{8.10.}$$

$$\sigma_s \leq 0.8\ f_{yk} \tag{8.11.}$$

$$\sigma_c \leq 0.45\ f_{ck} \tag{8.12.}$$

And according to Christian Menn [52], the deflection in bridges should be restricted by the Eq.8.13..

$$\delta < {}^{L_{span}}/_{750} \quad (8.13.)$$

8.4. CASE 0

8.4.1. OVERVIEW

This section aims to introduce the starting point of structural design of the Case 1 and Case 2. Structural analysis is performed to know its internal forces for all load cases and combinations. Additionally, limit states verifications are also performed. In Table 8.2. are defined the materials used in the real project as well their grades.

Table 8.2. – Case 0 - Structural materials.

Material	Structural Element	Grade
Concrete	Substructure	C30/37
	Superstructure	C40/50
Steel	Passive reinforcement	A500 NR SD
	Pre-stress strands	Y 1860 S7

The development of materials properties is modeled for the staged construction analysis. That is only considered for superstructure materials: pre-stress tendons and concrete C40/50. Some assumptions are made to develop concrete model according to EN1992-1-1:

- Cement class: N;
- A mid-span cross-section (Fig.8.3.) (A_c=6.4048m^2 and h_0=345.6mm);
- Outdoor temperature (T) equals to 20ºC;
- Relative Humidity (RH) equals to 60%;
- Several ages of permanent loading for concrete members occur during staged construction;
- Drying shrinkage starts at the time of formwork removal (t_s=3days).

The diagrams illustrating time dependent properties during time can be found on appendix A.3.

Tendon relaxation is internally modeled by the software according to CEB-FIP 90 (unique possibility provided by structural analysis software). The class of relaxation considered is class 2.

8.4.2. PRE-STRESS

From the existing execution project, it was gathered the following information:

- There are 6 pre-stressing tendons per web (Fig.8.19.) and they are tensioned with 6061kN (1397MPa) each;
- There are 31 strands per tendon with 0.6'' diameter which amounts 43.4 cm^2 per tendon;
- The ducts have 120 mm diameter and they are grouted after tensioning, which must occur after concrete reaches a minimum compressive strength of 30MPa;
- The steel has an elasticity modulus of 195GPa and low relaxation effects (Type R-2).

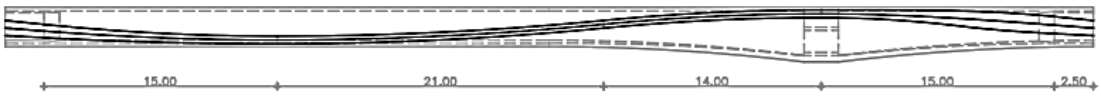

Fig.8.19. - Case 0 - Tendons lay-out per web for a typical segment cast in each stage.

This information is used for structure numerical modeling. Other missing data which is relevant for calculate short-term pre-stress losses are assumed as being:

- Friction coefficient - $\mu = 0.20$;
- Wobble coefficient - $k = 0.01\ m^{-1}$;
- Anchorage set slip - $\Delta s = 5$ mm.

Elastic shortening and long-term pre-stress losses are implicit in the numerical calculation performed by the structural analysis software. These losses are achieved through nonlinear staged construction analysis and providing the materials with time dependent properties definitions (creep, shrinkage, relaxation). This way of proceeding is possible by modeling pre-stress tendons as elements and not as simply loads, otherwise, these losses should be hand calculated and then inputted on software.

If elastic shortening losses were considered, all the single tendons would have to be modeled as also their staged tensioning sequence. For simplicity reasons, elastic shortening losses are not taken into account because it is only modeled one equivalent tendon per web. So, the equivalent tendons are modeled as they had been simultaneously tensioned until they attain 36366kN each (= 6 x 6061kN).

As aforementioned in load combinations during execution stage, is essential to know long-term pre-stressing effects after all losses have occurred. In order to evaluate that, the strategy adopted was the following:

- Add complete structure with 3 days of age;
- Tensioning all pre-stress tendons at the same age (t_0=3days);
- Add permanent loads (dead load and RPL) at the same age (t_0=3days);
- Perform a material non-linear analysis for 50 years;
- Remove permanent loads and output internal forces due to long-term pre-stress effects.

The resulting effects (P_k) at the end of that procedure are used to combine with the remaining effects in each load combination.

8.4.3. RESULTS

The stresses envelope (Fig.8.20.) shows that all spans were under identical maximum stresses. It was expected by knowing that every constructive stage follows the same tasks sequence during constructive process. Consequently, a unique stage of the constructive process may represent all stages so, for instance, 7th stage is analyzed task by task to know if compressive limit stress is respected. It is known that concrete is firstly loaded at 3 days of age but the highest stresses may also occur for higher concrete ages, thus, higher strength.

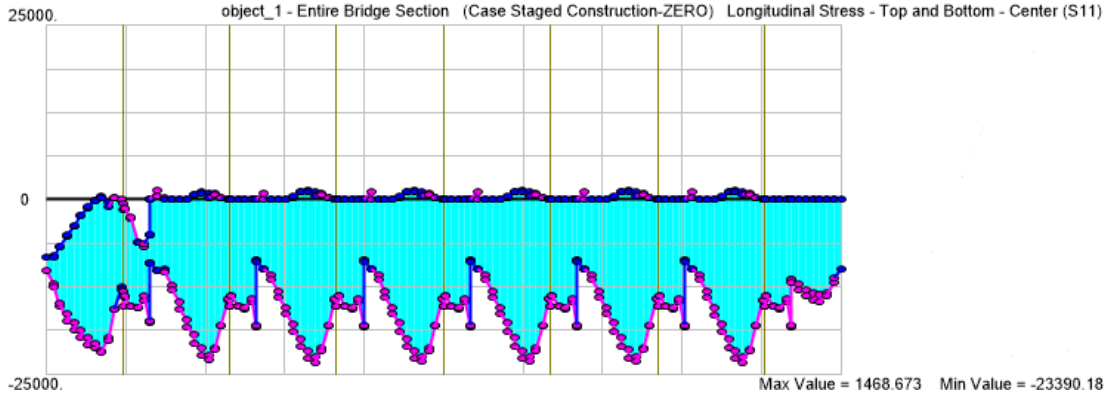

Fig.8.20. - Case 0 - Stresses envelope during constructive process [kPa].

Tensile limit stress is respected (Table 8.3.) during constructive process. Between task 1 and 4 and at the end of the task 6, the compressive limit stress assumed is not respected in the existing bridge. This problem had already been identified in a previous study [60] and the author was informed that this problem was noticed and properly solved before the execution. Additionally, the displacement of the cantilever end is 10.7 cm.

Table 8.3. - Case 0 - Verification of stress limits during constructive process.

Task	t	t_c	Maximum compressive stresses			Maximum tensile stresses		
			Top	Bottom	0.6 $f_{ck}(t_c)$	Top	Bottom	$f_{ctm}(t_c)$
	days	days	MPa	MPa	MPa	MPa	MPa	MPa
1	109	3	14.3	18.2	12.4	-	0.6	2.09
2	109	3	14.2	18.2	12.4	-	-	2.09
3	109	3	14.5	18.2	12.4	-	1.1	2.09
4	109	3	14.2	18.2	12.4	-	-	2.09
5	124	18	10.0	17.3	22.3	-	-	3.29
6	127	21	11.3	23.4	22.9	1.4	-	3.37
7	127	21	10	17.2	22.9	-	-	3.37

Stresses on an equivalent tendon (6 real tendons in a single web) are evaluated right after the tensioning procedure and, then, right after anchorage setting (Fig.8.21.).

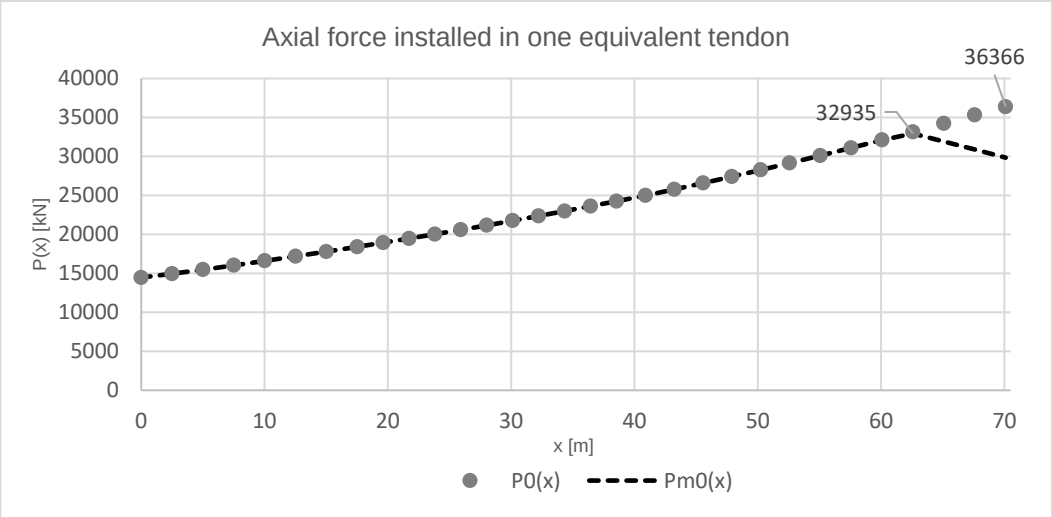

Fig.8.21. - Case 0 - Axial force installed in one equivalent tendon after friction losses (P_0) and anchorage setting (P_{m0}).

$$\sigma_p = \frac{36.366\ MN}{6\times43.33\times10^{-4}\ m^2} = 1399\ MPa\ (< \sigma_{p,max} = 1488\ MPa)$$

$$\sigma_p = \frac{32.935\ MN}{6\times43.33\times10^{-4}\ m^2} = 1267\ MPa\ (\sigma_{p,m0} < 1395\ MPa)$$

The maximum compressive stress installed on concrete under characteristic load combination is 16.1MPa (Fig.8.22.) and it respects the limit defined by the Eq.8.12.. Still in the same load combination, the maximum tensile stress installed in the tendons is 1130MPa which is under the limit defined by equation.

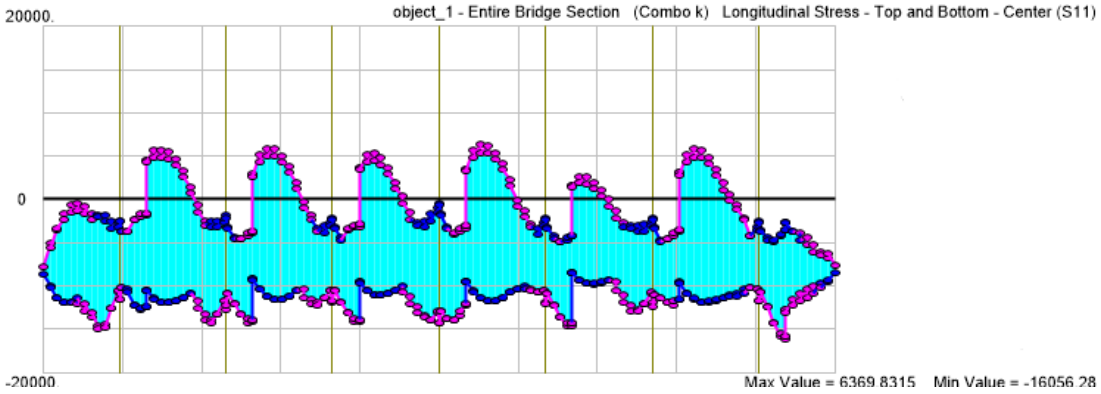

Fig.8.22. - Case 0 - Stresses envelope under characteristic load combination [kPa].

$$\sigma_p = 16.1\ MPa\ (< 24\ MPa)$$

$$\sigma_p = 1131\ MPa\ (< 1395\ MPa)$$

The frequent load combination results show that occurs cracking on the concrete (Fig.8.23.). The crack width should be determined and compared with the maximum admissible. However, it is not relevant for the current work.

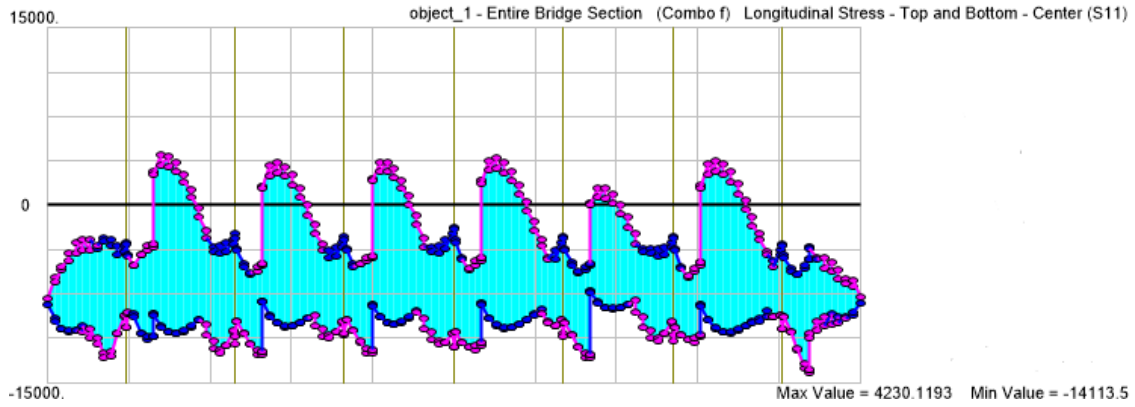

Fig.8.23. - Case 0 - Stresses envelope under frequent load combination [kPa].

The quasi-permanent load combination installs on the concrete a maximum compressive stress of 11.3MPa (Fig.8.24.) which is under the limit imposed by the Eq.8.9.. Furthermore, the decompression restriction under this load combination is not verified. Lastly, the deflection is controlled either in end or inner spans.

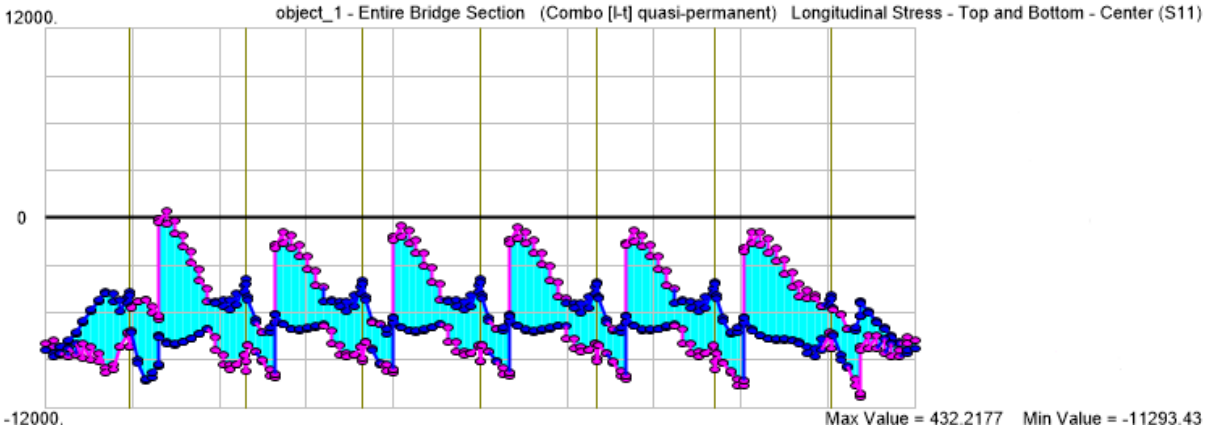

Fig.8.24. - Case 0 - Stresses envelope under quasi-permanent load combination [kPa]

To perform transversal analysis, it is modeled a single representative span with shell elements. In addition to the permanent loads, traffic loads are included and placed in unfavorable positions to aggravate transverse bending moments and shear forces. In Fig.8.25. tries to illustrate the model used and, for instance, it is represented a deformed shape for a fundamental load combination with traffic load arrangement corresponding to Fig.8.15. Additionally, in Fig.8.26. are shown the transverse bending moments used to fulfill the bending moment field for Section 1 on following Table 8.4..

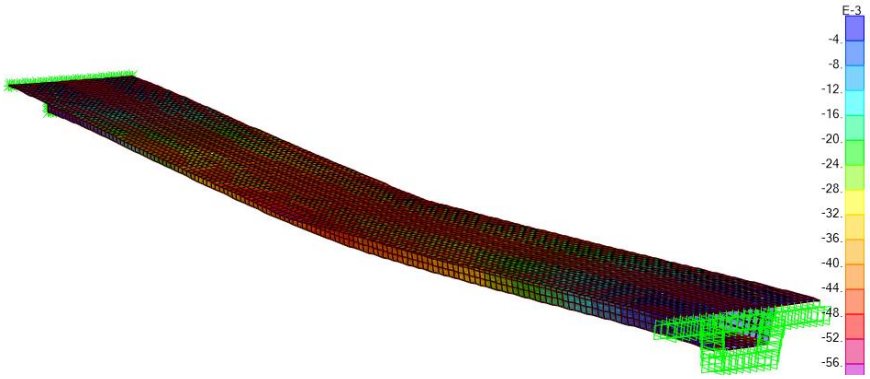

Fig.8.25. - Deformed shape of a representative single span with shell elements under a fundamental load combination.

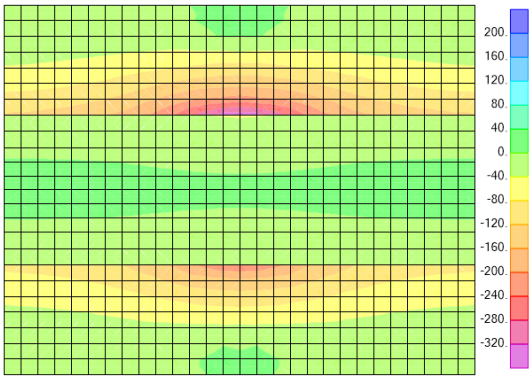

Fig.8.26. - Transverse bending moment at mid-span on top slab under a fundamental load combination [kN.m/m].

So, three different ULS combinations are considered which correspond to the arrangements illustrated in Fig.8.15., Fig.8.16., and Fig.8.17. where traffic load is the leading variable action. The maximum internal forces (Table 8.4.) are calculated for three different places (Fig.8.27.), from now on referred as Section 1, Section 2, and Section 3.

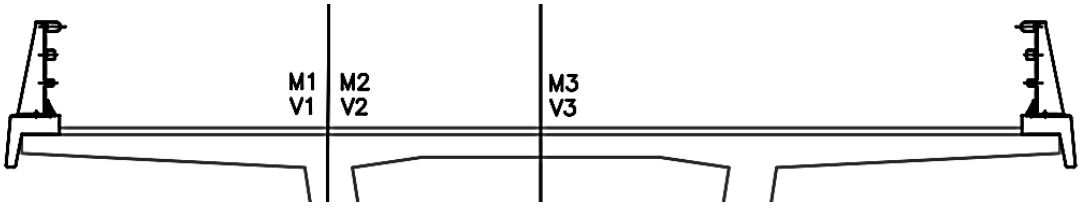

Fig.8.27. - Scheme illustrating where internal forces are measured

Table 8.4. - Case 0 - Local maximum internal forces in the top slab.

Section	1	2	3
M [kN.m/m]	-327	-152	+61
V [kN/m]	294	215	-

Conservatively, these internal forces correspond to maximum local values. However, it would be acceptable to consider a resultant value of, for example, 2-m cut around the maximum value and determine the average internal force per meter. This consideration is valid thanks to slabs capability of transverse redistribution of internal forces. For that case, the maximum internal forces would be that in Table 8.5..

Table 8.5 - Case 0 - Average internal forces along in a 2-m cut around the local maximum internal forces

Section	1	2	3
M [kN.m/m]	-320	-100	+61
V [kN/m]	255	152	-

Now, in the longitudinal direction, the most conditioning internal forces (Table 8.6.) considered for ULS occur near the piers and at mid spans.

Table 8.6. - Case 0 - Most governing global internal forces under fundamental load combination only containing pre-stressing second order effects.

Section	N [kN]	M [kN.m]	V [kN]	T [kN.m]
Above the pier	-	-155657	13724	7450
Mid-span	-	+100128	-	-

The truncated fields correspond to residual values. Notice that these results are based on the consideration that pre-stressing tendons are exclusively considered to contribute to cross-section strength, in ULS, meaning that only second order effects due to pre-stressing are considered acting on the structure.

However, in case of external unbounded tendons, pre-stressing effects can be compared to a simple load and it barely contributes to element strength. So, by considering this point of view, the ULS internal forces on the structure are presented in Table 8.7.. These internal forces contain pre-stressing effects on the structure, both isostatic and second order effects.

Table 8.7. - Case 0 - Most governing global internal forces under fundamental load combination containing pre-stressing effects.

Section	N [kN]	M [kN.m]	V [kN]	T [kN.m]
Above the pier	-45000	-97690	13380	7430
Mid-span	-23267	57715	-	-

The ultimate capacity of the existing structure is also evaluated. Sectional analysis of CC elements is performed with the same method that has been introduced for UHPC elements. Meaning that the worksheet tool addressed in chapter 7 was adjusted to CC design code, EC2. The results are in the following tables. The safety is checked as expected.

Table 8.8. - Case 0 - Bending capacity above the piers.

b_w [m]	A_c [m^2]	x [m]	x/d	ε_s [%]	A_s [cm^2]	ε_p [%]	A_p [cm^2]	ρ [%]	M_{rd} [kN.m]
0.60	8.19	1.11	0.33	0.72	173	0.56	521	0.85	178039

Table 8.9. - Case 0 - Shear capacity above the pier.

$b_{w,nom}$ [m]	$V_{rd,c,i}$ [kN]	A_{sw}/s [cm^2/m]	$V_{rd,s,i}$ [kN]	$V_{rd,max,i}$ [kN]	$V_{rd,i}$ [kN]	$V_{ed,V,i}$ [kN]	$V_{ed,T,i}$ [kN]	$V_{ed,Total,i}$ [kN]
0.48	1824	49	11186	10217	10217	6862	843	7705

Table 8.10. – Case 0 - Bending capacity at mid-span.

b_w [m]	A_c [m^2]	x [m]	x/d	ε_s [%]	A_s [cm^2]	ε_p [%]	A_p [cm^2]	ρ [%]	M_{rd} [kN.m]
0.60	6.40	0.73	0.30	0.83	69	0.67	521	0.11	137711

8.5. CASE 1

8.5.1. OVERVIEW

This chapter aims to describe the process followed for the design of Río Cabriel Bridge with pre-stressed UHPC. In the current study case, the superstructure is supposed to be materialized with UHPC along its length, uniquely. Additionally, the superstructure is modeled with shell elements so that an external pre-stressing solution can also be modeled. Furthermore, shell models do not require adjustments on cross-section shape to include shear-lag effect because shell models can catch that effect during numerical calculation. Finally, two simplified auxiliary models are developed to perform transverse analysis of the cross-section and as well buckling analysis.

An observation about constructive process have to be mentioned. It is reasonable to assume that the load of the fresh concrete that M70-S transfers to the structure may decrease while the cross-section area decreases too. For that reason, that load variation is simply considered directly proportional to the variation of the cross-section area during design.

Along design process, the minimum steel reinforcement necessary to verify safety conditions is calculated for both bending and shear ultimate limit states. Moreover, a constant cross-section is assumed in order to provide an expedite constructive processes. And finally, the substructure remains equal to that in Case 0. The materials grade used for this specific case are in Table 8.11..

Table 8.11. - Case 1 - Structural materials.

Material	Structural Element	Grade
Concrete	Substructure	C30/37
	Superstructure	UHPC150
Steel	Passive reinforcement	A500 NR SD
	Pre-stress strands	Y 1860 S7

8.5.2. PRE-STRESS

How it is already known, UHPC is a high cost material and, in order to reduce its consumption, it is vital to reduce cross-section dimensions. For that reason, and considering the enhanced strength and stiffness of the UHPC, a pre-stress solution with external tendons is assumed to this case study. It is expected to achieve a lighter superstructure by decreasing webs thickness. In addition to diaphragms above the piers, some more diaphragms are modeled at the anchorages and where the tendons deviate so that the pre-stress loads can be effectively transferred to the superstructure. Tendons lay-out are initially assumed having a polygonal theoretical configuration (Fig.8.28.).

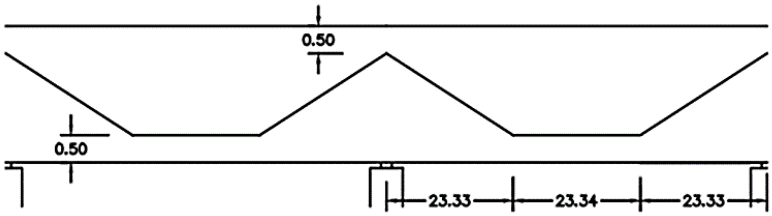

Fig.8.28. - Case 1 - Initial tendons lay-out [m].

Between deviators and anchorages, the tendons are out of section and then they are unbonded. In contrast, the tendons have compatibility of displacements in the deviators and anchorages. However, that has no great impact on superstructure internal forces. Furthermore, the friction between tendons and the deviators are neglected for short-term losses calculation. So, for the current case and Case 2, the following parameters are assumed for the full length of the tendons:

- Friction coefficient - $\mu = 0$;
- Wobble coefficient - $k = 0\ m^{-1}$;
- Anchorage set slip - $\Delta s = 5$ mm.

So, the short-term pre-stress losses occur only due to anchorage set slip and amounts:

$$\Delta\sigma_p = \frac{0.005}{70}\ 200{\times}10^3 = 14.3\ MPa$$

Consequently, the initial pre-stress force is governed by the allowed limit stress after short-term losses (Eq.8.4.) have occurred. Which means the maximum stress during tensioning must be limited to:

$$\sigma_{p,max} = \sigma_{pm0} + 14.3 = 0.75 \times 1860 + 14.3 = 1409.3\ MPa$$

8.5.3. DESIGN

The first step of design process is to calculate top slab thickness through ULS transverse analysis. The internal forces used in the first iteration are in Table 8.4.. The procedure of designing included reduction of slab thickness followed by flexural steel reinforcement design. Remember that an example explaining this procedure is presented in the appendix A.4..

All the solutions (Table 8.12) have sufficient strength to verify safety conditions and they also have enough ductility. Considering the amount of reinforcement and that cantilever self-weight is expected to reduce, solution 3 is selected for Section 1 (Fig.8.27.). The cantilever end remains its actual thickness of 0.20m.

Table 8.12 - Case 1 - First approach to assess minimum slab thickness on Section 1.

	h [m]	x [m]	x/d	ε_s [%]	A_s [cm^2/m]	ρ [%]	$V_{rd,c}$ [kN/m]	$V_{rd,f}$ [kN/m]	$V_{rd,s}$ [kN/m]	$V_{rd,max}$ [kN/m]	V_{rd} [kN/m]
1	0.35	0.06	0.19	0.5	11.2	0.32	532	821	0	4618	1353
2	0.30	0.05	0.19	0.6	18.3	0.61	446	734	0	4191	1180
3	0.25	0.04	0.20	0.8	27.8	1.11	360	628	0	3629	989
4	0.20	0.04	0.26	0.8	43.2	2.16	274	504	0	2875	779

In Table 8.13. are shown some possible solutions for Section 2. For the same reasons stated for Section 1, it was selected the solution 3.

Table 8.13 - Case 1 - First approach to assess minimum slab thickness on Section 2.

	h [m]	x [m]	x/d	ε_s [%]	A_s [cm^2/m]	ρ [%]	$V_{rd,c}$ [kN/m]	$V_{rd,f}$ [kN/m]	$V_{rd,s}$ [kN/m]	$V_{rd,max}$ [kN/m]	V_{rd} [kN/m]
1	0.35	0.03	-	-	0.0	0.00	532	509	0	3425	1041
2	0.25	0.04	0.18	0.5	6.4	0.25	360	564	0	3147	924
3	0.20	0.03	0.19	0.8	14.0	0.70	274	474	0	2691	749
4	0.15	0.03	0.26	0.8	27.6	1.84	189	355	0	1994	543

Finally, 3th solution could be adopted but solution 2 is selected (Table 8.14.) in order to have a constant thickness. Additionally, that solution does not require no steel reinforcement to face positive bending moments. Fig.8.29. illustrates the top slab geometry at this point of design.

Table 8.14 - Case 1 - First approach to assess minimum slab thickness on Section 3.

	h [m]	x [m]	x/d	ε_s [%]	A_s [cm^2/m]	ρ [%]	$V_{rd,c}$ [kN/m]	$V_{rd,f}$ [kN/m]	$V_{rd,s}$ [kN/m]	$V_{rd,max}$ [kN/m]	V_{rd} [kN/m]
1	0.24	0.02	-	-	0.0	0.00	343	291	0	2162	634
2	0.20	0.02	-	-	0.0	0.00	274	357	0	2109	631
3	0.15	0.02	0.19	0.7	5.6	0.37	189	331	0	1835	520
4	0.10	0.02	0.35	0.5	20.3	2.03	103	205	0	1117	308

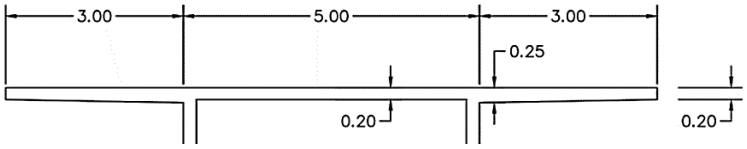

Fig.8.29. - Case 1 - Top slab solution [m].

During longitudinal analysis and design, girder depth is not going to be variable. It is assumed a reasonable value for that which remains constant for all bridge length. It is estimated by relating deck slenderness with existing UHPC box girders. As introduced in the State of the Art, the Batu 6 Bridge spans 100 m with a cross-section depth of 4 m. Whereas PS34 Bridge, with a sectional depth of 1.63 m, spans 48 m. This means that the deck slenderness (length/depth) ranges between 25 and 30. Moreover, those decks have widths of 5 and 4.4 meters, respectively. Another difference, when compared with the case study bridge, is that those decks are simply supported. However, in the case study bridge, the deck has 11 m width and, besides that, is continuously supported which may be an advantage to mid span deflection and maximum bending moment values by reducing them. Considering all just said, a sectional depth of 2.5 is assumed for the design. It means that the deck slenderness is 28.

The bottom slab thickness is initially assumed as being 0.20 m and constant although it may be conditioned by negative bending moments or instability above the piers. During ULS bending calculations, it is conservatively assumed that top slab, including cantilevers, has a constant thickness of 0.20 m.

The internal forces for longitudinal design are in table 8.7.. Firstly, the web thickness is iteratively reduced while both bending (Table 8.15.) and shear strength verify safety conditions (Table 8.16.) in a critical cross-section above the piers. Notice that the shear analysis is made for a single web with the superposition of longitudinal shear and torsion effects. The thinnest web which respects the minimum shear strength is in solution 5.

Table 8.15 - Case 1 - First approach to assess minimum web thickness (flexural reinforcement).

	b_w [m]	A_c [m^2]	x [m]	x/d	ε_s [%]	A_s [cm^2]	ρ [%]
1	0.36	4.86	0.44	0.18	0.9	597	1.23
2	0.30	4.61	0.46	0.19	0.8	605	1.31
3	0.25	4.40	0.47	0.20	0.8	613	1.39
4	0.23	4.32	0.48	0.20	0.8	616	1.43
5	0.22	4.27	0.49	0.20	0.8	617	1.44

Table 8.16. - Case 1 - First approach to assess minimum web thickness (shear reinforcement).

	$V_{rd,c,i}$ [kN]	$V_{rd,f,i}$ [kN]	A_{sw}/s [cm^2/m]	$V_{rd,s,i}$ [kN]	$V_{rd,max,i}$ [kN]	$V_{rd,i}$ [kN]	$V_{ed,V,i}$ [kN]	$V_{ed,T,i}$ [kN]	$V_{ed,Total,i}$ [kN]
1	1756	552	31.9	5183	12787	7491	6690	801	7491
2	1476	470	34.0	5534	10594	7480	6690	790	7480
3	1239	401	35.9	5832	8788	7472	6690	782	7472
4	1144	383	36.5	5942	8075	7469	6690	779	7469
5	1096	373	36.9	5999	7719	7467	6690	777	7467

Additionally, table 8.17. shows the reinforcement solution for mid-span cross-section. This first iteration on cross-section design concludes in the geometry illustrated in the Fig.8.30..

Table 8.17. - Case 1 - Assessment of longitudinal reinforcement at mid-span.

b_w [m]	A_c [m^2]	x [m]	x/d	ε_s [%]	A_s [cm^2]	ρ [%]
0.22	4.27	0.08	0.04	5.2	363	0.85

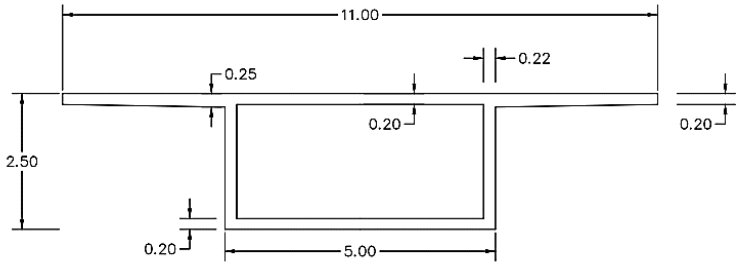

Fig.8.30. - Case 1 - Cross-section solution.

A pre-stress solution still missing before running structural analysis with this new cross-section geometry and material. The pre-stressing force after losses is estimated to avoid cracking under quasi-

permanent combination. This means that tensile stresses are limited to mean limit of elasticity under tension ($f_{ctm,el}$ = 8MPa). Top fiber near the pier and bottom fiber at mid span were subjected to this verification and the pre-stress solution after assuming 25% of total losses is:

- P_{max} = 18151 kN
- A_p= 128.8 cm^2 (92 strands)

With that pre-stress solution the deck remains uncracked in quasi-permanent load combination in both top and bottom fibers. However, the deflection at mid span takes unacceptable values (10.8 cm). The quantity of pre-stress is then governed by deflection limit. With the following quantity of pre-stress, it was possible to reduce mid span deflection to 8.61 which is now acceptable (Eq.8.13.).

- P_{max} = 26833 kN
- A_p = 190.4 cm^2 (136 strands)

Two problems arise during the constructive process. First, the maximum tensile stress on top fibers is not respected (Fig.8.31.). Second, the deflection at the cantilever end, before the tensioning process of the following span, is approximately 20.3 cm for all stages. It is recommended that this displacement may be as lower as possible, but a pre-camber may be foreseen to correct the final position of cantilever end.

The characteristic compressive strength of UHPC at the age of 3 days amounts 84.65MPa, thus, the compressive stress limit during execution is 50.79MPa. When compared with the maximum compressive stress installed during execution (38.3MPa), it is possible to conclude that the compressive stress limit is always respected.

Notice that there is a gap, or discontinuity, in the diagram where exists the constructive joint that connects two adjacent segments which are casted at different times. That gap is exclusively a result from numerical analysis considerations and does not represent the real response of the structure. That happens because the cantilever end has no null deflection, therefore, it is not in the same position where the following segment is added. Consequently, the software forces the continuity of displacements at that joint by bring those adjacent cross-sections together.

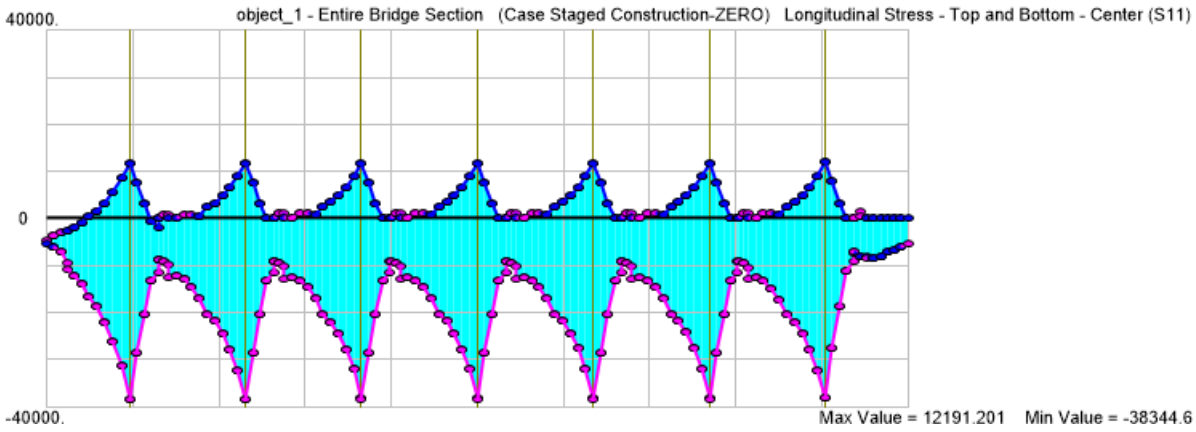

Fig.8.31. - Case 1 - Stresses envelop during constructive process with a polygonal lay-out of tendons [kPa].

To face those issues during constructive process, additional pre-stressing tendons were designed in order to compress and induce a positive bending moment in the cross-section near the piers. The aim is to reduce top fiber tensile stresses during constructive process. At the same time, the deflection at the end of the cantilever is also attenuated. The lay-out of the tendons is schematically illustrated in

Fig.8.32. which includes the additional tendons with a total length of 40.83m. All tendons are considered to be tensioned at the same time. The quantity of the additional pre-stressing is:

- P_{max} = 36765kN
- A_p = 259cm^2 (185 strands)

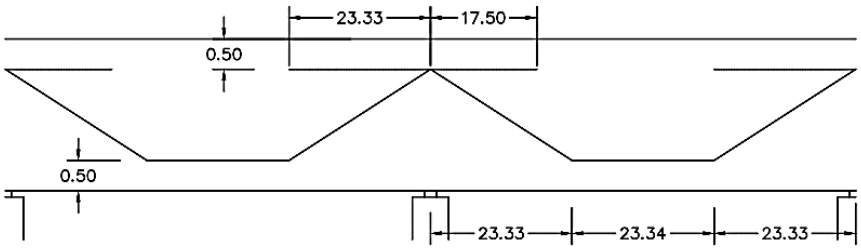

Fig.8.32. - Case 1 - External tendons lay-out [m].

8.5.4. RESULTS

The stresses control during constructive stage is similar with that described in Case 0. As it is shown in Table 8.18., there is no crack formation due to both compressive and tensile stresses. Moreover, the displacement at the end of the cantilever decreased to 14.0cm.

Table 8.18 - Case 1 - Stresses control during constructive stage.

Task	t	t_c	Maximum compressive stresses			Maximum tensile stresses		
			Top	Bottom	0.6 $f_{ck}(t_c)$	Top	Bottom	$f_{ctm,el}(t_c)$
	days	days	MPa	MPa	MPa	MPa	MPa	MPa
1	109	3	19.4	12.3	50.8	-	-	2.18
2	109	3	18.2	12.3	50.8	-	-	2.18
3	109	3	20.0	12.3	50.8	-	1.0	2.18
4	109	3	14.4	26.7	50.8	-	-	2.18
5	124	18	14.4	26.7	87.3	-	-	7.47
6	127	21	14.6	41.0	88.4	2.8	-	7.68
7	127	21	14.4	26.7	88.4	-	-	7.68

NF P 18-710 does not require decompression verification for UHPC elements with unbonded tendons and it only defines the maximum crack opening during quasi-permanent load combination. However, the strategy is to avoid crack opening by limiting tensile stresses installed on structure. Therefore, no crack opening calculations are necessary. Additionally, compressive limits (Eq.8.9.) are respected for the quasi-permanent load combination either in the bottom and top fibers (Fig.8.33.). Furthermore, the mid span deflection was reduced to 5.7cm.

The maximum stress installed in the tendons is 1200MPa and is under the limit admissible in characteristic combination of loads (Eq.8.10.). Besides that, in the characteristic load combination,

longitudinal cracking is avoided because compressive stresses (Fig.8.34.) are under the compressive stress limit (Eq.8.12.).

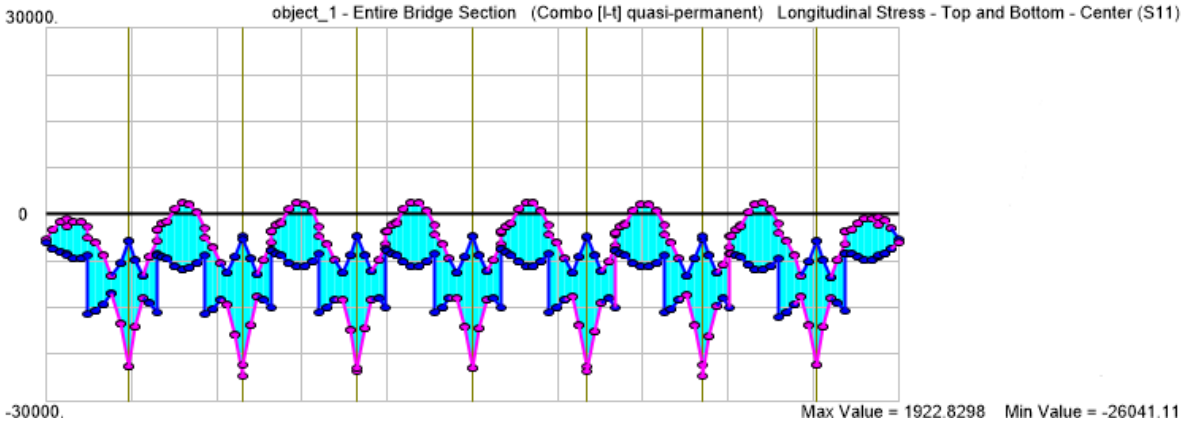

Fig.8.33. - Case 1 - Stresses envelope under quasi-permanent load combination [kPa].

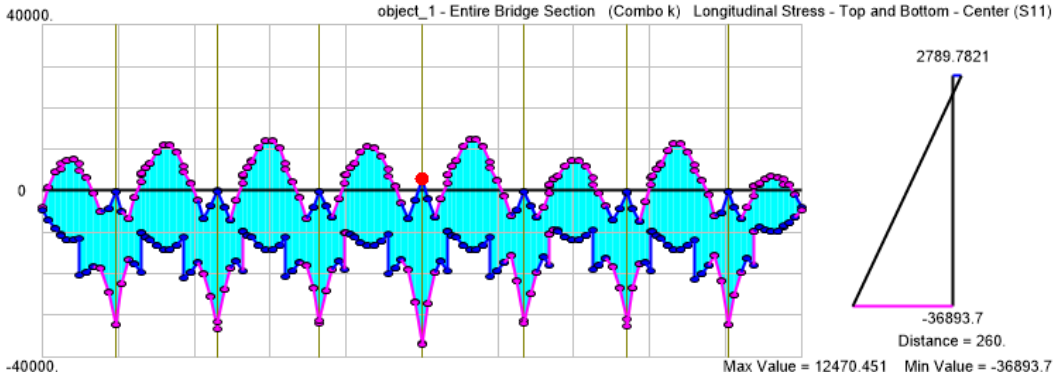

Fig.8.34. - Case 1 - Stresses envelope under characteristic load combination [kPa].

Then, it is described the ultimate limit state verifications and reinforcement design, first, in transverse direction followed by longitudinal direction. The maximum internal forces with the updated slab thickness have changed and are described in the Table 8.19..

Table 8.19. - Case 1 - Local maximum internal forces in the top slab.

Section	1	2	3
M [kN.m/m]	-260	-127	+79
V [kN/m]	223	203	-

In Section 1, the slab thickness of 0.25 m leads to an acceptable reinforcement solution (Table 8.20.) and also respects shear strength (notice, that this solution is the one that was used as practical example in the Appendix A.4.). For the top inner slab, the thickness of 0.20 m leads to a satisfactory solution to stand negative bending moments (Table 8.20.) but, the lower quantity of reinforcement to face positive bending moment suggests that slab thickness could be reduced at mid-span of top slab (Table 8.22.). However, no more optimization is going to be performed.

Table 8.20. - Case 1 - Local verification of Section 1

h [m]	x [m]	x/d	ε_s [%]	A_s [cm^2]	ρ [%]	$V_{rd,c}$ [kN/m]	$V_{rd,f}$ [kN/m]	$V_{rd,s}$ [kN/m]	$V_{rd,max}$ [kN/m]	V_{rd} [kN/m]
0.25	0.04	0.19	0.78	19.6	0.78	360	611	0	3511	972

Table 8.21. - Case 1 - Local verification of Section 2

h [m]	x [m]	x/d	ε_s [%]	A_s [cm^2]	ρ [%]	$V_{rd,c}$ [kN/m]	$V_{rd,f}$ [kN/m]	$V_{rd,s}$ [kN/m]	$V_{rd,max}$ [kN/m]	V_{rd} [kN/m]
0.20	0.03	0.18	0.70	10.0	0.50	274	465	0	2611	739

Table 8.22. - Case 1 - Local verification of Section 3

h [m]	x [m]	x/d	ε_s [%]	A_s [cm^2]	ρ [%]	$V_{rd,c}$ [kN/m]	$V_{rd,f}$ [kN/m]	$V_{rd,s}$ [kN/m]	$V_{rd,max}$ [kN/m]	V_{rd} [kN/m]
0.20	0.03	0.18	0.52	2.3	0.11	274	426	0	2351	701

Table 8.23. contains the governing internal forces for global verifications.

Table 8.23. - Case 1 - Most governing global internal forces under fundamental load combination.

Section	N [kN]	M [kN.m]	V [kN]	T [kN.m]
Above the pier	-52000	-98700	10950	8415
mid-span	-22140	66000	-	4500

The solutions in the tables bellow fulfill safety requirements. Those internal forces lead to feasible solutions of longitudinal reinforcement above the piers (Table 8.24. and Table 8.25.) and also in the mid-span (Table 8.26. and Table 8.27.).

Table 8.24. - Case 1 - Assessment of longitudinal reinforcement at above the piers.

b_w [m]	A_c [m_2]	x [m]	x/d	ε_s [%]	A_s [cm^2]	ρ [%]
0.22	4.27	0.61	0.26	0.6	577	1.35

Table 8.25. - Case 1 - Assessment of shear reinforcement above the piers.

$V_{rd,c,i}$ [kN]	$V_{rd,f,i}$ [kN]	A_{sw}/s [cm^2/m]	$V_{rd,s,i}$ [kN]	$V_{rd,max,i}$ [kN]	$V_{rd,i}$ [kN]	$V_{ed,V,i}$ [kN]	$V_{ed,T,i}$ [kN]	$V_{ed,Total,i}$ [kN]
1126	493	29.1	4737	7809	6355	5475	880	6355

Table 8.26. - Case 1 - Assessment of longitudinal reinforcement at mid-span.

b_w [m]	A_c [m_2]	x [m]	x/d	ε_s [%]	A_s [cm^2]	ρ [%]
0.22	4.27	0.09	0.04	5.4	453	1.06

Table 8.27. - Case 1 - Assessment of shear reinforcement at mid-span.

$V_{rd,c,i}$ [kN]	$V_{rd,f,i}$ [kN]	A_{sw}/s [cm^2/m]	$V_{rd,s,i}$ [kN]	$V_{rd,max,i}$ [kN]	$V_{rd,i}$ [kN]	$V_{ed,V,i}$ [kN]	$V_{ed,T,i}$ [kN]	$V_{ed,Total,i}$ [kN]
999	45	0.0	0	10095	1044	-	471	471

The purpose now is to know if local instability is conditioning in ULS. Once the design is done with high compressive strength material, the structure elements are likely to be slenderer. May occur that ULS is conditioned by buckling in turn of material strength.

First, a buckling analysis in ULS is performed to assess the stability of the bottom slab above the pier during constructive process. The critical moment occurs after task 6 has completed (Fig.8.8.) where the negative bending moment above the piers takes high values and the bottom flange is highly compressed. The elasticity modulus at that moment had attained 44.5GPa. The critical segment was modeled as a cantilever box girder beam. The first buckling mode occurred in the bottom slab near the support (Fig.8.35.) as expected. The buckling factor of that mode is 9.9 which lead to conclude that the ULS is governed by material strength capacity.

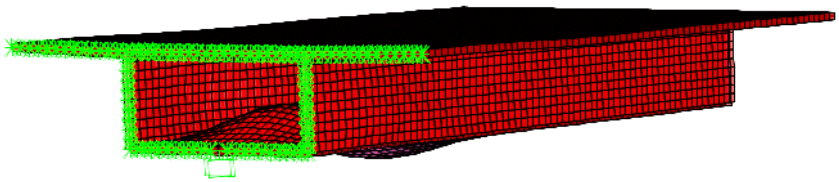

Fig.8.35. - Case 1 - Buckling mode during constructive process.

Second, a buckling analysis in ULS is performed to assess the stability during service stages. Again, for simplicity, it was modeled a standard span clamped in both ends and no pre-stressing losses were considered. It was expected to observe buckling modes on top slab at mid span and/or on bottom slab near the supports. However, the first buckling mode points to a buckling factor of 11.6 and it seems to be related to the a very high point load resulting from pre-stressing anchorage. Actually, that point load does not exist because that tendon represents a set of cables which are supposed to be distributed. The one that seems to be the first real buckling mode has a buckling factor of 13.4 and is associated with instability of bottom slab near the pier (Fig.8.36.). Again, it can be concluded that the thickness of structure members may be even more decreased if material strength allows it.

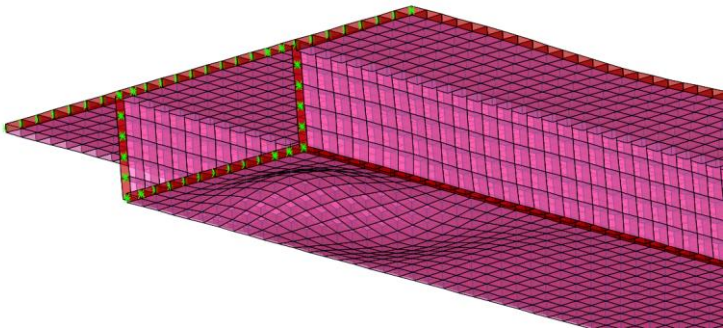

Fig.8.36. - Case 1 - Buckling mode during service stage.

8.6. CASE 2

8.6.1. OVERVIEW

The purpose of this case is to design the deck with UHPC near the piers and the CC segment at mid span where shear and bending forces take lower values. The reasoning is analogous to what happens during lightened slabs design where a solid slab is designed near supports to resist high internal forces. But, in this case, it would be the strength of the material changing instead of the cross-section. Again, it is assumed a constant bridge deck geometry. So, Table 8.28. identifies the materials involved in this case.

Table 8.28. - Case 2 - Structural materials.

Material	Structural Element	Grade
Concrete	Substructure	C30/37
	Superstructure	UHPC150
		C40/50
Steel	Passive reinforcement	A500 NR SD
	Pre-stress strands	Y 1860 S7

8.6.2. DESIGN

The thickness of the top slab is expected to be governed by ULS design in the deck part which is casted with CC. By acknowledging that top slab thickness is mainly influenced by transverse internal forces resulting from ULS, it is possible to conclude that, the existing solution (Case 0) for bridge deck already has the solution of top slab thickness which is going to be used in this case (Fig.8.37.). Then, it is going to be verified if that solution is admissible for longitudinal limit states.

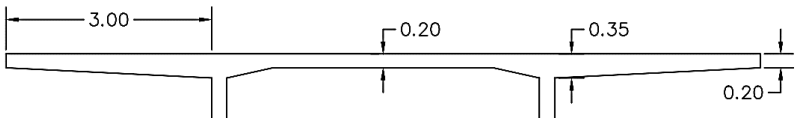

Fig.8.37. - Case 2 - Top slab solution [m].

Before going into the longitudinal analysis, the ULS internal forces are determined in the transverse direction to check safety. Now, when determining internal forces, it is going to be considered a 2-m edge around the maximum local value and estimate the average internal force per meter in that zone (Table 8.5.). The strength is determined with the existing thicknesses and reinforcements. As can be seen in Tables 8.29., 8.30., and 8.31., corresponding to Section 1, 2, and 3 (Fig.8.27.), the bending strength is high enough to resist the ultimate bending moments. However, shear strength is under the required in the cantilever part. That may be justified by overestimation of the shear forces and the underestimation of the shear strength, respectively:

- The internal forces induced by the wheels of the tandem system that are closest to the web may not enter thoroughly in the design values of shear forces because part of that load is directly transferred to the support (web) by means of a compressed strut.
- The positive contribution to shear strength provided by the slope of the bottom face of the cantilever is not being considered.

Table 8.29. - Bending and shear capacity of Section 1.

h [m]	M_{rd} [kN.m/m]	x [m]	x/d	ε_s [%]	A_s [cm^2]	ρ [%]	$V_{rd,c}$ [kN]	$V_{rd,max}$ [kN]	V_{rd} [kN]
0.35	323.07	0.05	0.17	1.8	25.8	0.74	166	1624	166

Table 8.30. - Bending and shear capacity of Section 2.

h [m]	M_{rd} [kN.m/m]	x [m]	x/d	ε_s [%]	A_s [cm^2]	ρ [%]	$V_{rd,c}$ [kN]	$V_{rd,max}$ [kN]	V_{rd} [kN]
0.35	323.07	0.05	0.17	1.8	25.8	0.74	166	1624	166

Table 8.31. - Bending and shear capacity of Section 3.

h [m]	M_{rd} [kN.m/m]	x [m]	x/d	ε_s [%]	A_s [cm^2]	ρ [%]	$V_{rd,c}$ [kN]	$V_{rd,max}$ [kN]	V_{rd} [kN]
0.24	83.72	0.02	0.10	3.4	10.1	0.42	123	1048	123

A cross-section depth of 2.5m is used which is justified by the same motivations mentioned in Case 1. The final internal forces results from previous case are used to realize a preliminary design on the material distribution along the bridge and the webs thickness. It is considered a valid start once that the few differences that are expected to occur in internal forces are result of the increase of self-weight due to the thickness of top slab and, maybe, due to the not so slender webs. Consequently, the solution of pre-stressing lay-out may not change but additional pre-stressing force may be required to balance the permanent load.

During 2^{nd} stage, 1^{st} task, it is installed in the bottom fiber of cantilever end a compressive stress of 14.1MPa (Fig.8.38.). It occurs when the CC only attained 20.72MPa of characteristic compressive strength which means that compressive limit stress is 12.43MPa. That fact requires that UHPC must go until 17.5m to the right side of each pier.

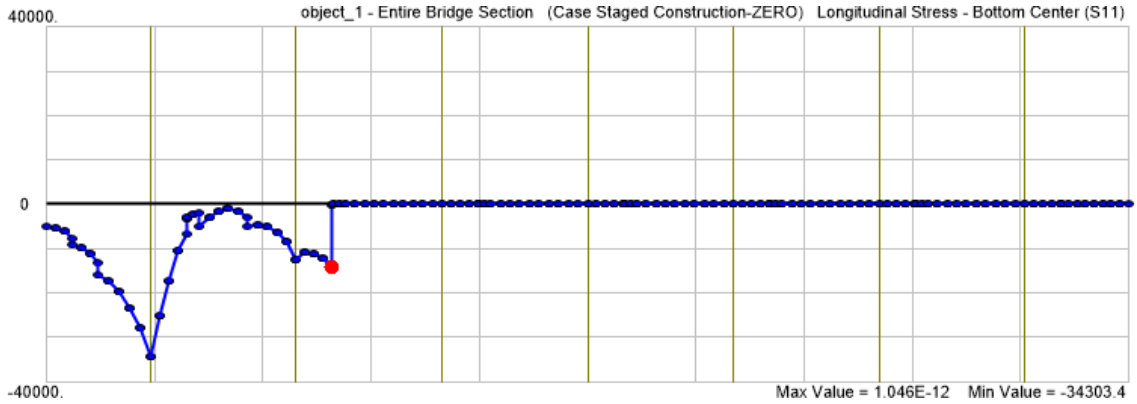

Fig.8.38. - Case 2 - Longitudinal stresses on bottom fibers during 2nd stage, 1st task of constructive process [kPa].

During 2nd stage, 6th task (Fig.8.39.), the CC has attained 38.18MPa of characteristic compressive strength, so, it is allowed to stand 22.9MPa in order to avoid longitudinal cracking. The compressive stress installed on bottom fiber is lower than that limit at 23.23m away from the pier (P-2). This means that between this cross-section and the pier, the deck must be casted with UHPC.

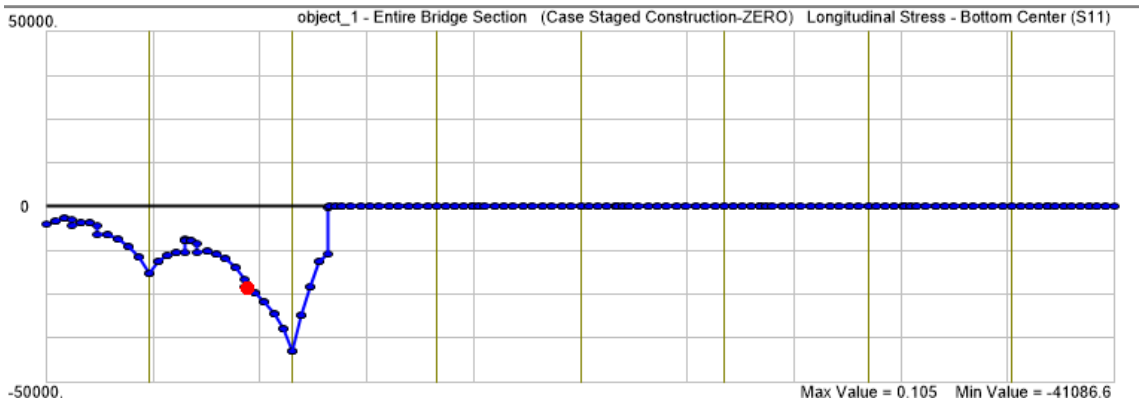

Fig.8.39. - Case 2 - Longitudinal stresses on bottom fibers during 2nd stage, 6th task of constructive process [kPa].

This reasoning concludes in a material distribution according with that illustrated in Fig.8.40..

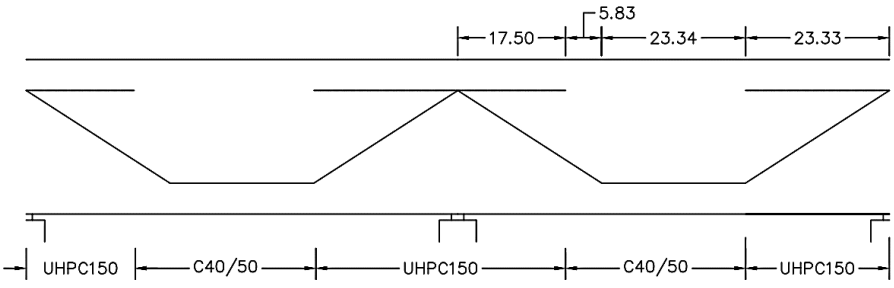

Fig.8.40. - Case 2 - Material distribution along deck length [m].

For this first iteration on longitudinal design, it is used the internal forces resulted from Case 1 with the addition of internal forces at constructive joints at both right and left side of each pier (Table 8.32.).

Table 8.32. - Case 2 - Most governing global internal forces under fundamental load combination.

Section	N [kN]	M [kN.m]	V [kN]	T [kN.m]
Constructive joint (right)	-17677	34363	4715	6694
Constructive joint (left)	-17677	41756	4279	5923
Above the pier	-52000	-98700	10950	8415
mid-span	-17677	66000	-	4500

The CC is the weakest material at constructive joints, therefore, the verification of UHPC is unnecessary. Thickness of the webs is going to be governed by CC in the constructive joint (right) or by UHPC above the piers. First, the web thickness is going to be reduced at the constructive join and, then, it is checked above the piers both bending (Table 8.33.) and shear capacity (Table 8.34.).

Table 8.33. - Case 2 - First approach to assess minimum web thickness (flexural reinforcement)

	b_w [m]	A_c [m^2]	x [m]	x/d	ε_s [%]	A_s [cm^2]	ρ [%]
1	0.36	5.40	0.15	0.06	6.3	351	0.65
2	0.30	5.16	0.15	0.06	6.3	351	0.68
3	0.25	4.95	0.15	0.06	6.3	351	0.71
4	0.22	4.83	0.15	0.06	6.3	351	0.73

Table 8.34. - Case 2 - First approach to assess minimum web thickness (shear reinforcement)

	$V_{rd,c,i}$ [kN]	A_{sw}/s [cm^2/m]	$V_{rd,s,i}$ [kN]	$V_{rd,max,i}$ [kN]	$V_{rd,i}$ [kN]	$V_{ed,V,i}$ [kN]	$V_{ed,T,i}$ [kN]	$V_{ed,Total,i}$ [kN]
1	704	19.0	3079	5081	3079	2358	721	3079
2	603	18.9	3070	4256	3070	2358	712	3070
3	516	18.9	3062	3563	3062	2358	705	3062
4	461	18.8	3058	3145	3058	2358	700	3058

The iteration stops here because is expected that structure self-weight will increase and, consequently, shear force increases too. The web thickness used in the following steps is 0.25 m. In the left constructive joint, the shear strength is enough and the reinforcement quantity is satisfactory, and Tables 8.35. and 8.36. show right that. At mid-span, shear forces (Table 8.38.) do not constitute a problem but the positive bending moment requires a high amount of steel reinforcement (Table 8.37.). The maximum reinforcement ratio (4%) is respected but 1.36% may lead to an infeasible constructive solution. However, the study is going to continue without any change on geometry or pre-stress

solution. Above the piers, UHPC resists to internal forces with satisfactory quantity of steel reinforcement both in the longitudinal direction (Table 8.39.) and in the transverse direction (Table 8.40.).

Table 8.35. - Case 2 - Bending capacity in the left constructive joint.

b_w [m]	A_c [m^2]	x [m]	x/d	ε_s [%]	A_s [cm^2]	ρ [%]
0.25	4.95	0.16	0.07	5.7	427	0.86

Table 8.36. - Case 2 - Shear capacity in the left constructive joint.

$V_{rd,c,i}$ [kN]	A_{sw}/s [cm^2/m]	$V_{rd,s,i}$ [kN]	$V_{rd,max,i}$ [kN]	$V_{rd,i}$ [kN]	$V_{ed,V,i}$ [kN]	$V_{ed,T,i}$ [kN]	$V_{ed,Total,i}$ [kN]
516	17.0	2763	3563	2763	2140	623	2763

Table 8.37. - Case 2 - Bending capacity at mid-span.

b_w [m]	A_c [m^2]	x [m]	x/d	ε_s [%]	A_s [cm^2]	ρ [%]
0.25	4.95	0.21	0.09	4.2	675	1.36

Table 8.38. - Case 2 - Shear capacity at mid-span.

$V_{rd,c,i}$ [kN]	A_{sw}/s [cm^2/m]	$V_{rd,s,i}$ [kN]	$V_{rd,max,i}$ [kN]	$V_{rd,i}$ [kN]	$V_{ed,V,i}$ [kN]	$V_{ed,T,i}$ [kN]	$V_{ed,Total,i}$ [kN]
516	0.0	0	3563	516	-	474	474

Table 8.39. - Case 2 - Bending capacity above the piers.

b_w [m]	A_c [m^2]	x [m]	x/d	ε_s [%]	A_s [cm^2]	ρ [%]
0.25	4.95	0.64	0.27	0.5	611	1.23

Table 8.40. - Case 2 - Shear capacity above the piers.

$V_{rd,c,i}$ [kN]	$V_{rd,f,i}$ [kN]	A_{sw}/s [cm^2/m]	$V_{rd,s,i}$ [kN]	$V_{rd,max,i}$ [kN]	$V_{rd,i}$ [kN]	$V_{ed,V,i}$ [kN]	$V_{ed,T,i}$ [kN]	$V_{ed,Total,i}$ [kN]
1245	589	27.83	4527	8934	6361	5475	886	6361

With the pre-design concluded, the deck geometry used to run the analysis is illustrated in the Fig.8.41.. The change of the load that M70-S transfers to the bridge deck due to fresh concrete self-weight is assumed to be proportional to the variation of the cross-section area. So, the load corresponding to task 6 and 7 (Fig.8.8.) is now 2865kN.

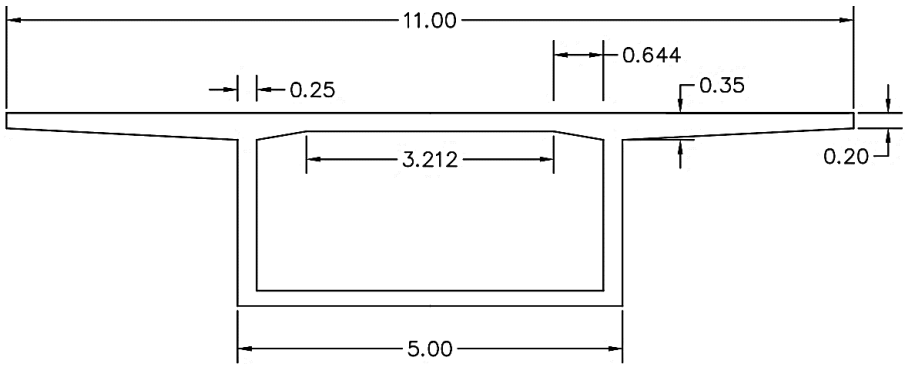

Fig.8.41. - Case 2 - Cross-section solution [m].

The same pre-stressing solution, lay-out and force, was used from Case 1 solution. The self-weight of the superstructure naturally increased when compared with the solution of Case 1. However, the solution of pre-stress of Case 1 have left room to increase superstructure self-weight without disrespecting stresses and deflections limits in service stage and that was what happened.

In the other hand, during constructive process, undesirable tensile stresses occur in bottom fibers at mid-span at the age of the concrete of 3 days which will cause crack opening. Those bottom fibers are under tensile stresses for the quasi-permanent load combination, thus, those cracks still opened during service stage and they may comprise serviceability behavior.

In order to solve this problem, the pre-stressing force of the tendons with polygonal layout is increased to avoid cracking during constructive process. Then, the pre-stressing force in tendons with polygonal lay-out totals:

- P_{max} = 29596kN
- A_p= 210cm^2 (150 strands)

And for the pre-stressing tendons disposed only near the piers, the amount is:

- P_{max} = 36765kN
- A_p = 259cm^2 (185 strands)

At this point it was possible to run analysis again with the cross-section proposed in the Fig.8.40., and with the pre-stress solution, as aforementioned.

8.6.3. RESULTS

During construction stages, there is no stresses above the limits assumed, as is shown in Table 8.41. for maximum compressive stresses, and in Table 8.42. for maximum tensile stresses. Those tables are referred to stage 7 which is assumed to be representative of all other stages. Additionally, the deflection of the cantilever end is 16.8 cm.

Table 8.40 - Case 2 - Control of compressive stresses control during constructive stage.

Task	t	t_c	C40/50			UHPC150		
			Top	Bottom	0.6 $f_{ck}(t_c)$	Top	Bottom	0.6 $f_{ck}(t_c)$
	days	days	MPa	MPa	MPa	MPa	MPa	MPa
1	109	3	8.9	4.6	12.4	17.4	12.3	50.8
2	109	3	7.0	9.7	12.4	16.4	12.3	50.8
3	109	3	9.8	2.1	12.4	17.8	12.3	50.8
4	109	3	4.3	12.2	12.4	13.3	26.4	50.8
5	124	18	4.3	12.2	22.3	11.5	26.4	87.3
6	127	21	2.5	20.9	22.9	11.5	42.5	88.4
7	127	21	4.4	11.9	22.9	11.4	26.3	88.4

Table 8.42. - Case 2 - Control of tensile stresses control during constructive stage.

			C40/50			UHPC150		
Task	t	t_c	Top	Bottom	$f_{ctm}(t_c)$	Top	Bottom	$f_{ctm,el}(t_c)$
	days	days	MPa	MPa	MPa	MPa	MPa	MPa
1	109	3	-	-	2.09	-	-	2.18
2	109	3	-	-	2.09	-	-	2.18
3	109	3	-	1.5	2.09	-	-	2.18
4	109	3	-	-	2.09	-	-	2.18
5	124	18	-	-	3.29	-	-	7.47
6	127	21	2.1	-	3.37	4.5	-	7.68
7	127	21	-	-	3.37	-	-	7.68

During quasi-permanent load combination, all the deck remains uncracked and the creep effects may be considered linear because of the maximum compressive stress is under the limit establish (Eq.8.12.). The maximum compressive stresses installed in the concrete and UHPC are 8.2MPa and 26.4MPa (Fig.8.42.) which have as limits 18MPa and 67.5MPa, respectively. Moreover, the maximum tensile stress verified does not induce cracking. The deflection limit established is also respected in inner spans (8.0 cm) and end spans (3.5 cm).

Longitudinal crack opening is also controlled either in the concrete or in the UHPC. For the characteristic load combination (Fig.8.43.), the maximum compressive stress in the concrete and in the UHPC are 13.2MPa and 37.7MPa which have as limits 24MPa and 90MPa. Furthermore, the maximum tensile stress in the tendons is 1272MPa which is under the limit established (Eq.8.10.).

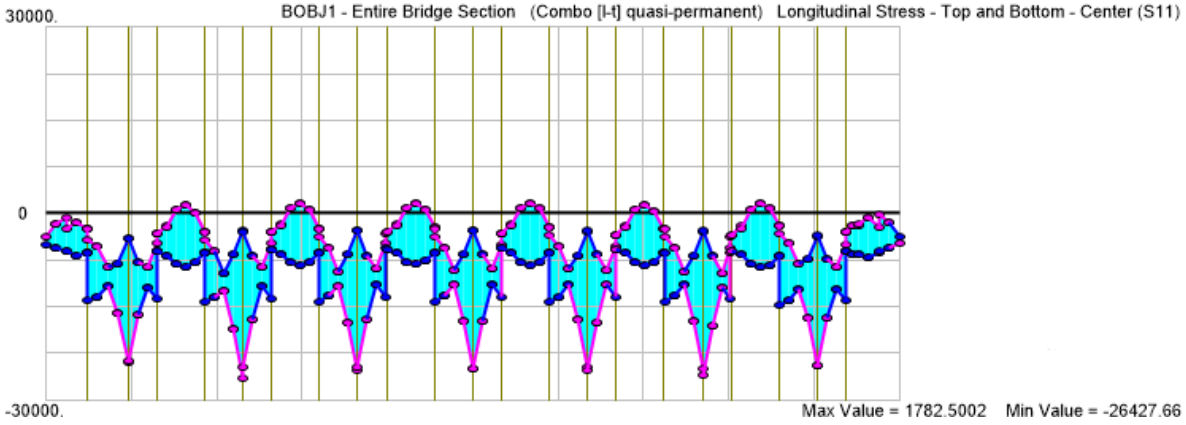

Fig.8.42. - Case 2 - Stresses envelope under quasi-permanent load combination [kPa]

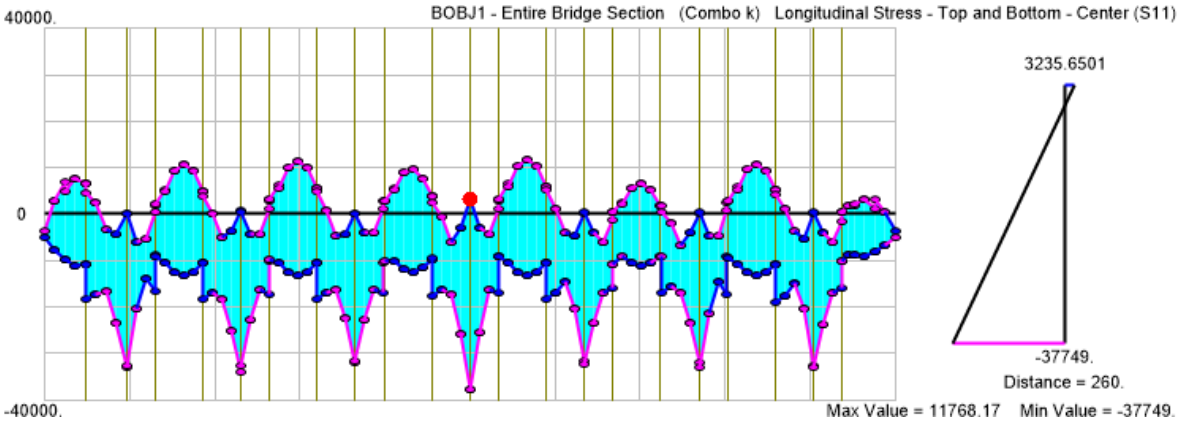

Fig.8.43. - Case 2 - Stresses envelope under characteristic load combination [kPa].

In Table 8.43. are presented the internal forces required to evaluate the amount of reinforcement and check safety conditions. These internal forces lead to reasonable reinforcement solutions for the CC segment at constructive joints at the right (Tables 8.44. and 8.45.) and at the left side of the piers (Tables 8.46. and 8.47.).

Table 8.43. - Case 2 - Most governing global internal forces under fundamental load combination.

Section	N [kN]	M [kN.m]	V [kN]	T [kN.m]
Constructive joint (right)	-27115	31800	4932	6257
Constructive joint (left)	-27115	38690	4494	5629
Above the pier	-56867	-109601	10157	8014
Mid-span	-27115	65975	-	4513

Table 8.44. - Case 2 - Assessment of longitudinal reinforcement in the right constructive joint.

b_w [m]	A_c [m^2]	x [m]	x/d	ε_s [%]	A_s [cm^2]	ρ [%]
0.25	4.95	0.19	0.08	4.8	339	0.69

Table 8.45. - Case 2 - Assessment of shear reinforcement in the right constructive joint.

$V_{rd,c,i}$ [kN]	A_{sw}/s [cm^2/m]	$V_{rd,s,i}$ [kN]	$V_{rd,max,i}$ [kN]	$V_{rd,i}$ [kN]	$V_{ed,V,i}$ [kN]	$V_{ed,T,i}$ [kN]	$V_{ed,Total,i}$ [kN]
687	19.2	3125	3788	3125	2466	659	3125

Table 8.46. - Case 2 - Assessment of longitudinal reinforcement in the left constructive joint.

b_w [m]	A_c [m^2]	x [m]	x/d	ε_s [%]	A_s [cm^2]	ρ [%]
0.25	4.95	0.20	0.08	4.4	410	0.83

Table 8.47. - Case 2 - Assessment of shear reinforcement in the left constructive joint.

$V_{rd,c,i}$ [kN]	A_{sw}/s [cm^2/m]	$V_{rd,s,i}$ [kN]	$V_{rd,max,i}$ [kN]	$V_{rd,i}$ [kN]	$V_{ed,V,i}$ [kN]	$V_{ed,T,i}$ [kN]	$V_{ed,Total,i}$ [kN]
687	17.5	2840	3788	2840	2247	593	2840

However, the longitudinal reinforcement at mid span (Table 8.48.) may be restricted by constructive constraints even knowing that the maximum quantity of longitudinal steel reinforcement is respected (4%). There is no shear reinforcement needed (Table 8.49.) but the minimum quantity of that must be respected for CC.

Table 8.48. - Case 2 - Assessment of longitudinal reinforcement at mid-span.

b_w [m]	A_c [m^2]	x [m]	x/d	ε_s [%]	A_s [cm^2]	ρ [%]
0.25	4.95	0.29	0.12	2.8	693	1.40

Table 8.49. - Case 2 - Assessment of shear reinforcement at mid-span

$V_{rd,c,i}$ [kN]	A_{sw}/s [cm^2/m]	$V_{rd,s,i}$ [kN]	$V_{rd,max,i}$ [kN]	$V_{rd,i}$ [kN]	$V_{ed,V,i}$ [kN]	$V_{ed,T,i}$ [kN]	$V_{ed,Total,i}$ [kN]
687	0.0	0	3788	687	0	475	475

There is a problem with the reinforcement solution above the piers is related with lack of ductility. As can be noticed in Table 8.50., the steel reinforcement yields ($\varepsilon_s \geq 0.217$ %) almost when the cross-section reaches its maximum bending strength. It could be achieved more ductility just by increasing the bottom slab thickness, for instance, to 0.30 m. This would approximate the compression resultant force to extreme fiber, and neutral axis too. With that, cross-section curvature in ULS would increase and the strain of the reinforcement would also become higher. Other measure with the same effects

would be the adoption of compressive steel reinforcement. In last case, superstructure depth should be increased. Finally, with shear (Table 8.51.) there is no problems to be noticed.

Table 8.50. - Case 2 - Assessment of longitudinal reinforcement above the piers.

b_w [m]	A_c [m^2]	x [m]	x/d	ε_s [%]	A_s [cm^2]	ρ [%]
0.25	4.95	1.09	0.46	0.217	683	1.38

Table 8.51. - Case 2 - Assessment of shear reinforcement above the piers.

$V_{rd,c,i}$ [kN]	$V_{rd,f,i}$ [kN]	A_{sw}/s [cm^2/m]	$V_{rd,s,i}$ [kN]	$V_{rd,max,i}$ [kN]	$V_{rd,i}$ [kN]	$V_{ed,V,i}$ [kN]	$V_{ed,T,i}$ [kN]	$V_{ed,Total,i}$ [kN]
1265	1471	19.7	3210	9505	5947	5105	842	5947

The considerations described in Case 1, about buckling analysis, are also applied in this case on what concerns assessment of the stability during constructive process and service stage. In first place, during execution, the first buckling mode configuration is like the one occurred in Case 1 (Fig.8.44.) but the correspondent buckling factor slightly increased to 10.0. Nevertheless, the result shows that instability is unexpected during the constructive process.

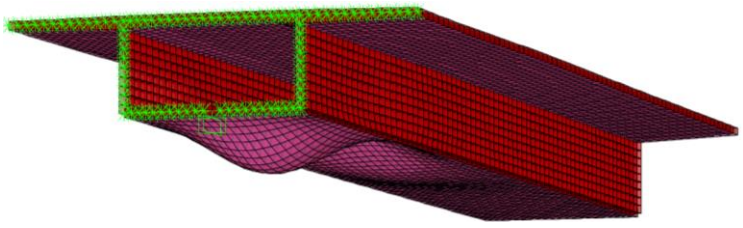

Fig.8.44. - Case 2 - Buckling mode during constructive process.

In second place, during service stage, the first buckling mode configuration is an instability in the bottom slab near the support (Fig.8.45.) where the axial and negative bending moments are high. This time, that buckling mode has a slightly higher buckling factor of 13.7. One more time, there is no instability problems conditioning the design.

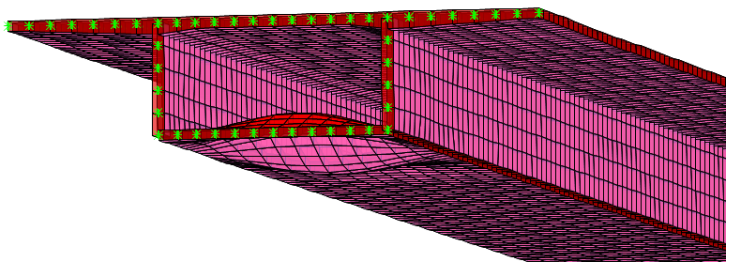

Fig.8.45. - Case 2 - Buckling mode during service stage.

8.7. COMPARATIVE ANALYSIS

8.7.1. SUBSTRUCTURE

By decreasing superstructures self-weight, it is understandable that substructure members like piers and foundations may also have some reduction of volume once they are less loaded. At the Appendix A.6. can be found the axial forces installed on piers base for each case and under quasi-permanent load combination of actions (RPL and self-weight). In Table 8.52. is shown the relative variation of axial force at piers base.

Table 8.52. - Variation of axial force at piers base when compared with Case 0.

Pier	ΔN [%]	
	Case 1	Case 2
P1	-28.1	-20.6
P2	-22.9	-16.7
P3	-22.8	-16.7
P4	-23.0	-16.8
P5	-23.0	-16.8
P6	-23.2	-17.0
P7	-26.3	-19.2

Notice that not only vertical loads transferred to substructure may change. Lateral loads induced by seismic action may also decrease. As superstructure mass decreases, the inertial forces resulting from ground acceleration may also decrease. However, it is not that simple because natural frequency of the structure is expected to become higher making the structure more susceptible develop higher accelerations during seismic action. A better understanding of seismic action and its effects on substructure, it is performed a modal analysis followed by a seismic analysis based on response spectrum given by 1998-1 and considering that the piers are unchanged.

Square Root of the Sum of the Squares (SRSS) method is used to combine modal responses and perform directional combination. The seismic action is defined according to EN 1998-2, with the following parameters:

- Ground type B;
- Importance Class 1 (average importance);
- Behavior factor: q = 1;
- Both types of seismic actions are analyzed according to NP EN 1998-1
  - Type 1 - Near Earthquake (Seismic Zone 1.4) with ground acceleration of 1.0 m/s^2
  - Type 2 - Distant Earthquake (Seismic Zone 2.4) with ground acceleration of 1.1 m/s^2
- Equivalented viscous damping ratio for all modes of 0.05;
- Bridge mass defined by characteristic value of self-weight and characteristic value of remaining permanent loads (RPL).

Fig.8.46. shows the directions whose results are referred. Direction 3 corresponds to deck alignment whereas direction 2 is transversally oriented. The global base reactions in the superstructure alignment and in the perpendicular direction resulting from seismic action are detailed in the Appendix A.6.. It can also be found there the base reactions for each pier, for each case study, and for each seismic action. From those tables is possible to conclude that the bridge is more vulnerable to seismic type 1 which, by other words, induces higher internal forces than seismic type 2 does.

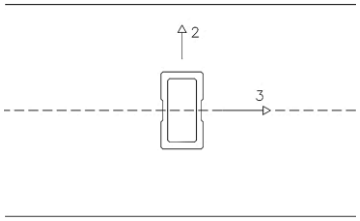

Fig.8.46. - Axis orientation regarding bridge alignment.

In Table 8.53. are described variations of the global base reactions. In a first approach, the results referred to seismic type 1 in the direction 3 are quite unexpected but, if it is looked closer, easily is understood why it has occurred.

Translation of bridge deck along its longitudinal axis alignment constitutes the first fundamental dynamic mode of the structure and the unique contributing in that direction. For that mode, the period of vibration is 3.52s for Case 0 and 2.98s for Case 1. Which means that for that dynamic mode and for those, the corresponding accelerations (a) are 0.33 m/s^2 and 0.45 m/s^2, respectively. Whereas the mass (M) of the structure has reduced 24%, the acceleration has increased 26%. Consequently, the seismic action ($M \times a$) barely does not change in that direction. The same reasoning is applied between Case 0 and Case 2. Nevertheless, piers should first be redesigned and then the modal and seismic analysis should be repeated, because both mass and stiffness may reduce, and consequently the seismic action too.

In seismic type 2, direction 3, the acceleration does not change and the equivalent seismic action relies only on mass. In the other hand, the transverse direction (2) does not has a fundamental mode and the seismic response results from the combination of several modes so, hand calculation may be more complex.

Table 8.53. - Variation of global base reactions when compared with Case 0.

Case	Seismic type 1		Seismic type 2	
	ΔF3	ΔF2	ΔF3	ΔF2
	%	%	%	%
1	0.9	-14.6	-26.9	-14.4
2	-0.9	-8.0	-19.8	-7.7

Naturally, the same impact on internal forces of piers base is foreseen and described in tables 8.54. and 8.55.. There is a significant reduction on internal forces for seismic type 2 but the internal forces resulting from seismic type 1 are the ones that count because are higher. For this last, only in transverse direction is verified a general reduction of internal forces. Additionally, the shorter piers

which are stiffer and are susceptible to balance most of the seismic action (P1 and P7) are also subjected to higher internal forces reductions.

Table 8.54. - Variation of piers base reactions from Case 0 to Case 1.

Piers	Seismic type 1					Seismic type 2				
	ΔV3	ΔM2	ΔV2	ΔM3	ΔT	ΔV3	ΔM2	ΔV2	ΔM3	ΔT
	%	%	%	%	%	%	%	%	%	%
P1	-	-	-30.2	-28.5	-	-	-	-29.7	-27.9	-
P2	0.7	0.1	-11.0	-11.7	-11.3	-27.2	-27.5	-10.3	-11.2	-11.1
P3	1.1	0.3	-9.2	-9.5	-10.8	-26.7	-27.3	-9.0	-9.3	-10.3
P4	1.1	0.2	-9.9	-9.8	-23.8	-26.8	-27.4	-9.6	-9.6	-22.6
P5	0.9	0.2	-9.5	-9.9	-13.1	-26.7	-27.4	-9.3	-9.7	-12.5
P6	0.8	0.1	-11.7	-12.2	-12.7	-26.9	-27.4	-11.2	-11.8	-12.5
P7	-	-	-23.3	-22.2	-	-	-	-22.7	-21.6	-

Table 8.55. - Variation of piers base reactions from Case 0 to Case 2.

Piers	Seismic type 1					Seismic type 2				
	ΔV3	ΔM2	ΔV2	ΔM3	ΔT	ΔV3	ΔM2	ΔV2	ΔM3	ΔT
	%	%	%	%	%	%	%	%	%	%
P1	-	-	-13.2	-11.5	-	-	-	-12.2	-10.4	-
P2	0.4	0.0	-7.9	-8.1	-4.6	-18.7	-19.0	-7.6	-7.8	-4.3
P3	0.7	0.2	-5.6	-5.8	-5.7	-18.4	-18.9	-5.5	-5.6	-5.3
P4	0.7	0.1	-6.1	-5.9	-2.9	-18.4	-18.9	-6.0	-5.8	-1.7
P5	0.5	0.1	-5.7	-5.8	-6.8	-18.4	-18.9	-5.5	-5.7	-6.3
P6	-6.3	-4.7	-7.5	-7.7	-5.0	-24.1	-22.8	-7.3	-7.5	-4.7
P7	-	-	-12.1	-10.8	-	-	-	-11.4	-10.2	-

8.7.2. QUANTITIES

The gross area of the cross-section (Table 8.56.) is a simple parameter that gives a good perception on the quantity of material used on bridge deck. The cross-section area of Case 0 is a mean value because it changes along the bridge. The volume is easily calculated by multiplying the area by bridge length. In Case 0, the volume of concrete takes into account the volume occupied by internal tendons. The quantity of pre-stressing strands is also quantified (Table 8.57.). For simplicity, the length measured corresponds to the horizontal projection of the tendons.

Table 8.56. - Amount of concrete and/or UHPC

Case	Area	C40/50		UHPC150	
		Volume	Mass	Volume	Mass
	[m^2]	[m^3]	[t]	[m^3]	[t]
0	6.67	3441	8777	-	-
1	4.27 (-36%)	-	-	2220	5663
2	4.95 (-26%)	1151	2934	1423	3627

Table 8.57. - Amount of pre-stressing steel

Case	Total strands length	Volume	Mass
	[m]	[m^3]	[t]
0	193440	27.08	212.6
1	123904 (-36%)	17.35	136.2
2	131184 (-32%)	18.47	145.0

8.7.3. COST ASSESSMENT

There is considerable scatter on UHPC unit cost when compared to what happens with CC. For that reason, and by remembering the information addressed about UHPC cost in chapter 3, it is considered two extreme scenarios

1. UHPC costs 2000€/m^3
2. UHPC costs 500€/m^3.

Additionally:

- C40/50 cost 95€/m^3 including concreting works
- Pre-stressing streel is assumed to cost 2800€/t with positioning work

Finally, considering the amount of each material and their unit cost, it is now possible to estimate total materials cost for each scenario. In Table 8.58. is presented the total cost for each case and for each scenario and, in Table 8.59. can be found the variation of cost when compared with case 0. Furthermore, Fig.8.47. and 8.48. illustrate stacked column charts where partial costs can be better compared.

Table 8.58. - Total cost.

Case	Scenario 1	Scenario 2
	€	€
0	922108	922108
1	4824323	1492100
2	3360939	1226739

Table 8.59. - Variation of total cost when compared with Case 0.

Case	Scenario 1	Scenario 2
	%	%
1	423	61
2	264	33

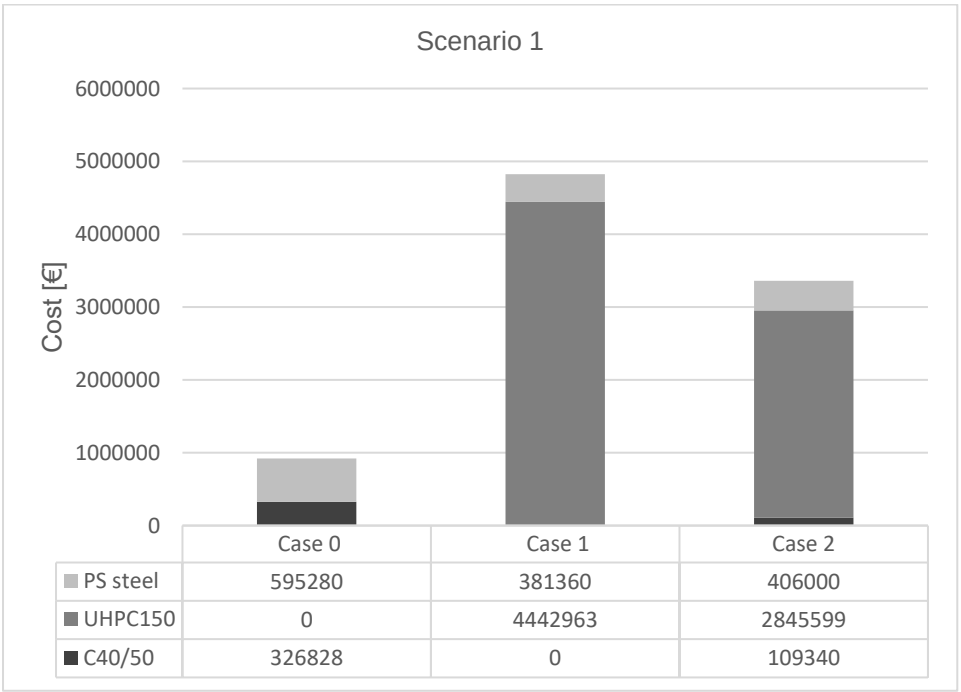

Fig.8.47. - Partial costs of scenario 1

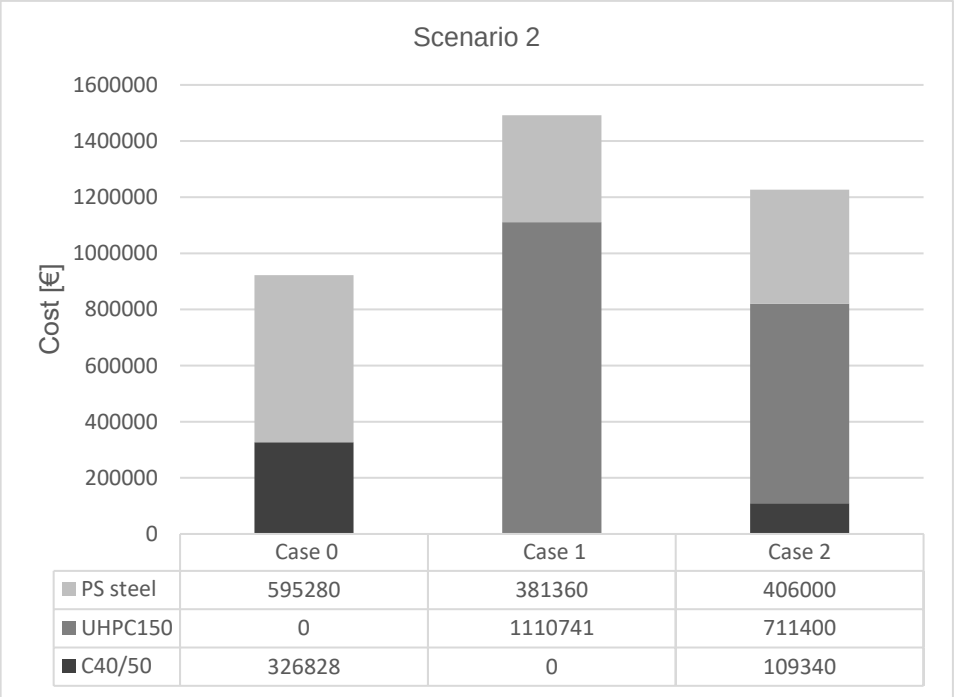

Fig.8.48. - Partial costs of scenario 2

Even though the amount of steel reinforcement for Case 1 and 2 was not counted, it is estimated how much the steel rebar should be reduced to match the total cost of Case 0. The total amount of steel reinforcement for the deck in the existing bridge is 410.6 t and the unit cost assumed for it is 750€/t, including positioning works. Then, the total cost of steel rebar used on existing bridge deck (Case 0) is 307950€. Thus, in Table 8.60. is shown how much the total of steel rebar should cost, the corresponding quantity, and the corresponding variation in order to satisfy the condition aforementioned.

The negative values for cost and quantity means that even if the bridge deck had not steel rebar, it would not be enough to match the cost of deck of Case 0. Only for Case 2 combined with scenario 2 it would be hypothetically possible to match the cost of the existing deck.

Table 8.60. - Quantity of steel reinforcement allowed, per case, to match the total cost of existing bridge deck.

Case	Scenario 1			Scenario 2		
	Total Cost	Quantity	ΔQuantity	Total Cost	Quantity	ΔQuantity
	€	t	%	€	t	%
1	-3594265	-4792	-1267	-262043	-349	-185
2	-210881	-2841	-792	3318	4.42	-99

9
CONCLUSION

1.1. DISCUSSION

Concrete have been improved during decades in order to increase its performance and a formulation for that material have been stabilized since twenty years ago. That formulation is referred to UHPC and its high-performance characteristics are related to ductility, compressive strength and durability, mainly. However, its high raw materials cost and restrict conditions during production make it difficult to compete against CC. Nevertheless, it has been applied in several bridges while proper design codes have been developed. Initially there was only recommendations and guidelines supporting the designers but at the moment of this study, there is design codes addressing almost the same matters that reinforced CC structures codes do. It is the case of French national annex to EC2, NF P 18-710 and which was used during the study case.

A brief review on internal and external pre-stressing solutions showed that the last may permit reduce web thickness and short-term pre-stress losses. However, the tendons contribution to stiffness and strength is negligible. Also, an overview on constructive methods able to be used on case study bridge was made with more focus on Movable Scaffolding System (MSS) which was used to execute *Río Cabriel* Bridge. The concluding remark of this chapter was that constructive staged analysis and the resulting internal forces must be considered at the moment of design. Essentially because the structure changes during time, equipment loads, and finally internal forces redistribution due to viscoelasticity.

About the case study itself, it was possible conclude the following:

- In contrast with the real project (Case 0), the design of both Case 1 and Case 2 respect compressive stress limit during constructive process;
- The loads imposed by constructive equipments to the structure are reduced as result of the decrease of fresh material that the equipment must support. Regardless, the constructive process remained with major influence on structure design;
- It is possible to decrease the top slab thickness while maintaining the transverse bending moment reinforcement ratio and without include shear reinforcement. In fact, shear strength is far away of being the internal force governing slab thickness;
- It is verified an important contribution of steel fibers to shear and bending strength in slab elements;
- In one hand, it is possible to decrease webs thickness up to 63% (Case 1) by using external pre-stress solution. In the other hand, more quantity of passive steel reinforcement in longitudinal direction in needed because pre-stress tendons are no longer contributing to cross-section strength;

- The safety is governed by material strength and instead of instability issues despite the elements slenderness;
- Lower amount of cementitious composite material in both cases studied, less 36% for Case 1 and less 26% for Case 2;
- Lower amount of pre-stressing tendons in both cases studied. In the Case 1 that quantity is reduced 36% whereas in the case 2 it is reduced 32%;
- Substructure ends up being less loaded, naturally. The axial force on piers base is generally reduced by 25% in Case 1 and 17% in Case 2;
- Equivalented seismic action did not decrease as much as expected, considering the superstructure mass reduction. Despite mass reduction, equivalent seismic action along bridge alignment barely does not changed because acceleration has increased. In transverse direction, the seismic action was reduced by 14.6 % for Case 1 and 8% for Case 2;
- The large range of unit cost of UHPC material leads to high scatter on bridge deck total cost and, under those circumstances, it is difficult to achieve precise conclusions about economic feasibility. However, the solutions proposed in Case 1 and 2 are economically infeasible regardless the UHPC cost scenario.
- The best-case scenario occurs when UHPC costs 500€/m^3 and it is adopted a mix solution of UHPC and CC for bridge deck design (Case 2). The total cost increased 33% when compared with actual bridge deck (Case 0).
- Still in that case scenario, it would be needed almost total reduction (-99%) of steel reinforcement amount on bridge deck which is impossible is both cases studies.

One final note about steel reinforcement in UHPC elements. In 2nd chapter were introduced cases where passive steel reinforcement is not needed. In the case study performed it was concluded that in the longitudinal direction, due to external pre-stressing solution, the amount of flexural reinforcement is higher than in the real bridge. In the other hand, shear reinforcement decreased. The EC2 requires minimum shear reinforcement, minimum bending reinforcement, distribution reinforcement in slabs, and minimum steel reinforcement to control cracks. Those minimum quantities may have high impact on total steel rebar used in a bridge. However, NF P18-710 states that all of those minimum quantities are no more applicable to UHPC structures and, consequently, it can be a great aspect to take advantage of.

Finally, the design developed along this study has not included sophisticated optimization of the solution and much other variables that may change and influence economic feasibility assessment are not considered. As could be seen, and considering the particular circumstances in which the study was done regarding the span length, cross-section type, and constructive method, it is concluded that a superstructure solution that makes use of UHPC as main structural element (Case 1) or even combined with CC, in the way it was done in Case 2, is economically infeasible.

1.2. RECOMMENDATIONS FOR FURTHER RESEARCH

In the point of view of the author, studies about the design of bridges with UHPC should continue. With the steel and conventional concrete, it is possible to design different and uncountable of solutions for bridges. With this new material, UHPC, more solutions may arise and some of them may be even better than those first mentioned. To evaluate that, the author recommends future research, in first place, on continuing the study that has been done with this *Río Cabriel* Bridge:

- Perform deeper optimization of cross-section geometry;

- Test different solutions of pre-stress and the corresponding lay-out;
- Study the impact the usage of UHPC has on constructive equipment and the changes that may occur in the construction schedule;
- Design and quantify steel reinforcement;
- Design of substructure with CC and/or UHPC considering the decreasing of internal forces.

And in second, extend the study to other type of bridge projects where UHPC is expected to become profitable either as a main structural material or not.

REFERENCES

[1] AFGC, *Bétons fibrés à ultra-hautes performances–Recommandations,* in *Recommandations*. 2013.

[2] Standardization, E.C.f., *Eurocode 1: Actions on structures - Part 2: Traffic loads on bridges*

2003.

[3] Engineers, J.S.o.C., *Recommendations for Design and Construction of High Performance Fiber Reinforced Cement Composites with Multiple Fine Cracks*. 2008.

[4] Qualidade, I.P.d., *NP EN1991 - Acções em estruturas - Parte 1-5: Acções gerais - Acções térmicas*. 2009.

[5] Magalhães, F., *Influence of the construction phases on the bridges forces and stresses,* in *Redistribution of bridges forces and stresses*. 2015.

[6] AFNOR, *Calcul des structures en béton – Règles spécifiques pour les bétons fibrés à ultra-hautes performances* in *Complément national à l'Eurocode 2*. 2016: France.

[7] Hajar, Z., et al. *Design and construction of the world first ultra-high performance concrete road bridges*. in *Proceedings of the International Symposium on Ultra High Performance Concrete. Kassel, Germany*. 2004.

[8] Fehling, E., T. Leutbecher, and K. Bunje. *Design relevant properties of hardened ultra high performance concrete*. in *Proceedings of the International Symposium on Ultra High Performance Concrete. Kassel, Germany*. 2004.

[9] Graybeal, B.A. and F. Baby, *Development of Direct Tension Test Method for Ultra-High-Performance Fiber-Reinforced Concrete.* ACI Materials Journal, 2013. **110**(2).

[10] Costa, A., *Estruturas de Betão II*, in *Folhas de apoio às aulas*. 2013, Departamento de Engenharia Civil e Arquitetura: Instituto Superior Técnico de Lisboa.

[11] Delauzun, O., et al., *Construction of the PS34 UHPFRC bridge.* Designing and building withUHPFRC, 2011: p. 137-148.

[12] Amorim, M., *Estudo do tabuleiro de um viaduto de betão pré-esforçado construído tramo a tramo com vãos de 90m*, in *Engenharia Civil*. 2008, Universidade do Porto: Faculdade de Engenharia da Universidade do Porto.

[13] Manterola, J., *Puentes : apuntes para su diseño, cálculo y construcción*. Vol. II. 2006, Madrid: Colegio de Ingenieros de Caminos, Canales y Puertos.

[14] Endicott, W.A., *A Whole New Cast*, in *ASPIRE*. 2007, Precast/Prestressed Concrete Institute, James G. Toscas, President. p. 26-29.

[15] Gowripalan, N. and R. Gilbert, *Design Guidelines for Ductal Prestressed Concrete Beams. Design Guide.* Civil & Environmental Engineering School, University of NSW, Sydney, Australia, 2000.

[16] Uchida, Y., et al. *Outlines of" Recommendations for Design and Construction of Ultra High Strength Fiber Reinforced Concrete Structures" by JSCE*. in *International RILEM Workshop on High Performance Fiber Reinforced Cementitious Composites in Structural Applications*. 2006. RILEM Publications SARL.

[17] Stráský, J. *The power of prestressing*. in *Role of Concrete Bridges in Sustainable Development: Proceedings of the International Symposium held at the University of Dundee, Scotland, UK on 3–4 September 2003*. 2003. Thomas Telford Publishing.

[18] Behloul, M. and R. Ricciotti. *Footbridge of Peace–Seoul*. in *Role of Concrete Bridges in Sustainable Development: Proceedings of the International Symposium*. 2003. University of Dundee, Scotland, UK Thomas Telford Publishing.

[19] Blais, P.Y. and M. Couture, *Precast, prestressed pedestrian bridge: World's first Reactive Powder Concrete structure.* PCI journal, 1999. **44**(5): p. 60-71.

[20] Roy, D.M., G. Gouda, and A. Bobrowsky, *Very high strength cement pastes prepared by hot pressing and other high pressure techniques.* Cement and Concrete Research, 1972. **2**(3): p. 349-366.

[21] Yudenfreund, M., I. Odler, and S. Brunauer, *Hardened portland cement pastes of low porosity I. Materials and experimental methods.* Cement and Concrete Research, 1972. **2**(3): p. 313-330.

[22] Birchall, J., A. Howard, and K. Kendall, *Flexural strength and porosity of cements.* Nature, 1981. **289**(5796): p. 388-390.

[23] Bache, H.H., *Densified cement ultra-fine particle-based materials*. 1981, Aalborg, Portland.

[24] Richard, P. and M. Cheyrezy, *Composition of reactive powder concretes.* Cement and concrete research, 1995. **25**(7): p. 1501-1511.

[25] Fehling, E., et al., *Ultra-High Performance Concrete UHPC: Fundamentals, Design, Examples*. 2014: John Wiley & Sons.

[26] Orgass, M. and Y. Klug. *Fibre reinforced ultra-high strength concretes*. in *Proceedings of the International Symposium on Ultra High Performance Concrete. Kassel, Germany*. 2004.

[27] Russell, H.G., et al., *Ultra-high performance concrete : a state-of-the-art report for the bridge community*. 2013, McLean, VA: U.S. Department of Transportation, Federal Highway

Administration, Research, Development, and Technology, Turner-Fairbank Highway Research Center. vii, 163 pages.

[28] Thibaux, T., *UHPFRC Development: The Experience of BSI® Applications.* Designing and Building with UHPFRC, 2010: p. 63-76.

[29] AFGC, S., *Bétons fibrés à ultra-hautes performances*, in *Recommandations provisoires*. 2002.

[30] AFGC, S., *Bétons fibrés à ultra-hautes performances–Recommandations*, in *Recommandations*. 2013.

[31] Kim, B., et al. *R&D activities and application of ultra high performance concrete to cable-stayed bridges*. in *Proceedings of Hipermat 2012 3rd International Symposium on UHPC and Nanotechnology for High Performance Construction Materials, Kassel University Press, Kassel*. 2012.

[32] Voo, Y.L., S.J. Foster, and C.C. Voo, *Ultrahigh-performance concrete segmental bridge technology: Toward sustainable bridge construction.* Journal of Bridge Engineering, 2014. **20**(8): p. B5014001.

[33] Tanaka, Y., et al. *Design and construction of Sakata-Mirai footbridge using reactive powder concrete*. in *Proceedings of the 1st fib Congress*. 2002.

[34] Voo, Y.L. and S.J. Foster, *Design and Construction of the 100 metre Span UHPC Batu 6 Segmental Box Girder Bridge*, in *Proceedings of Hipermat 2016 - 4th International Symposium on Ultra-High Performance Concrete and High Performance Construction Materials Kassel*. 2016, Kassel University Press: Kassel, Germany.

[35] Strunge, J. and T. Deuse. *Special cements for ultra high performance concrete*. in *Proceedings of the Second International Symposium on UHPC, Kassel, Germany*. 2008.

[36] Camacho, E., J.Á. López, and P.S. Ros. *Definition of three levels of performance for UHPFRC-VHPFRC with available materials*. in *Proceedings of Hipermat 2012 3rd International Symposium on UHPC and Nanotechnology for High Performance Construction Materials, Kassel University Press, Kassel*. 2012. kassel university press GmbH.

[37] Heinz, D., L. Urbonas, and T. Gerlicher. *Effect of heat treatment method on the properties of UHPC*. in *Proceedings of Hipermat 2012 3rd International Symposium on UHPC and Nanotechnology for High Performance Construction Materials, Kassel University Press, Kassel*. 2012.

[38] Schröfl, C., M. Gruber, and J. Plank, *Preferential adsorption of polycarboxylate superplasticizers on cement and silica fume in ultra-high performance concrete (UHPC).* Cement and Concrete Research, 2012. **42**(11): p. 1401-1408.

[39] Hirschi, T. and F. Wombacher. *Influence of different superplasticizers on UHPC*. in *Proceedings of the Second International Symposium on UHPC, Kassel, Germany*. 2008.

[40] Engineers, J.S.o.C., *JSCE Guidelines for Concrete No.9*, in *Recommendations for Design and Construction of Ultra High Strength Fiber Reinforced Concrete Structures (draft)*. 2006.

[41] Resplendino, J., *Introduction: What is a UHPFRC?* Designing and Building with UHPFRC, 2011: p. 3-14.

[42] Graybeal, B., *Ultra-high performance concrete*. 2011.

[43] Mazanec, O., D. Lowke, and P. Schießl, *Mixing of high performance concrete: effect of concrete composition and mixing intensity on mixing time.* Materials and structures, 2010. **43**(3): p. 357-365.

[44] Yang, S. and B. Diao, *Influence of curing regime on the ductility of ultra-high performance fiber reinforced concrete (UHPFRC)*, in *ICCTP 2009: Critical Issues In Transportation Systems Planning, Development, and Management*. 2009. p. 1-7.

[45] Habel, K., et al., *Development of the mechanical properties of an ultra-high performance fiber reinforced concrete (UHPFRC).* Cement and Concrete Research, 2006. **36**(7): p. 1362-1370.

[46] AFNOR, *Bétons fibrés à Ultra Hautes Performances - Spécification, performance, production et conformité*, in *Bétons*. 2016: France.

[47] des Architectes, Société S.des Ingénieurs e., *Béton fibré ultra-performant (BFUP) - Matériaux, dimensionnement et exécution*, in *prSIA 2052 :2014-04*. 2014.

[48] Wille, K. and B. Graybeal, *Development of Non-Proprietary Ultra-High Performance Concrete for Use in the Highway Bridge Sector*. 2013.

[49] G.tecz, *Quantz®- The Next Generation of cement bonded materials!* Kassel.

[50] Ductal. *UHPC Standards & Recommendations*. 2017 16-06-2017]; Available from: http://www.ductal.com/en/architecture/uhpc-standards-recommendations.

[51] Naaman, A.E., *Prestressed concrete analysis and design: fundamentals*. 1982: McGraw-Hill New York.

[52] Menn, C., *Prestressed concrete bridges*. 2012: Birkhäuser.

[53] Naaman, A.E. and J.E. Breen. *External prestressing in bridges*. 1990. American Concrete Institute.

[54] Powell, L., J.E. Breen, and M.E. Kreger, *State of the Art Externally Post-tensioned Bridges with Deviators*. 1988: The Center.

[55] Pacheco, P., et al. *A new concept of overhead movable scaffolding system for bridge construction*. in *IABSE Symposium Report*. 2008. International Association for Bridge and Structural Engineering.

[56] Pacheco, P., et al., *Technical challenges of large movable scaffolding systems.* Structural Engineering International, 2011. **21**(4): p. 450-455.

[57] Hendy, C.R. and D.A. Smith, *Designers' Guide to EN 1992-2: Eurocode 2: Design of Concrete Structures. Concrete bridges*. 2007: Thomas Telford.

[58] Yoo, D.-Y. and Y.-S. Yoon, *Structural performance of ultra-high-performance concrete beams with different steel fibers.* Engineering Structures, 2015. **102**: p. 409-423.

[59] Calgaro, J.-A., M. Tschumi, and H. Gulvanessian, *DESIGNERS'GUIDE TO EUROCODE 1: ACTIONS ON BRIDGES: EN 1991-2, EN 1991-1-1,-1-3 TO-1-7 AND EN 1990 ANNEX A2*. 2010: Thomas Telford Ltd.

[60] Alves, G.C., *Determinação de esforços em tabuleiros de pontes de betão armado contruídos tramo a tramo - Estudo de um caso concreto*, in *Engenharia Civil*. 2009, Universidade do Porto: Faculdade de Engenharia p. 157.

A
APPENDICES

A.1. INDICATIVE VALUES FOR UHPC PROPERTIES

A.1.1. FOREWORD

NF P 18-710 provides some indicative values and models of UHPC properties in its appendix T. This information is intended to be used by designers in preliminary studies due to inexistence of characterization tests and identity card of the material. Only relevant information for this work is herein summarized.

A.1.2. MECHANICAL PROPERTIES

Elasticity Modulus	E_{cm}	45 – 65 GPa
Characteristic compressive strength	f_{ck}	150 – 200 MPa
Mean compressive strength	f_{cm}	160 – 230 MPa
Characteristic limit of elasticity under tension	$f_{ctk,el}$	7.0 – 10.0 MPa
Mean limit of elasticity under tension	$f_{ctm,el}$	8.0 – 12.0 MPa
Characteristic maximal post-cracking stress	f_{ctfk}	6.0 – 10.0 MPa
Mean maximal post-cracking stress	f_{ctfm}	7.0 – 12.0 MPa
Fibers length	L_f	12 – 20 mm
Global fiber orientation factor	K_{global}	1.25
Local Fiber orientation factor	K_{local}	1.75
Thermal expansion coefficient	α_t	11 µm/m/ºC
Crack opening corresponding to local peak	w_{pic}	0.3
Mean post-cracking stress corresponding to a crack with of 0.01H	$f_{ctf1\%}$	0.8 f_{ctfk}

A.1.3. SHRINKAGE

$$\varepsilon_{ca} = \begin{cases} 0, & \frac{f_{cm}(t)}{f_{ck}} < 1 \\ \beta_{ca}\left[1 - e^{-\frac{t}{\tau_{ca}}}\right]10^{-6}, & \frac{f_{cm}(t)}{f_{ck}} > 1 \end{cases}$$

$$\varepsilon_{cd} = \frac{K[80 - RH](t - t_s)10^{-6}}{(t - t_s) + \beta_{cd}\ {h_0}^2}$$

β_{ca}	300 – 600 µm/m
τ_{ca}	100 days
β_{cd}	0.003 – 0.01 days/mm^2
K	5

A.1.4. CREEP

$$\varphi b(t, t_0) = \beta_{bc1}\, \varphi_{b0} \frac{\sqrt{t - t_0}}{\sqrt{t - t_0} + \beta_{bc}}$$

$$\beta_{bc} = \beta_{bc2}\, e^{2.8 \frac{f_{cm}(t_0)}{f_{ck}}}$$

$$\varphi_{b0} = \frac{3.6}{f_{cm}(t_0)^{0.37}}$$

$$\varphi_d(t, t_0) = \varphi_{d0}\, [\varepsilon_{cd}(t) - \varepsilon_{cd}(t_0)]$$

β_{bc1}	1.5 – 2.5
β_{bc2}	0.7
φ_{d0}	20 – 50

A.2. UHPC150 - TIME DEPENDENT PROPERTIES

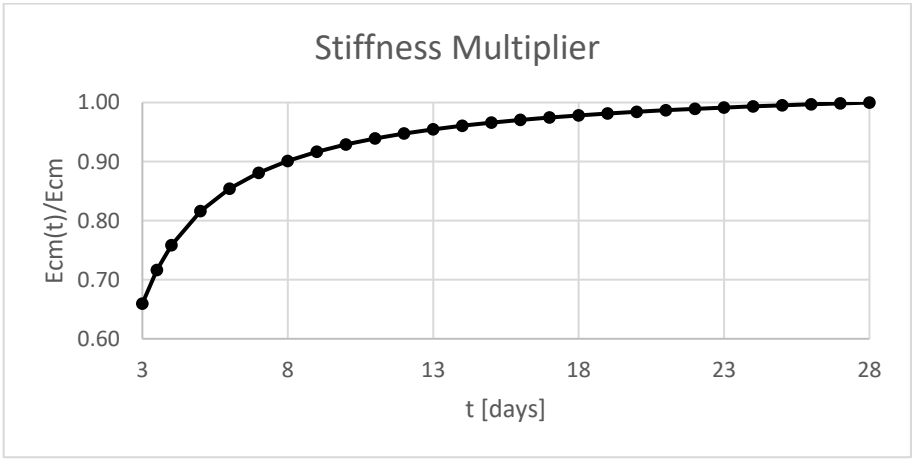

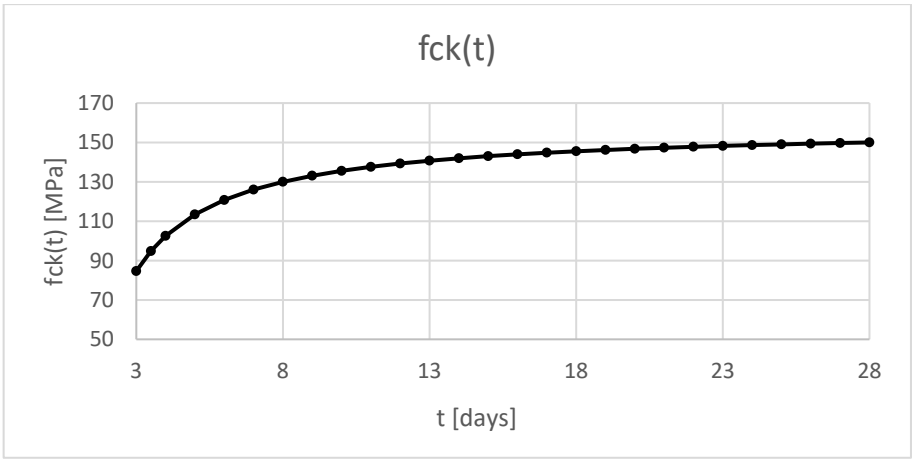

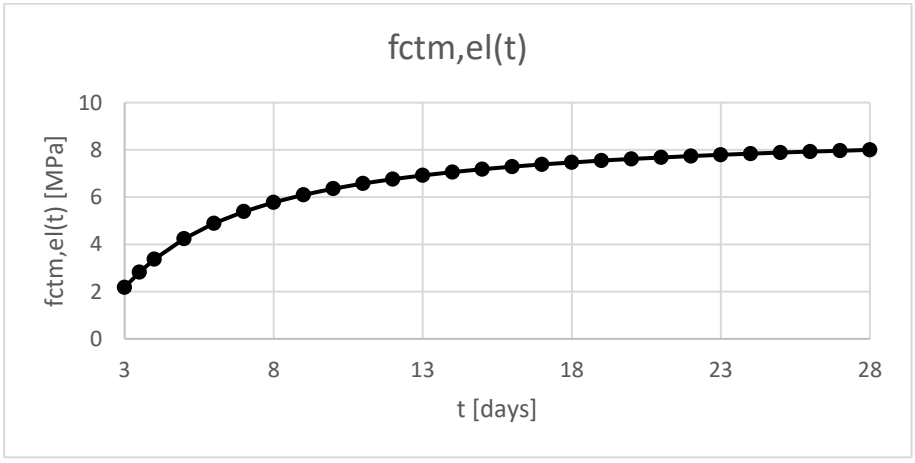

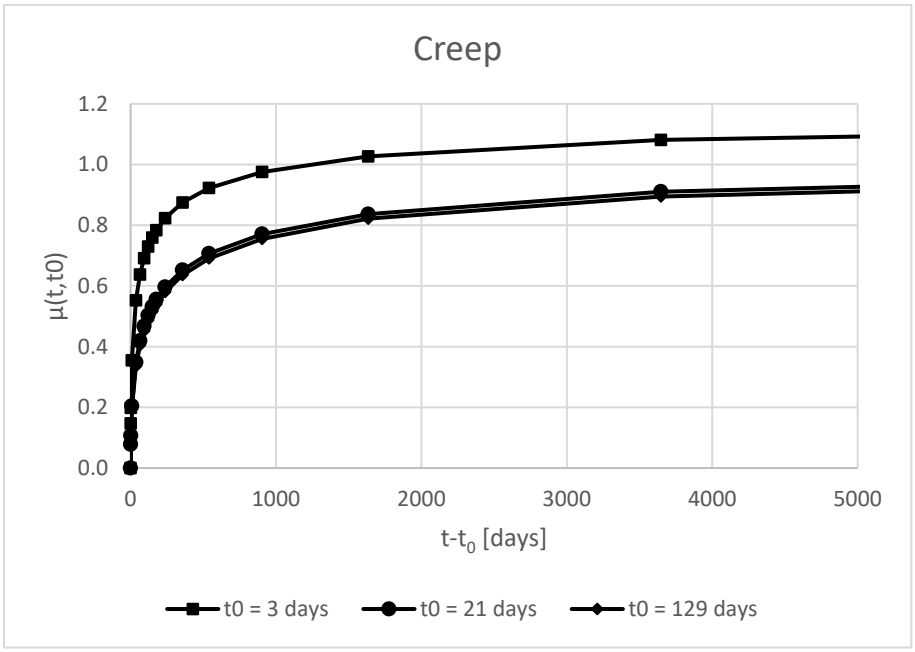

It is assumed that for shrinkage model that A_c, h_0, and RH values do not change from Case 0.

- A mid-span cross section (Ac=6.4048m2 and h0=345.6mm)
- Relative Humidity (RH) equals to 60%

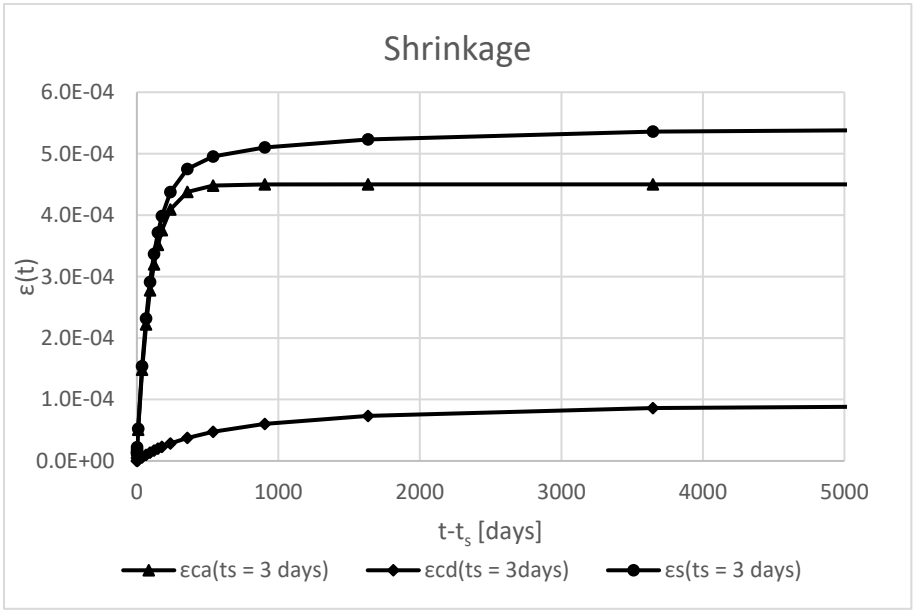

A.3. C40/50 - TIME DEPENDENT PROPERTIES

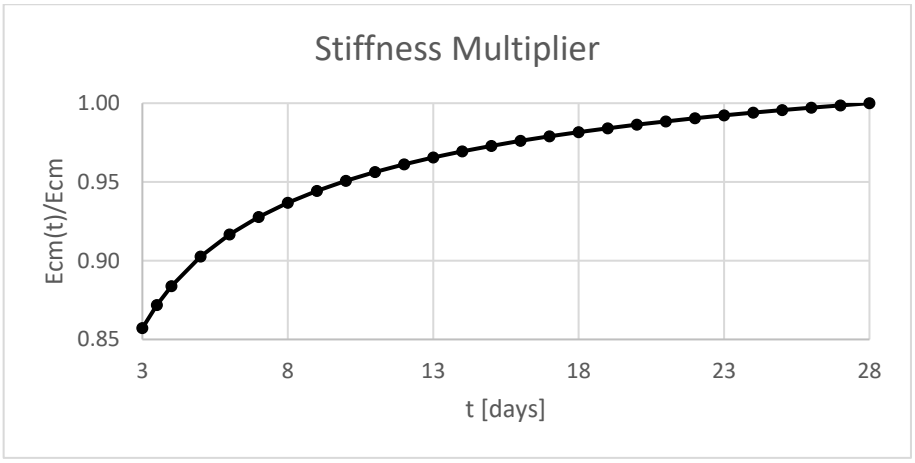

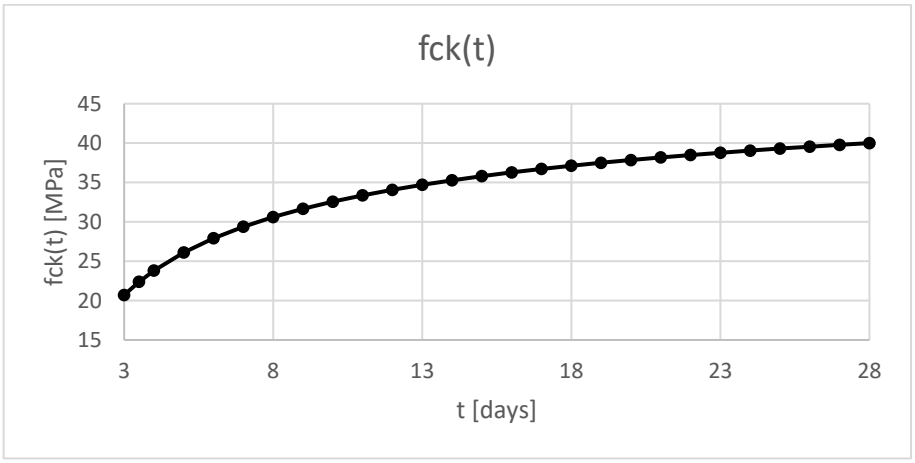

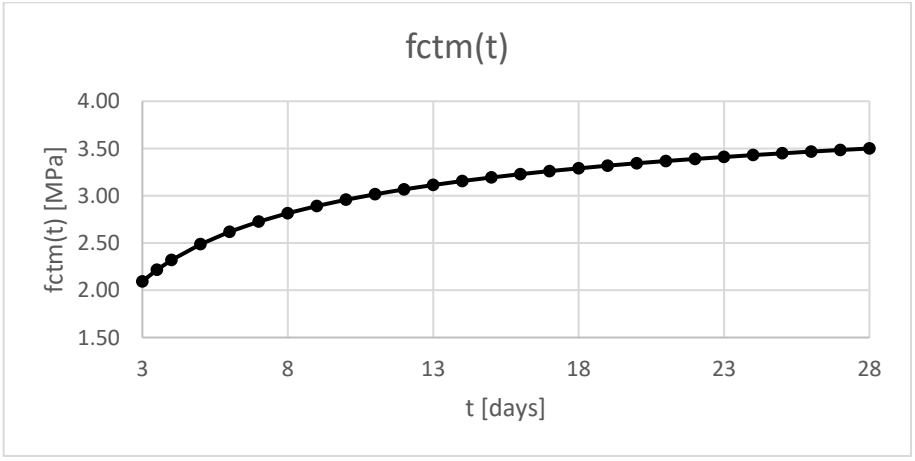

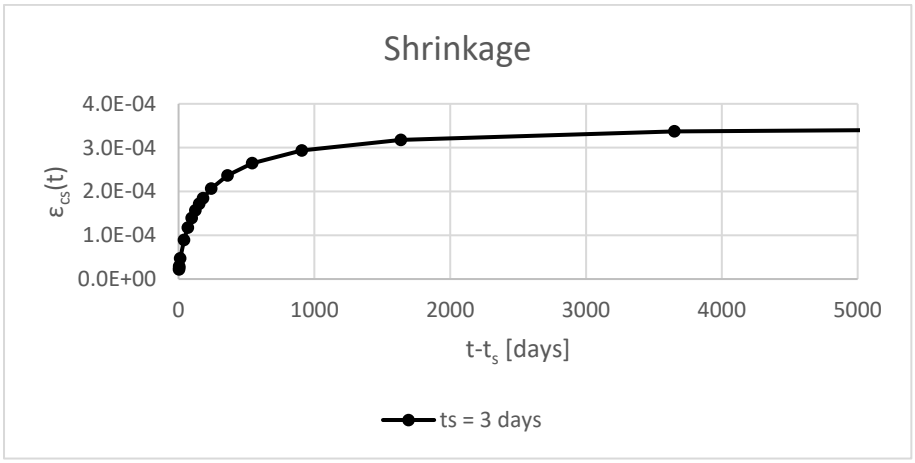
Shrinkage
4.0E-04
3.0E-04
2.0E-04
1.0E-04
0.0E+00
$\varepsilon_{cs}(t)$
0
1000
2000
3000
4000
5000
t-t_s [days]
ts = 3 days

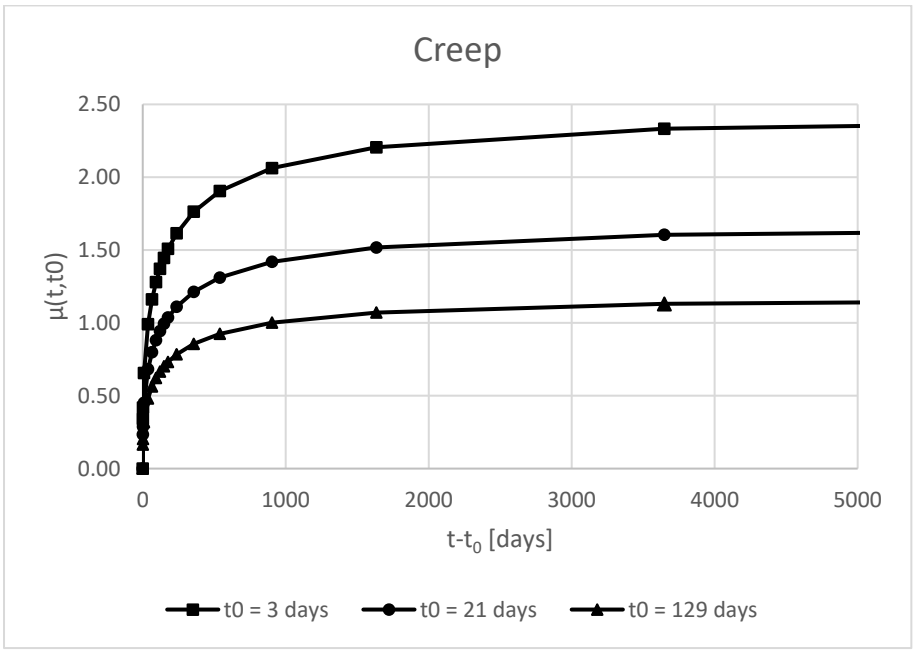
Creep
2.50
2.00
1.50
1.00
0.50
0.00
μ(t,t0)
0
1000
2000
3000
4000
5000
t-t_0 [days]
t0 = 3 days
t0 = 21 days
t0 = 129 days

A.4. ULS SECTIONAL ANALYSIS

The following tables describe the values of the parameters to define compressive constitutive law and tensile constitutive law.

α_{cc}	0.85
γ_c	1.5
f_{cd} [kPa]	-85000
ε_{c0d}	-0.001889
ε_{cud}	-0.00295

w_{pic} [m]	0.0003
L_c [m]	0.1666
L_f [m]	0.016
H [m]	0.2
$w_{1\%}$ [m]	0.002
$f_{ctf1\%,k}$ [Mpa]	4.8
K	1.25
$f_{ctfk,u}$ [kPa]	3692
$f_{ctf1\%,u}$ [kPa]	2954
$\varepsilon_{u,el}$	8.20E-05
$\varepsilon_{u,pic}$	0.00192
$\varepsilon_{u1\%}$	0.0121
$\varepsilon_{u,lim}$	0.0240

This is the stress-strain relationship for a particular UHPC class and cross-section geometry already described in chapter 7. Should be remembered that constitutive law in tension depends on cross-section depth and not only on material properties.

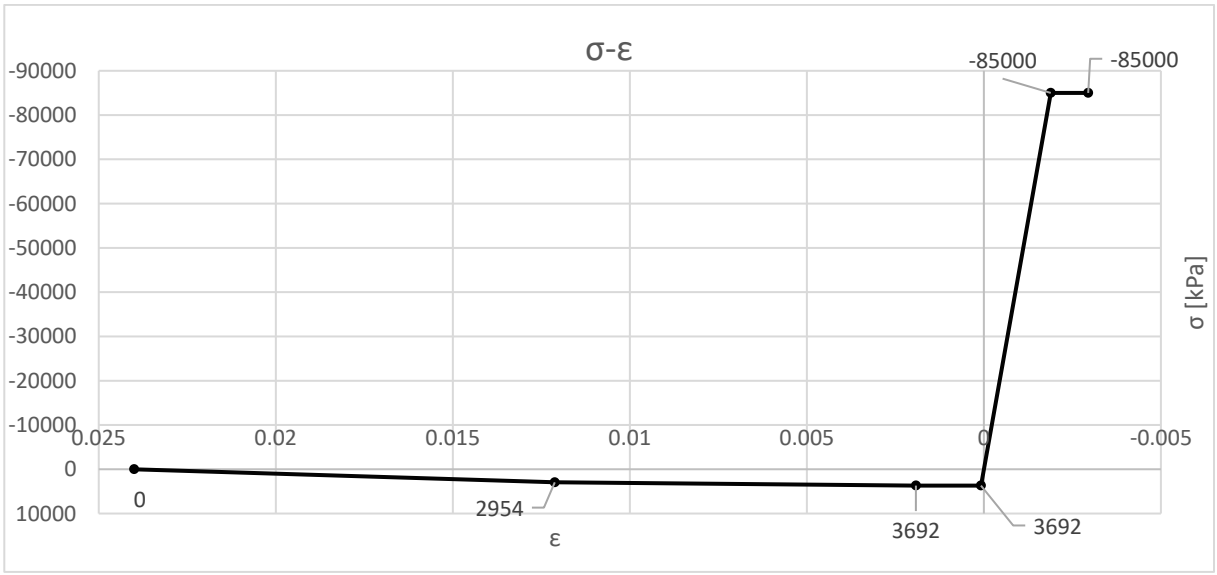

For a design bending moment of 260 kN.m combined with a null axial force, the worksheet tool was used to calculate the minimum longitudinal reinforcement area needed to verify safety conditions. In the following tables are the results curvature (φ) and the position of neutral axis (x). Thus, the strains field is defined as well as the stresses field. It can be noticed that the maximum compressive strain is not fully exploited when the maximum bending resisting moment is achieved.

φ [m^{-1}]	0.044697347
x [m]	0.03957524

x_i [m]	$b_{(xi)}$ [m]	$\varepsilon_{(xi)}$	$\sigma_{(xi)}$ [kPa]	$F_{(xi)}$ [kN]	x_i [m]	$b_{(xi)}$ [m]	$\varepsilon_{(xi)}$	$\sigma_{(xi)}$ [kPa]	$F_{(xi)}$ [kN]
0.001	1.00	-0.00171	-77087	-193	0.126	1.00	0.00387	3551	9
0.004	1.00	-0.0016	-72058	-180	0.129	1.00	0.00399	3543	9
0.006	1.00	-0.00149	-67030	-168	0.131	1.00	0.0041	3535	9
0.009	1.00	-0.00138	-62001	-155	0.134	1.00	0.00421	3527	9
0.011	1.00	-0.00127	-56973	-142	0.136	1.00	0.00432	3518	9
0.014	1.00	-0.00115	-51944	-130	0.139	1.00	0.00443	3510	9
0.016	1.00	-0.00104	-46916	-117	0.141	1.00	0.00454	3502	9
0.019	1.00	-0.00093	-41887	-105	0.144	1.00	0.00466	3494	9
0.021	1.00	-0.00082	-36859	-92	0.146	1.00	0.00477	3486	9
0.024	1.00	-0.00071	-31831	-80	0.149	1.00	0.00488	3478	9
0.026	1.00	-0.0006	-26802	-67	0.151	1.00	0.00499	3470	9

x_i	$b_{(xi)}$	$\varepsilon_{(xi)}$	$\sigma_{(xi)}$	$F_{(xi)}$	x_i	$b_{(xi)}$	$\varepsilon_{(xi)}$	$\sigma_{(xi)}$	$F_{(xi)}$
[m]	[m]		[kPa]	[kN]	[m]	[m]		[kPa]	[kN]
0.029	1.00	-0.00048	-21774	-54	0.154	1.00	0.0051	3462	9
0.031	1.00	-0.00037	-16745	-42	0.156	1.00	0.00522	3454	9
0.034	1.00	-0.00026	-11717	-29	0.159	1.00	0.00533	3446	9
0.036	1.00	-0.00015	-6688	-17	0.161	1.00	0.00544	3438	9
0.039	1.00	-3.7E-05	-1660	-4	0.164	1.00	0.00555	3429	9
0.041	1.00	7.5E-05	3369	8	0.166	1.00	0.00566	3421	9
0.044	1.00	0.00019	3692	9	0.169	1.00	0.00577	3413	9
0.046	1.00	0.0003	3692	9	0.171	1.00	0.00589	3405	9
0.049	1.00	0.00041	3692	9	0.174	1.00	0.006	3397	8
0.051	1.00	0.00052	3692	9	0.176	1.00	0.00611	3389	8
0.054	1.00	0.00063	3692	9	0.179	1.00	0.00622	3381	8
0.056	1.00	0.00075	3692	9	0.181	1.00	0.00633	3373	8
0.059	1.00	0.00086	3692	9	0.184	1.00	0.00644	3365	8
0.061	1.00	0.00097	3692	9	0.186	1.00	0.00656	3357	8
0.064	1.00	0.00108	3692	9	0.189	1.00	0.00667	3349	8
0.066	1.00	0.00119	3692	9	0.191	1.00	0.00678	3340	8
0.069	1.00	0.0013	3692	9	0.194	1.00	0.00689	3332	8
0.071	1.00	0.00142	3692	9	0.196	1.00	0.007	3324	8
0.074	1.00	0.00153	3692	9	0.199	1.00	0.00711	3316	8
0.076	1.00	0.00164	3692	9	0.201	1.00	0.00723	3308	8
0.079	1.00	0.00175	3692	9	0.204	1.00	0.00734	3300	8
0.081	1.00	0.00186	3692	9	0.206	1.00	0.00745	3292	8
0.084	1.00	0.00197	3688	9	0.209	1.00	0.00756	3284	8
0.086	1.00	0.00209	3680	9	0.211	1.00	0.00767	3276	8
0.089	1.00	0.0022	3672	9	0.214	1.00	0.00779	3268	8
0.091	1.00	0.00231	3664	9	0.216	1.00	0.0079	3260	8
0.094	1.00	0.00242	3656	9	0.219	1.00	0.00801	3251	8
0.096	1.00	0.00253	3648	9	0.221	1.00	0.00812	3243	8
0.099	1.00	0.00264	3640	9	0.224	1.00	0.00823	3235	8
0.101	1.00	0.00276	3632	9	0.226	1.00	0.00834	3227	8

x_i	$b_{(xi)}$	$\varepsilon_{(xi)}$	$\sigma_{(xi)}$	$F_{(xi)}$	x_i	$b_{(xi)}$	$\varepsilon_{(xi)}$	$\sigma_{(xi)}$	$F_{(xi)}$
[m]	[m]		[kPa]	[kN]	[m]	[m]		[kPa]	[kN]
0.104	1.00	0.00287	3624	9	0.229	1.00	0.00846	3219	8
0.106	1.00	0.00298	3616	9	0.231	1.00	0.00857	3211	8
0.109	1.00	0.00309	3607	9	0.234	1.00	0.00868	3203	8
0.111	1.00	0.0032	3599	9	0.236	1.00	0.00879	3195	8
0.114	1.00	0.00332	3591	9	0.239	1.00	0.0089	3187	8
0.116	1.00	0.00343	3583	9	0.241	1.00	0.00901	3179	8
0.119	1.00	0.00354	3575	9	0.244	1.00	0.00913	3171	8
0.121	1.00	0.00365	3567	9	0.246	1.00	0.00924	3162	8
0.124	1.00	0.00376	3559	9	0.249	1.00	0.00935	3154	8

For design calculation, the yield stress remains constant after yielding with no ultimate strain limit. Some information referred to steel reinforcement is shown in table which includes the solution of steel reinforcement needed.

A_s [m^2]	1.96E-03
d [m]	0.21
f_{ywd} [kPa]	434782.6087
E_s [kPa]	200000000
ε_{syd}	0.002173913
ε_s	0.192482338
σ_s [kPa]	434782.6087
F_s [kN]	852.173913
$F_{s,correction}$ [kN]	-6.436320028
$F_{s,corrected}$[kN]	845.737593

Additionally, the figure shows the Moment-curvature (M-φ) diagram for this solution of reinforcement and for a solution without reinforcement. This is achieved by determining the bending moment that satisfies the equilibrium and other constrains for each curvature value (φ).

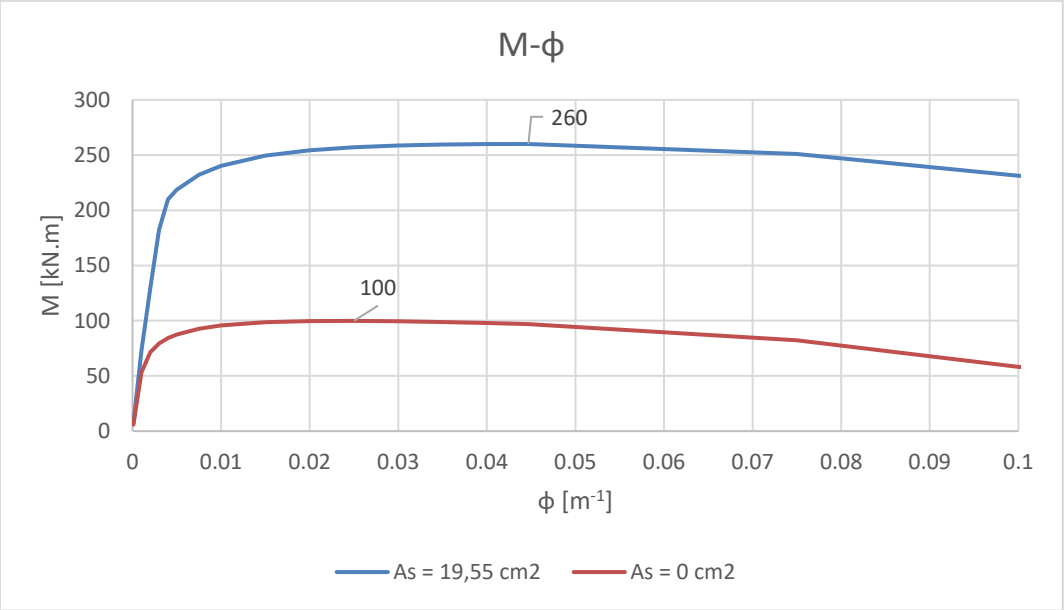

In the following table are described partial results from shear strength calculation.

$V_{rd,c}$		$V_{rd,f}$		$V_{rd,s}$		$V_{rd,max}$	
$Y_{cf}Y_E$	1.5	A_{fv} [m^2]	0.165	A_{sw} [m^2]	0	α_{cc}	0.85
N_{ed} [kN]	0	K	1.25	s [m]	1	Y_c	1.5
A [m^2]	0.21	Y_{cf}	1.3	z [m]	0.165	b_w [m]	1
σ_{cp} [Mpa]	0	$\sigma_{t,average}$ [kPa]	3474	f_{ywd} [kPa]	434782	z [m]	0.165
f_{ck} [Mpa]	150	$\sigma_{rd,f}$ [kPa]	2137	θ (°)	30	f_{ck} [Mpa]	150
k	1	θ (°)	30	cot(θ)	1.732	θ (°)	30
z [m]	0.165	cot(θ)	1.732	α (°)	90	tan(θ)	0.577
Φ_{ducts}	0			cot(α)	0	cot(θ)	1.732
n_{ducts}	0			sin(α)	1	α (°)	90
b_w [m]	1					cot(α)	0
$b_{w,nom}$ [m]	1					$V_{rd,f}$ [Mpa]	0.612
d [m]	0.21					$V_{rd,s}$ [Mpa]	0

$V_{rd,c}$ = 360 kN	$V_{rd,f}$ = 612 kN	$V_{rd,s}$ = 0 kN	

V_{rd} = 972 kN	$V_{rd,max}$ = 3512 kN

A.5. CONSTRUCTIVE SCHEDULE

Stage	Task	duration	Start	End	segment 1					segment 2				
		day(s)	day	day	t_c [days]	C40/50		UHPC150		t_c [days]	C40/50		UHPC150	
						f_{ck}	f_{ctm}	f_{ck}	$f_{ctm,el}$		f_{ck}	f_{ctm}	f_{ck}	$f_{ctm,el}$
1	1	1	0	1	3	20.72	2.09	84.65	2.18	-	-	-	-	-
	3	1	0	1	3	20.72	2.09	84.65	2.18	-	-	-	-	-
	4	1	0	1	3	20.72	2.09	84.65	2.18	-	-	-	-	-
	5	16	0	16	18	37.12	3.29	145.53	7.47	-	-	-	-	-
	6	3	16	19	21	38.18	3.37	147.32	7.68	-	-	-	-	-
	7	1	18	19	21	38.18	3.37	147.32	7.68	-	-	-	-	-
2	1	1	18	19	21	38.18	3.37	147.32	7.68	3	20.72	2.09	84.65	2.18
	2	1	18	19	21	38.18	3.37	147.32	7.68	3	20.72	2.09	84.65	2.18
	3	1	18	19	21	38.18	3.37	147.32	7.68	3	20.72	2.09	84.65	2.18
	4	1	18	19	21	38.18	3.37	147.32	7.68	3	20.72	2.09	84.65	2.18
	5	16	18	34	36	40.00	3.50	150.00	8.00	18	37.12	3.29	145.53	7.47
	6	3	34	37	39	⋮				21	38.18	3.37	147.32	7.68
	7	1	36	37	39					21	38.18	3.37	147.32	7.68
3	1	1	36	37	39					21	38.18	3.37	147.32	7.68
	2	1	36	37	39					21	38.18	3.37	147.32	7.68
	3	1	36	37	39					21	38.18	3.37	147.32	7.68
	4	1	36	37	39					21	38.18	3.37	147.32	7.68
	5	16	36	52	54					36	40.00	3.50	150.00	8.00
	6	3	52	55	57					39	⋮			
	7	1	54	55	57					39				
4	1	1	54	55	57					39				
	2	1	54	55	57					39				
	3	1	54	55	57					39				
	4	1	54	55	57					39				
	5	16	54	70	72					54				
	6	3	70	73	75					57				
	7	1	72	73	75					57				
5	1	1	72	73	75					57				

	2	1	72	73	75	57
	3	1	72	73	75	57
	4	1	72	73	75	57
	5	16	72	88	90	72
	6	3	88	91	93	75
	7	1	90	91	93	75
6	1	1	90	91	93	75
	2	1	90	91	93	75
	3	1	90	91	93	75
	4	1	90	91	93	75
	5	16	90	106	108	90
	6	3	106	109	111	93
	7	1	108	109	111	93
7	1	1	108	109	111	93
	2	1	108	109	111	93
	3	1	108	109	111	93
	4	1	108	109	111	93
	5	16	108	124	126	108
	6	3	124	127	129	111
	7	1	126	127	129	111
8	1	1	126	127	129	111
	2	1	126	127	129	111

A.6. SUBSTRUCTURE INTERNAL FORCES

A.6.1. AXIAL LOADS DUE TO PERMANENT LOADS

Pier	N]		
	[kN]		
	Case 0	Case 1	Case 2
P1	16393	11784	13016
P2	20094	15494	16733
P3	20058	15483	16706
P4	20016	15419	16652
P5	19919	15347	16569
P6	19842	15232	16474
P7	17390	12816	14042

A.6.2. GLOBAL BASE REACTIONS

Case	Seismic type 1		Seismic type 2	
	F3	F2	F3	F2
	[kN]	[kN]	[kN]	[kN]
0	4125	8471	2747	3894
1	4162	7231	2008	3332
2	4086	7797	2204	3595

A.6.3. CASE 0

Case 0	Seismic type 1					Seismic type 2				
	V3	M2	V2	M3	T	V3	M2	V2	M3	T
	[kN]	[kN.m]	[kN]	[kN.m]	[kN.m]	[kN]	[kN.m]	[kN]	[kN.m]	[kN.m]
P1	0	0	2223	42824	0	0	0	1033	19905	0
P2	1012	44450	1057	47618	3375	674	29598	485	21842	1552
P3	703	32672	1454	68500	3016	468	21755	667	31410	1384
P4	751	34167	1980	90280	761	500	22751	907	41389	354
P5	759	34417	1573	72836	3119	505	22917	721	33386	1435
P6	898	38570	1111	48819	2979	598	25683	510	22397	1370
P7	0	0	1820	50607	0	0	0	840	23355	0

A.6.4. CASE 1

Case 1	Seismic type 1					Seismic type 2				
	V3	M2	V2	M3	T	V3	M2	V2	M3	T
	[kN]	[kN.m]	[kN]	[kN.m]	[kN.m]	[kN]	[kN.m]	[kN]	[kN.m]	[kN.m]
P1	0	0	1551	30615	0	0	0	726	14345	0
P2	1019	44480	941	42031	2993	491	21469	435	19392	1379
P3	711	32755	1320	61978	2689	343	15809	607	28496	1242
P4	759	34236	1784	81409	580	366	16524	820	37435	274
P5	766	34488	1423	65593	2709	370	16646	654	30147	1255
P6	905	38615	981	42855	2601	437	18638	453	19759	1199
P7	0	0	1396	39377	0	0	0	649	18319	0

A.6.5. CASE 2

Case 2	Seismic type 1					Seismic type 2				
	V3	M2	V2	M3	T	V3	M2	V2	M3	T
	[kN]	[kN.m]	[kN]	[kN.m]	[kN.m]	[kN]	[kN.m]	[kN]	[kN.m]	[kN.m]
P1	0	0	1929	37915	0	0	0	907	17827	0
P2	1016	44455	974	43775	3221	548	23977	448	20133	1485
P3	708	32724	1372	64553	2845	381	17650	630	29637	1311
P4	756	34214	1859	84925	739	407	18453	853	38985	348
P5	763	34456	1483	68643	2906	411	18583	681	31497	1344
P6	841	36748	1028	45058	2831	454	19820	473	20723	1305
P7	0	0	1600	45122	0	0	0	744	20971	0